Novel Pathways Linking Mammalian Septins and the DNA Damage Response

Timothy Michael Errington
Buffalo, New York

M.A., Molecular and Cell Biology, University of California at Berkeley, 2007
B.S. Biology; Chemistry, St. Lawrence University, 2002

A Dissertation presented to the Graduate Faculty
of the University of Virginia in Candidacy for the Degree of
Doctor of Philosophy

Department of Microbiology, Immunology, and Cancer Biology

University of Virginia
December, 2013

Abstract

A cellular response to damaged DNA, known as the DNA damage response (DDR), has evolved to combat damage that occurs from exposure to genotoxic agents or byproducts of normal cellular metabolism. Upon recognition of DNA damage, the cell arrests the cell cycle and repairs damaged DNA to maintain genome integrity. However, if the damage is severe, cells undergo apoptosis or initiate cellular senescence. The DDR is a highly coordinated event linking many pathways involved in various cellular processes. A previous study from this lab implicated mammalian septins in the DDR, although through an unknown mechanism. These cytoskeletal proteins function as signaling platforms and diffusion barriers and associate with various proteins including the adaptor proteins SOCS7 and NCK. In response to multiple types of DNA damage, NCK relocalizes from the cytoplasm to the nucleus, using the nucleocytoplasmic shuttling protein SOCS7. The nuclear accumulation of NCK in response to UV irradiation is dependent on the kinase activity of ATR, a member of the PIKK family that is activated early in the DDR. Depletion of NCK results in elevated phosphorylation of the transcription factor p53 and an early induction of apoptosis. Depletion of SOCS7, which blocks the nuclear accumulation of NCK, also increases phosphorylation of p53 and also results in an early induction of apoptosis. This indicates the anti-apoptotic role of NCK is dependent on its nuclear translocation during the DDR. Another septin interacting protein was identified using a proteomic approach. This novel nuclease called Septin Associated Nuclease 1 (SAN1) possesses unique 5' exonuclease activity mediated

by a FEN1-related nuclease domain necessary for the proper repair of DNA interstrand crosslinks (ICL). Depletion of SAN1 results in a low rate of homologous recombination (HR) due to a decrease in end-resection of double-strand breaks generated during ICL repair. Additionally, SAN1 is mostly localized in the cytoplasm but accumulates in the nucleus following treatment with ICL-inducing agents. However, in the absence of septins, SAN1 becomes mislocalized and distributed throughout the cell. Depletion of septins also results in a decrease in HR and end-resection. This suggests septins are necessary for the proper response to ICL by regulating SAN1 localization and activation. Taken together, these data demonstrate that mammalian septins play a role in the DDR and highlight an unexpected link between cytoskeletal elements and DNA damage signaling.

Table of Contents

List of Figures

List of Abbrevations

CDC	cell division cycle
SNARE	soluble NSF attachment protein receptors
DDR	DNA damage response
SOCS7	suppressor of cytokine signaling 7
NCK	non-catalytic region of tyrosine kinase
UV	ultraviolet radiation
DSB	double-strand breaks
ICL	interstrand crosslink
ATM	ataxia telangiectasia mutated
ATR	ataxia telangiectasia and Rad3 related
DNA-PK	DNA-dependent protein kinase
PIKK	phosphoinositide 3-kinase-like kinase
MRN	MRE11-RAD50-NBS1
ATRIP	ATR-interacting protein
RPA	replication protein A
ssDNA	single-stranded DNA
DNA-PKcs	DNA-PK catalytic subunit
γH2AX	phospho-serine 139 H2AX
FHA	Forkhead associated
BRCT	BRCA1 C-terminal

BER	base excision repair
SSB	single strand break
MMR	mismatch repair
NER	nucleotide excision repair
NHEJ	non-homologous end joining
HR	homologous recombination
AP	apurinic/apyrimidinic
ROS	reactive oxygen species
PCNA	proliferating cell nuclear antigen
GG-NER	global genome NER
TC-NER	transcription-coupled NER
MMEJ	microhomology-mediated end-joining
SSA	single-strand annealing
CDK	cyclin-dependent kinase
CtIP	C-terminal binding protein interacting protein
PALB2	partner and localizer of BRCA2
dsDNA	double-stranded DNA
SDSA	synthesis-dependent strand annealing
BIR	break-induced replication
TLS	translesion synthesis
FA	Fanconi anaemia
SCAN1	spinocerebellar ataxia with axonal neuropathy

AOA1	ataxia with oculomotor apraxia 1
AT	ataxia telangiectasia
NBS	Nijmegen breakage syndrome
XP	Xeroderma pigmentosum
CS	Cockayne syndrome
TTD	tricothiodystrophy
KIN	karyomegalic interstitial nephritis
IκB	interaction with inhibitor κB
NEMO	NF-κB essential modulator
PIP	PCNA-interacting peptide
APIM	AlkB homologue 2 PCNA-interacting motif
SMC	structural maintenance of chromosomes
SCE	sister-chromatid exchange

Acknowledgements

This work would not be possible without the help and support of many other people. First, I would like to thank my mentor, Dr. Ian Macara, who not only provided guidance and support throughout my training, but also had an enthusiasm about science that was contagious. He also gave me the freedom and confidence to follow the direction my thesis project took. I was also fortunate to be apart of a laboratory group that was supportive, collaborative, smart, and just fun to be around. The Macara lab members during my tenure were a vital part of my scientific development and remain close colleagues and friends of mine. I also want to thank my thesis committee for their insight and constructive criticism during the course of this research. I always enjoyed my committee meetings and felt fortunate to have the attention and assistance they provided.

I also want to thank the many people who provided me with a strong academic and scientific framework that this work was built upon, including the numerous teachers, professors and mentors I had before I started graduate school at UVA. This includes my graduate training in the lab of Dr. Kathleen Collins at UC Berkeley, where I met wonderful classmates and labmates and Dr. Deborah Lannigan at UVA, where I obtained the early foundations of my training at the bench. I also want to thank David Clark for his help in training me in numerous techniques and for his friendship since our time at St. Lawrence.

Lastly, and most importantly, I want to thank my wife, Dr. Anne Allison who is a gifted scientist and teacher, and a wonderful partner. In addition to her support and

encouragement she constantly reminded me why science is so much fun and always wanted to listen to what I was up to in lab. Finally, I want to thank my son Henry, who I hope will one day be excited about the discovery process just like his parents.

Chapter 1: Introduction

The coordination of many molecular processes is essential for cellular survival. Discrete molecular pathways are becoming increasingly well understood, but the interconnectivity and coordination of multiple pathways remains less clear. This thesis work illustrates this by connecting cytoplasmic scaffolding proteins, namely septins, and cellular events in response to DNA damage, such as DNA repair. The inability of cells to properly respond to DNA damage can lead to apoptosis (cell death), genomic instability, and ultimately disease, premature aging and cancer.

Septins

Septins are ubiquitous GTP-binding proteins that have been identified in nearly all eukaryotes, with the exception of land plants [1, 2]. They were first discovered in *S. cerevisiae*, as cell division cycle (CDC) genes, named *cdc3, cdc10, cdc11, cdc12*, with mutations in any of these four genes resulting in defects in cytokinesis [3]. The protein products of these genes were named septins and were shown to localize as rings at the site of the emerging bud neck [4-6]. There is variability in the number of septin genes between organisms, with humans having 13 genes (SEPT1-SEPT12 and SEPT14), many of which undergo alternative splicing in addition to multiple pseudogenes [7]. These genes are further divided into four subgroups named after their founding members, SEPT2, SEPT3, SEPT6 and SEPT7 [2, 7, 8]. Seven of the septin genes, with at least one

from each subgroup, are expressed in all tissues, while the other six are tissue specific [2].

There are multiple conserved features among all septins (Fig. 1.1A). The N-terminus contains a variable proline-rich region and a polybasic region, which has been demonstrated to bind phosphoinositides and might target septins to the plasma membrane [8-10]. The central region contains a GTP-binding domain, through which septins interact with each other [11]. GTP hydrolysis has been observed from purified and recombinant septin complexes, and might regulate septin-septin interactions through conformational changes [8, 12-16]. The SEPT6 subgroup, however, is unable to hydrolyse GTP to GDP, and thus cannot be regulated by GTP hydrolysis like the other subgroups [8, 12]. C-terminal to the GTP-binding domain are 53 highly conserved amino acids, with unknown function, called the septin unique element [17]. Except the SEPT3 subgroup, there also contains a C-terminal extension with a coiled-coil domain of varying length [8, 18]. This domain is important for septin-septin interactions in combination with the N-terminus, as well as interaction of septins with other proteins, such as the Cdc42 effector Borg3 [11, 12, 16, 19, 20].

Septins form as rod-shaped hetero-oligomers in a non-polar manner (Fig. 1.1B) and form as either six or eight subunit complexes containing members of SEPT2, SEPT6 and SEPT7 in both complexes, with SEPT3 also present in the eight subunit complexes [11, 21-25]. In mammalian cells, similar to yeast, higher-order structures, such as rings, are found. Septin rings have been observed in the spermatozoa annulus, the base of primary cilia, at the base of dendritic spines, and during bacterial infection [26-36]. These

Figure 1.1: Septin domain structure and filament assembly. (A) Schematic drawing of each septin group (figure from [8]). The 13 individual septin proteins are classified into four groups according to sequence homology and the ability to substitute for each other within a septin multimer. Domains consist of: N-terminal proline-rich domain (Pro-rich), phosphoinositide-binding polybasic region (Polybasic), GTP-binding domain (GTP binding), septin unique element (SUE), and C-terminal coiled-coil domain (Coiled-coil). The N- and C-terminal regions vary in length and sequence. The SEPT6 group lacks a threonine residue (indicated by *), which prevents the proteins from hydrolyzing GTP-GDP. (B) Surface representation of the SEPT2-SEPT6-SEPT7 complex, with two copies of each septin generating a hexameric complex (figure from [11]). The hexamer makes contacts with SEPT7 (in grey) to form septin filaments. Arrows indicate the presumed orientations of the coiled-coil domains, which are absent from the crystal structure.

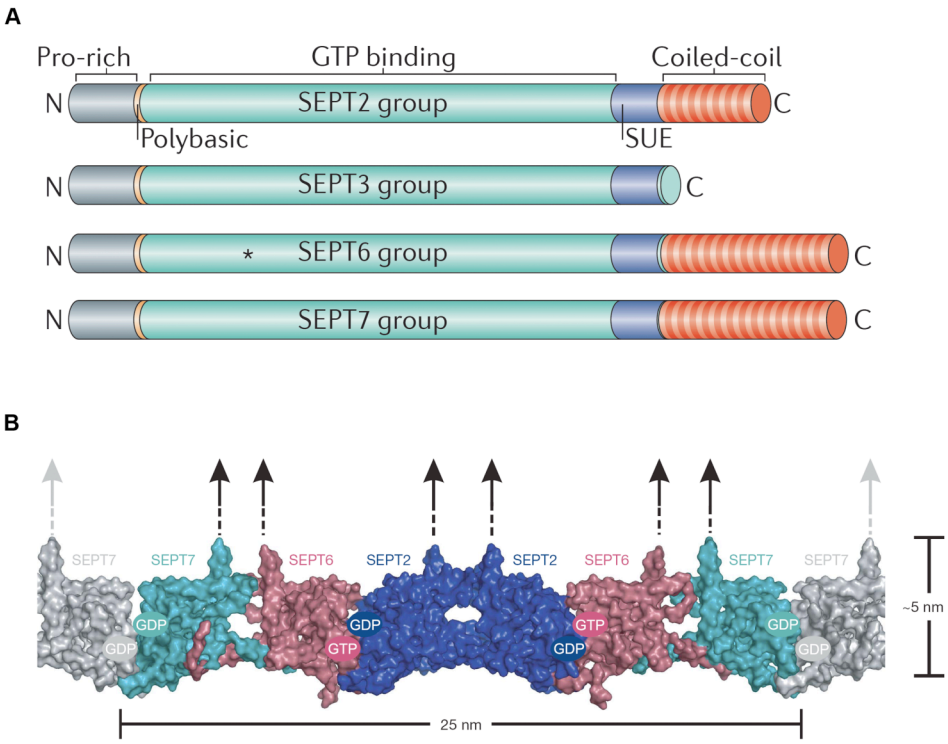
A
Pro-rich
GTP binding
Coiled-coil
N
SEPT2 group
C
Polybasic
SUE
N
SEPT3 group
C
N
*
SEPT6 group
C
N
SEPT7 group
C
B
SEPT7
SEPT7
SEPT6
SEPT2
SEPT2
SEPT6
SEPT7
SEPT7
GDP
GDP
GDP
GTP
GTP
GDP
GDP
GDP
~5 nm
25 nm

ring-like structures are thought to act as subcellular scaffolds for protein recruitment and as diffusion barriers to compartmentalize membrane proteins to specific cellular domains [2, 37]. However these functions can also be attributed to septins not forming higher-order structures, especially as a scaffold since there are many interacting partners and diverse molecular roles of mammalian septins.

As described above, septins were initially characterized as genes with a role in cytokinesis, and this function is conserved to humans. Multiple septins have been shown to localize to the cleavage furrow during anaphase, and depletion of most septins results in cytokinetic defects, such as multinucleation, however the phenotype is not completely penetrant [14, 38-42]. The defects in cytokinesis caused by septin depletion can be attributed by a failure of certain factors to be recruited. This has been suggested by different studies, such as SEPT9, which has been implicated in mediating exocyst complex localization to the midbody during abscission [42]. In addition, SEPT1 and the SEPT2, SEPT6, SEPT7 complex have been shown to be necessary for proper localization of the Aurora B kinase and the motor protein CENP-E, respectively [41, 43, 44]. Consistent with this, septins also interact with the actin cytokeleton and microtubules [14, 15, 39, 41, 45-50]. Septins interact with actin through proteins like anillin, which recruits septins to the actomyosin ring during cell division, non-muscle myosin II during interphase, a septin associated RhoGEF, and the Rho effector rhotekin [46, 51-53]. Septin association with microtubules is less well understood, with the microtuble-associated protein, MAP4, as the only known protein known to bridge this interaction [38, 54].

In addition to their roles in cytokinesis, septins are associated with various other cellular processes. This includes acting as a scaffold at the plasma membrane, where they regulate the distribution of surface receptors, like the receptor tyrosine kinase MET [55]. Septin scaffolds also play a role in vesicle trafficking. Multiple septins interact with the exocyst complex and soluble NSF attachment protein receptors (SNARE), thus mediating vesicle fusion events by localizing the exocyst complex and regulating the availability of SNAREs for fusion [42, 49, 56-61]. Septins have also been involved in the endocytosis of receptors, such as GLAST, possibly through their interaction with dynamin [62, 63]. The involvement of septins at the membrane may also involve their direct interaction with phospholipids, which assemble into filaments and facilitate tubule formation of phospholipid-based liposomes using purified proteins [64]. In addition, septins have been shown to be important for cell motility by providing a scaffold for membrane reabsorption, and for contraction of the leading edge in cooperation with the actomyosin cytoskeleton [65, 66].

Septins are also implicated in other cellular process, although less well understood. Examples of these are a role in platelet function, cardiac myocyte development, parkinson's pathogenesis, angiogenesis, cell proliferation, and tumorigenesis [67-75]. In addition, septins have been implicated in the DNA damage response (DDR) [76-78]. In humans, septins interact with suppressor of cytokine signaling 7 (SOCS7) and its binding partner non-catalytic region of tyrosine kinase (NCK), and retain these adaptor proteins in the cytoplasm at a steady state to regulate actin organization. However, following DNA damage SOCS7 translocates NCK to the

nucleus where it accumulates, although the significance of this accumulation is not well understood [76]. Although septin interaction with the actin cytoskeleton is well documented, the connection to the DDR is not well characterized.

DNA Damage Response

Damage to DNA can occur from endogenous sources, such as natural products of metabolism, or exogenous sources, such as ultraviolet radiation (UV) and chemotherapeutic reagents (De Bont van Larebeke 2004). Although there are many agents that cause damage to DNA, they differ in the way they alter the DNA molecule. These include base-pair mismatches, stalled replication forks, oxidized and alkylated base modifications, pyrimidine dimers, a nick, single-stranded gaps, double-strand breaks (DSB), and interstrand crosslinks (ICL) (Fig. 1.2) [79-81]. Since undamaged DNA is far more abundant then damaged DNA, proteins are continuously monitoring for aberrant DNA structures and the magnitude of the response is amplified by the presence of DNA damage [81]. Some of the biochemical pathways elicited by DNA damage are DNA repair, transcriptional response, DNA damage checkpoints, chromatin remodeling, and apoptosis, collectively known as the DDR [82].

Figure 1.2: DNA lesions. DNA base and noncanonical DNA structures that elicit a DNA damage response (figure from [81]). O^6MeGua indicates O^6-methyldeoxyguanosine; T< > T indicates cyclobutane thymine dimer; Cross-link indicates a cisplatin G-G interstrand crosslink.

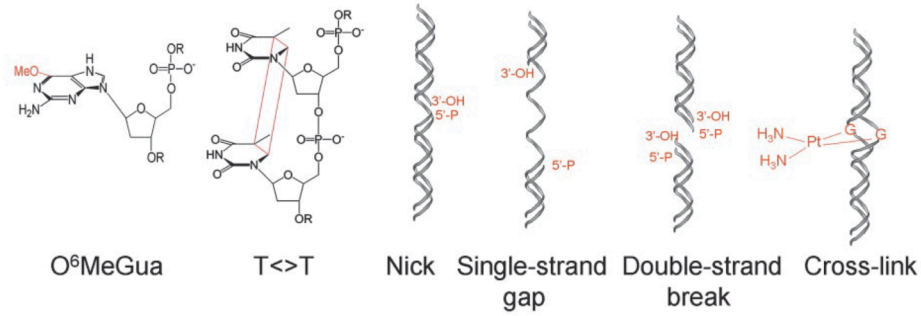

O^{6}MeGua T<>T Nick Single-strand gap Double-strand break Cross-link

DNA Damage Checkpoints

DNA damage checkpoints are signaling transduction pathways to delay or arrest cell cycle progression in the presence of DNA lesions thus preventing chromosome alterations and cell death [83]. Four checkpoints have been described in eukaryotic cells. The G1/S checkpoint prevents cells from entering S phase by inhibiting replication, the intra-S-phase checkpoint blocks replication, the G2/M checkpoint prevents mitosis, and the replication (S/M) checkpoint inhibits mitosis and suppresses initiation of DNA replication [81, 84, 85].

Like other signal transduction pathways, DNA damage checkpoints can be divided into components: sensors, mediators, transducers, and effectors. Sensors are recruited to sites of DNA damage and are necessary to initiate subsequent events [86]. Mediator proteins provide specificity by associating with sensors and transducers at certain cell cycle phases [81]. Transducers are kinases, which propagate the signal by phosphorylating and regulating downstream effectors to control cellular responses, such as cell cycle progression and DNA synthesis [85]. Proteins in the DNA damage checkpoint pathway are not restricted to a role in one component; for example sensors can also function as transducers.

The earliest event in the DDR, and one of the most well studied, is the activation of the sensors ataxia telangiectasia mutated (ATM), ataxia telangiectasia and Rad3 related (ATR) and DNA-dependent protein kinase (DNA-PK). ATM, ATR, and DNA-PK belong to the phosphoinositide 3-kinase-like kinase (PIKK) family of serine/threonine

kinases. Through the MRE11-RAD50-NBS1 (MRN) complex, a sensor of DSBs, ATM becomes activated by autophosphorylation at serine 1981, which dissociates inactive dimers to monomers [87, 88]. Although the MRN complex is necessary for activation of ATM at DSBs, ATM is regulated by other mediators, and even in the absence of damage through direct tethering to chromatin [89, 90]. Unlike ATM, the recruitment of ATR to DNA lesions is mediated by its binding partner ATR-interacting protein (ATRIP), which is recruited to replication protein A (RPA)-coated single-stranded DNA (ssDNA) [91]. DNA-PK is a heterotrimer of a catalytic subunit (DNA-PKcs) and the KU70/KU80 dimer, which binds DNA ends and recruits and activates DNA-PKcs [92].

According to the canonical model of PIKK activation, ATM and DNA-PK are activated by DSBs, while ATR responds primarily by stalled replication forks [81]. However, the sensing of damage and initial signaling of the DDR is more complex then this simplified model. Besides activating ATM, DSBs activate ATR, through ATM/MRE11-dependent end resection, which generates ssDNA [93, 94]. In addition, during replication fork stalling, or UV treatment, ATM and DNA-PK are phosphorylated and activated in an ATR dependent manner [95-97]. Thus, the PIKKs do not function independently of each other only in response to distinct types of DNA lesions, but instead act in concert.

Once activated, the PIKK family initiates a signaling cascade with mediator proteins as the immediate downstream substrates, which act to recruit additional substrates, as scaffolds for complexes to form, and to maintain different DDR proteins at sites of damage. One of the earliest events is the phosphorylation of the histone variant

H2AX on serine 139 (γH2AX), which promotes recruitment of other DDR proteins including chromatin modifying complexes [98, 99]. Because of the prominence of phosphorylation as a mark of DNA damage signaling, many proteins also contain phospho-binding domains. These include Forkhead associated (FHA) and BRCA1 C-terminal (BRCT) domains, which preferentially bind to phospho-serines and phospho-threonines motifs in substrates phosphorylated by the PIKK family [100-102]. Proteins with FHA and BRCT domains interact with specific PIKK substrates, which leads to an accumulation of proteins near sites of DNA damage, which is observed as nuclear foci when visualized by indirect immunofluorescence or by expressing fluorescently tagged proteins [99, 103]. This leads to an amplification of the DNA damage signal and activation of the downstream kinases CHK1, CHK2, and MK2.

Traditionally the DDR has been divided into two signaling branches, the ATR/CHK1 arm and the ATM/CHK2 module, with the more recently discovered MK2 kinase sharing substrate homology with CHK1 and CHK2 [104]. The CHK1 protein plays a prominent role in the intra-S and G2/M checkpoints and is active in the absence of DNA damage [105-107]. The importance of CHK1 in the cell cycle is highlighted by the embryonic lethality in *Chk1*-deficient mice [108, 109]. However, CHK2 null mice are viable and display only a mild defect in the intra-S and G1/S checkpoints [110, 111]. CHK2 is largely inactive, yet stable, throughout the cell cycle, but following DNA damage, CHK2 is phosphorylated on threonine 68, which then leads to autophosphorylation and oligomerization activating the kinase [112-114]. However, similar to which types of DNA lesions activate the PIKK family, there is also overlap in

the activation of the checkpoint kinases with both checkpoint kinases being phosphorylated and activated by the other PIKK family members [115-118]. The targets of CHK1 and CHK2 are proteins involved in chromatin remodeling, damage-induced transcription, DNA repair, cell cycle arrest and apoptosis. Examples of these effector proteins include the cell cycle proteins CDC25A and CDC25C, the transcription factor E2F1, and the tumor suppressors BRCA1 and p53 [119-122].

DNA damage can induce cell cycle arrest or apoptosis, which is implemented primarily by p53. Multiple models exist that explain how this decision is determined, with none of them being mutually exclusive, and probably a combination of all of them contributing to the process. A common model suggests the amount of accumulated p53 dictates cell fate, where a low level of p53 results in cell cycle arrest, and it is not until higher levels are reached when apoptosis occurs [80, 123]. Under normal conditions, p53 protein stability and activity are inhibited through its interaction with the ubiquitin ligase, MDM2, which targets p53 for degradation [124]. In response to a variety of stimuli, including DNA damage, p53 is rapidly stabilized and activated [125]. Stability occurs through post-translational modifications of p53, or MDM2, leading to accumulation of the p53 protein [126].

There are over 30 different sites of modification on p53 including phosphorylation, ubiquitination, sumoylation, acetylation, methylation, and ADP-ribosylation [127]. The majority of these modifications are phosphorylations, which occur in the amino-terminus, where they mostly regulate protein stability, and the carboxyl-terminus, where they mostly enhance DNA binding [126]. Phosphorylation of

p53 at serine 15 occurs rapidly in response to DNA damage and has been proposed as a priming event for other modifications to occur [128, 129]. Multiple DDR kinases phosphorylate p53, including ATM, ATR, DNA-PK, CHK1, and CHK2 [120, 125, 130-132]. It has also been shown that p53 binds to DNA strand breaks, suggesting p53 might play a role in detection or amplification of DNA damage signaling [126, 133]. Thus, the influence of upstream signals may also drive cell fate decisions, which could affect p53 levels and post-translational modifications to accommodate the appropriate cellular response.

The primary role of p53 in apoptosis is to act as a transcriptional activator of multiple pro-apoptotic genes, such as BAX, and transcriptional repressor of a subset of genes, such as Survivin [134, 135]. In mammalian cells, apoptosis occurs through either an extrinsic or intrinsic pathway. The extrinsic pathway is induced by pro-apoptotic and pro-inflammatory cytokines, which bind to death-domain receptors resulting in the formation of intracellular death-induced signaling complexes [136]. These complexes can lead to direct activation of caspases, by activating upstream caspases, such as Caspase-8, or amplification of the cell death signal, by activating the pro-apoptotic proteins, which cause mitochondrial damage [136, 137]. The intrinsic apoptotic pathway is initiated by transcriptional upregulation, or activation, of pro-apoptotic members of the BCL2 family [138]. Activation of pro-apoptotic proteins leads to inhibition of anti-apoptotic members of the BCL2 family. Anti-apoptotic members of the BCL2 family protect cells by preventing caspase activation, via adaptor molecules, as well as protecting the integrity of the mitochondria, through inhibition of the pro-apoptotic BCL2 family members BAX

and BAK [138]. Activation of BAX and BAK lead to mitochondrial damage and cytochrome *c* release, which promotes the formation of the heptameric apoptosome complex [136, 138]. This leads to activation of Caspase-9, which in turn cleaves and activates downstream caspases, including Caspase-3, that carry out apoptosis [139].

Another possible outcome if DNA damage is especially severe, besides apoptosis, is for cells to undergo senescence. Cellular senescence is an irreversible cell-cycle arrest that is implemented by the DDR, however the mechanism of choice between apoptosis ad senescence is not clear [140]. The establishment of cellular senescence is associated with prolonged DNA damage signaling leading to persistent foci of DDR proteins, especially at short telomeres [141, 142]. These foci are likely a result of DNA lesions unable to be repaired, thus prompting cellular senescence, or death, presumable to eliminate cells with potentially dangerous mutations.

DNA Repair

A major element of the DDR is the detection and repair of DNA damage to prevent genomic instability and to avoid transmission to progeny. The initiation of cell cycle checkpoints and execution of DNA repair are intertwined, and although they are discussed independently, they occur simultaneously and utilize some of the same proteins. Multiple repair pathways have evolved, which act independently although there is often crosstalk, to combat the variety of DNA lesions that can occur. These include base excision repair (BER), single strand break (SSB) repair, mismatch repair (MMR),

nucleotide excision repair (NER), non-homologous end joining (NHEJ), and homologous recombination (HR) (Fig. 1.3). Another repair pathway that is thought to integrate components of all the other repair pathways is DNA ICL repair. It remains perplexing how a cell decides which repair pathway to utilize given the plethora of DNA lesions and the overlap among detection and repair pathways.

Base Excision and Single Strand Break Repair

The BER pathway is the most adaptable repair pathway, responsible for the repair of damage to DNA bases produced by oxidation, alkylation, hydroxylation, or deamination [143, 144]. BER is initiated with excision of a damaged base by a damage-specific DNA glycosylase, leaving an apurinic or apyrimidinic (AP) site [144]. These AP sites, which also occur by the spontaneous hydrolysis of bases, are removed by an AP-endonuclease, or the AP lyase activity of bifunctional DNA glycosylases [143, 144]. This leaves a SSB, which can also arise through reactive oxygen species (ROS) or stalled topoisomerase activity, and where BER and SSB repair converge [145]. Although the detection of the SSB is different between BER and SSB repair, the latter utilizing PARP, the two pathways share similar end processing and gap filling mechanisms [145, 146]. The processed SSB is filled in by one of two sub-pathways, short-patch BER, which fills a one-nucleotide gap through DNA polymerases, or long-patch BER, where the repair size is two to eight nucleotides and removed as a ssDNA flap, before the final step of DNA ligation [144, 145].

Figure 1.3: DNA repair mechanisms. Simplified models of various forms of DNA repair pathways (figure from [157]). See text for details.

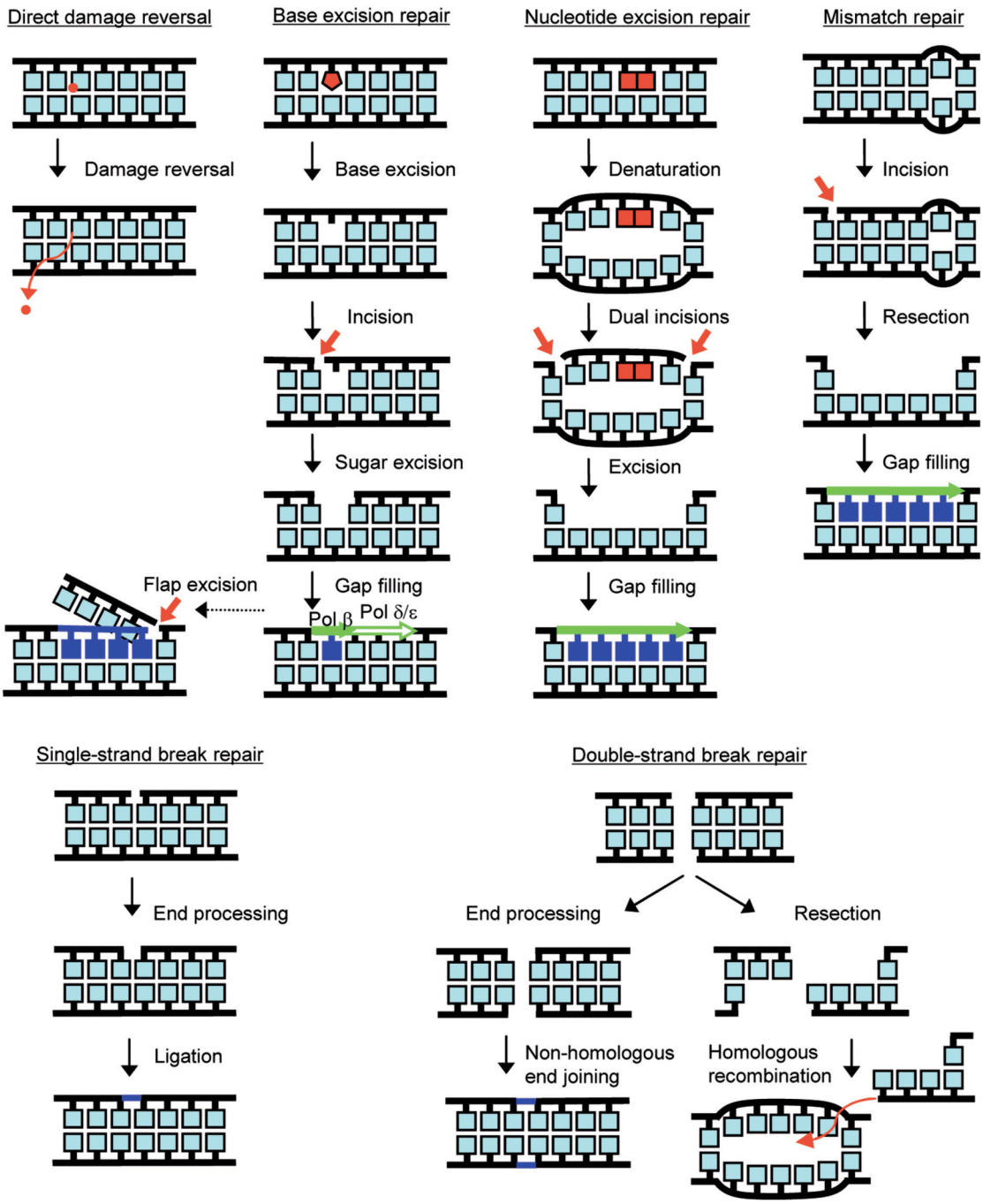
Direct damage reversal
Damage reversal
Base excision repair
Base excision
Incision
Sugar excision
Flap excision
Gap filling
Pol β
Pol δ/ε
Nucleotide excision repair
Denaturation
Dual incisions
Excision
Gap filling
Mismatch repair
Incision
Resection
Gap filling
Single-strand break repair
End processing
Ligation
Double-strand break repair
End processing
Resection
Non-homologous end joining
Homologous recombination

Mismatch Repair

Unlike other DNA repair pathways that recognize aberrant DNA structures, MMR has evolved to correct errors that escape the DNA proofreading capabilities of DNA polymerases during replication. MMR can be broken up into three steps, licensing, or recognition of the mismatch, degradation of the strand with the mismatch, and resynthesis to restore the damaged DNA [147, 148]. Also unique to MMR is strand discrimination, which is vital to restore the genetic information. In prokaryotes this is determined by recognition of a hemimethylated *dam* site located near the mismatch [143, 149]. However, in eukaryotes the strand containing the mismatch is marked with proliferating cell nuclear antigen (PCNA), which activates and orientates the nucleases involved in the degradation of the damaged strand [147, 150]. In addition to repairing a single nucleotide mismatch, MMR also corrects insert and deletion loops and is involved in the metabolism of trinucleotide repeats and antibody maturation [147].

Nucleotide Excision Repair

The NER pathway recognizes bulky, helix-distorting lesions occurring from chemical modification of DNA bases, such as generated from UV, which is not repaired by BER [151]. There are two subpathways of NER, global genome NER (GG-NER), which senses reduced rigidity of DNA from helix distortion, and transcription-coupled NER (TC-NER), which recognizes lesions which block RNA polymerase II during

transcription [152]. Although, GG-NER and TC-NER differ in how they sense DNA damage, they share a common mechanism for the remaining repair steps. During this process, two incisions, one on the 5' side of the lesion by ERCC1-XPF, and one on the 3' side by XPG, release 24-32 nucleotides containing the lesion, which is then filled in by one of three polymerases using the undamaged strand as a template [153-156].

Double-Strand Break Repair

One of the most lethal DNA lesions is the DSB, generated by environmental factors like ionizing radiation and chemical agents, or from replication fork stalling and as intermediates of recombination, of which a single unrepaired DSB is sufficient to cause cell death [157-159]. There are two major pathways devoted to repairing DSB, NHEJ and HR. These two pathways differ, as their names suggest, in whether they use a homologous sequence to repair the break. They also differ in when they are utilized during the cell cycle and the context of the DSB, such as during the collapse of a replication fork, where there is only one end available and thus NHEJ can not be used [157]. NHEJ is active throughout the cell cycle, while HR, since it requires a homologous sequence for repair, is generally restricted to S and G2 phases [99, 160, 161]. Although these two pathways are complementary there is also competition in determining the choice between the two pathways, which mainly resides in DSB recognition and initial end processing.

Non-Homologous End Joining

NHEJ is the dominant DSB repair pathway in higher eukaryotes and essentially rejoins the broken ends. During NHEJ, the DSB is recognized by the Ku70/Ku80 dimer, which binds to each side of the break and recruits DNA-PKcs, forming the DNA-PK holoenzme [92]. If the ends are not compatible, minimal end processing occurs by nucleases and polymerase to either remove or fill-in ssDNA overhangs to form ligatable termini for the DNA ligase IV/XRCC4 and XLF/Cernunnos complex [162-165]. Since NHEJ may result in small insertions or deletions of DNA at the DSB location it has been considered an error-prone repair mechanism. There are also alternative end-joining pathways, microhomology-mediated end-joining (MMEJ) and single-strand annealing (SSA), that rely on terminal microhomologies for the joining reactions, leading to larger deletions, 5-25 basepairs and more than 30 basepairs respectively, opposed to the 1-4 nucleotide deletions and insertions of the classical NHEJ pathway [166, 167]. These alternative end-joining subpathways utilize components of the NHEJ and HR pathways, however because of their propensity to delete genetic information are likely to be highly mutagenic *in vivo* [168].

Homologous Recombination

Unlike NHEJ and alternative end-joining, HR is an error-free pathway for DSB repair, utilizing duplicate DNA as a source of sequence homology. During HR, the DSB

is recognized by the MRN complex, which besides binding and tethering the broken DNA ends, also, through Mre11, processes the ends, possible removing modified ends [169, 170]. The DNA ends are then further processed by 5' to 3' degradation creating 3' ssDNA, which is coated with RPA before being displaced by the recombinase Rad51, which invades a homologous DNA region to use as a template for DNA synthesis [171].

A shared step among the different DSB repair pathways, and a process thought to influence the choice of pathway is DNA end resection. DNA end resection, once started, makes the DNA ends poor substrates for the Ku70/Ku80 dimers, thus directing repair of DSB towards the HR pathway [172-174]. The initiation of DNA end resection is promoted by cyclin-dependent kinases (CDK), thus providing a mechanistic link to cell cycle control of pathway choice [172]. CDK phosphorylation of NBS1 of the MRN complex, and its cofactor C-terminal binding protein interacting protein (CtIP) are important steps in controlling the initiation of DNA end resection [175-177]. CtIP is required for promoting the nuclease activity of MRE11 of the MRN complex to carry out initial limited end resection [178]. Phosphorylation of CtIP by CDKs, besides facilitating its association with NBS1 and CtIP, also facilitate its association with BRCA1 [177, 179, 180]. One way in which BRCA1 promotes DNA end resection is through displacing 53BP1 at DSB ends [181, 182]. 53BP1 promotes NHEJ, particularily during DSB repair of heterochromatic DNA, uncapped telomere rejoining, long range V(D)J recombination and class switch recombination [183]. However, 53BP1 also blocks HR through RIF1 to impair DNA end resection illustrating a competition between 53BP1 promoted NHEJ and BRCA1 promoted HR [184-187]. This is further supported in *Brca1*-deficient mice where

the embryonic lethality, genomic instability, and HR defect is rescued by deletion of 53BP1 [182, 188, 189].

While the MRN/CtIP complex initiates end resection, the nuclease and helicase activity of other proteins are responsible for generating extensive ssDNA. The two activities, helical unwinding and single-strand specific degradation, are a conserved mechanism [174, 190]. The multifunctional enzyme, RecBCD, or the combined activities of the RecQ helicase and the RecJ exonuclease, in *E. coli* performs end resection [174, 191]. In yeast, two similar pathways, perform this function. A RecQ homolog, Sgs1, along with Dna2, a helicase and flap-endonuclease, or the exonuclease Exo1, perform extensive resection [173, 174, 192-194]. In human cells, the RecQ homolog, BLM, has been shown to stimulate end resection *in vivo* and *in vitro* through direct interactions with either the exonuclease EXO1 or endonuclease DNA2 [192, 195-197]. However, unlike yeast where Exo1 can function independently of Sgs1, in human cells, EXO1 is stimulated by BLM by increasing EXO1 affinity for DNA ends [195]. In addition to BLM, humans have four other RecQ homologs, WRN, RECQ4, RECQ1, and RECQ5 [198]. RECQ5 has been shown to be recruited to sites of DSB by MRE11, and WRN has been implicated as an alternative end resection pathway with EXO1, but not DNA2 [195, 197, 199]. Although in Xenopus cell-free extracts, WRN and DNA2 function in end resection [200]. Extensive end resection leaves long stretches of ssDNA, which are coated with RPA. As a result, RPA foci can be used as an indirect measurement of end resection [173].

RPA coated ssDNA serves many roles during DNA repair and signaling besides protecting the unstable ssDNA from further degradation. RPA is a target of phosphorylation by the PIKK family in response to DNA damage, recruits ATR through ATRIP binding to RPA-coated ssDNA, and stimulates DNA2 and EXO1 mediated end resection [93, 195, 201]. Although RPA coated ssDNA is a prerequisite for RAD51 loading, RPA also exerts an inhibitory effect by excluding the loading of the recombinase [202]. Recombination mediators overcome this inhibition by facilitating the loading of RAD51 to form the presynaptic filament. A key mediator is BRCA2, which promotes RAD51 filament assembly onto ssDNA and stabilizes RAD51 nucleoprotein filaments by blocking its ATPase activity, which inactivates and turns over RAD51 [203-205]. BRCA2 also interacts with other proteins to mediate RAD51 loading, specifically partner and localizer of BRCA2 (PALB2) [206]. PALB2 interacts with BRCA1 and BRCA2, thus linking end resection and presynaptic filament formation [207-209]. There are also five paralogues to RAD51 in humans (RAD51B, RAD51C, RAD51D, XRCC2, XRCC3), which are thought to influence the stability and assembly of the RAD51 presynaptic filament [202].

Once formed, the RAD51 coated ssDNA nucleoprotein filament invades and searches for homologous sequence in double-stranded DNA (dsDNA), forming a displaced strand called a D-loop [210]. This process is performed by RAD54, or the paralogue RAD54B, which interacts with RAD51 during homology search, chromatin remodeling, and D-loop formation, and finally displaces RAD51 in a dsDNA and ATPase dependent manner [202]. A factor promoting D-loop formation is RAD51AP1, which

interacts and enhances the recombinase activity of RAD51 [211, 212]. Also, in BRCA2-defective cells, RAD52 interacts with RAD51 and performs a stimulatory role in strand invasion and homologous pairing, in addition to mediating the alternative end-joining pathways SSA [167, 213, 214]. After DNA strand invasion, synthesis is performed by a number of DNA polymerases to restore the nucleotides removed during end resection using the donor strand as a template [210]. Depending on how the newly synthesized DNA is resolved there are three different subpathways of HR. In the classical HR pathway second end capture occurs, where the other end of the break is captured by the displaced template strand during D-loop formation, extended, and the newly synthesized DNA is ligated with the end of the resected strands forming Holliday junction intermediates, which are then resolved to form crossover or non-crossover products [210, 215]. Alternatively, the newly synthesized DNA can be displaced and reannealed in a process called synthesis-dependent strand annealing (SDSA), or after the initial strand invasion the synthesis can continue to the end of the chromosome in a process called break-induced replication (BIR) [174].

Interstrand Crosslink Repair

An especially toxic DNA lesion is an ICL, which covalently links the two DNA strands together, thus preventing cellular processes such as replication and transcription. Although ICLs can form from the by-products of lipid peroxidation, most arise from exposure to environmental mutagens, such as chemotherapeutic drugs [216]. There are

four main classes of ICL-inducing agents (platinum compounds, mitomycin C and furocoumarins, psoralens, and nitrogen mustards), with differences in their cellular uptake, base and sequence specificity, DNA distortion, and other types of DNA lesions they produce, but the mechanism of action of all ICL are generally the same [216-219]. One reason for this is that even though ICLs may represent only a small fraction of total DNA adducts formed, they are thought to be the main cause of toxicity such that cytotoxicity is linked to the number of ICLs formed [217].

Cellular recognition of ICLs occurs during S phase, by replication fork collision, but also during G1 phase, by a block in transcription, and in untranscribed regions of the genome [219]. In general, when an ICL is detected by a block in transcription, or in quiescent DNA, the TC-NER, or GG-NER pathways, respectively, are recruited to remove the lesion [218, 219]. When an ICL is detected during S-phase, a HR component is necessary to repair a DSB generated during the repair process [220-223]. In both cases, because the ICL binds to both strands of the DNA, there is not a copy for retaining genetic information, thus leading to the accumulation of mutations at the site of the ICL [219, 221]. A simplified model of ICL repair includes components of the NER pathway, translesion synthesis (TLS), which is an adduct tolerance pathway, and HR when a homologous template is present (Fig. 1.4). In this model, the NER proteins recognize the ICL and unhook the lesion by performing incisions on either side of the ICL on one of the DNA strands [218, 224]. The now mono-adduct is flipped-out and the resulting gap is filled in by TLS polymerases before the remaining adduct is excised in a NER dependent manner [218, 224]. If repair is in the context of a replication fork, a DSB is formed,

Figure 1.4: Model of interstrand crosslink repair. In G0/G1 phase of the cell cycle, NER proteins make an initial excision of the ICL, and if a futile cycle of ligation and excision does not occur, the flipped out lesion is followed by translesion synthesis and excision of the damaged DNA. During S phase of the cell cycle a replication fork encounters the damaged lesion leading to the collapse of the fork. If the ICL was partially processed this would lead to a one-sided double-strand break. If the ICL is first recognized by a replication fork, HR-mediated replication fork stabilization by components of the Fanconi anaemia pathway, allows coordinated incisions 5' and 3' of the lesion. After unhooking, translesion synthesis past the flipped out lesion occurs, HR is then completed along with removal of the lesion and replication is re-established. If a second replication fork encounters the ICL from the opposite direction, unhooking and translesion synthesis occurs as described for a single replication fork. However, extension of the leading strand of one fork would join with the lagging strand of the other fork, followed by end capture, extension and joining of the other lagging and leading strands. This would generate a double Holliday junction, which would be resolved either by a helicase or structure-specific nucleases. (Figure from [216]).

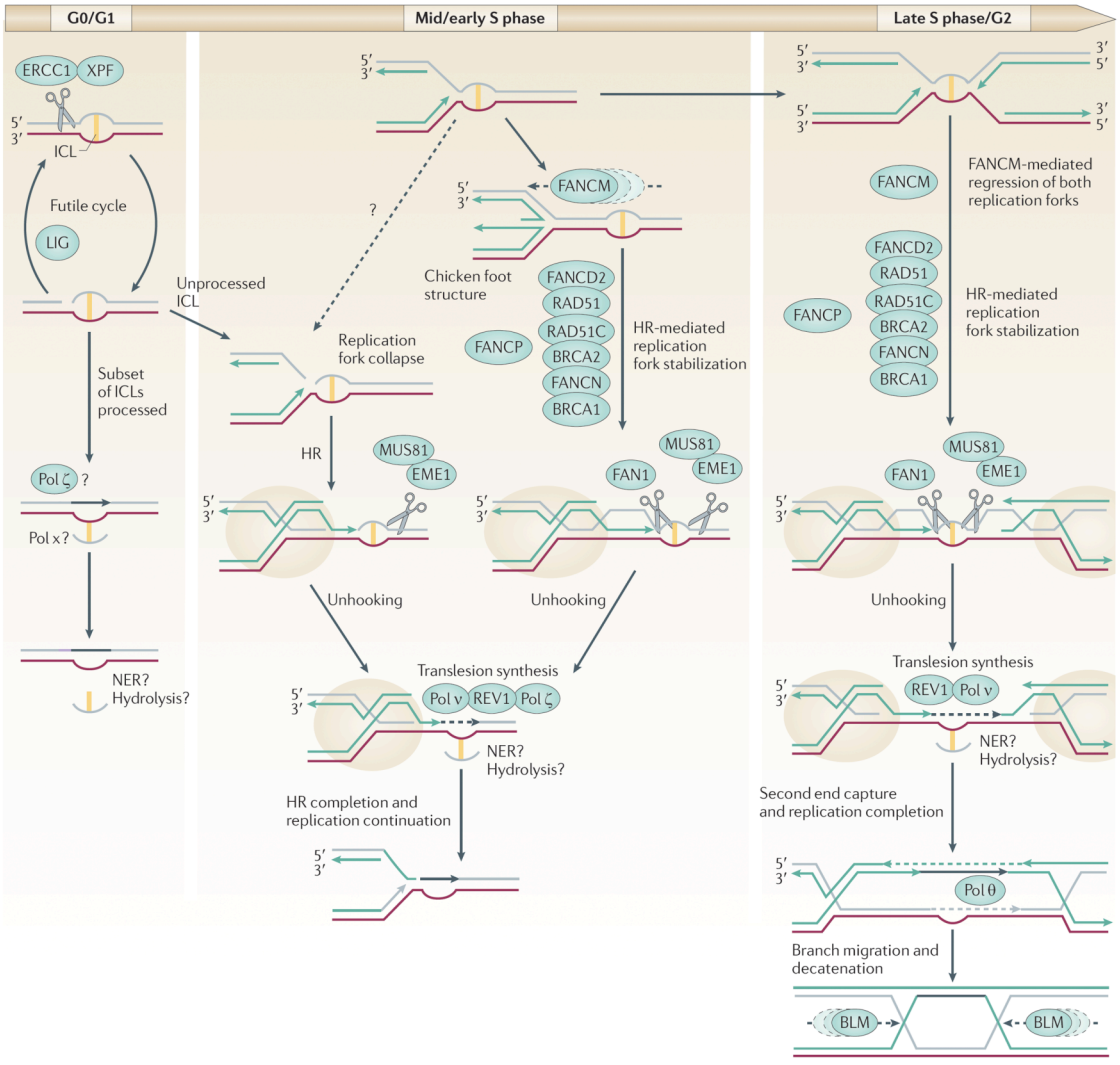
G0/G1
Mid/early S phase
Late S phase/G2
ERCC1
XPF
ICL
Futile cycle
LIG
Subset of ICLs processed
Pol ζ ?
Pol x?
NER? Hydrolysis?
Unprocessed ICL
?
Replication fork collapse
HR
MUS81
EME1
Unhooking
Translesion synthesis
Pol ν
REV1
Pol ζ
NER? Hydrolysis?
HR completion and replication continuation
Chicken foot structure
FANCM
FANCD2
RAD51
RAD51C
BRCA2
FANCN
BRCA1
FANCP
HR-mediated replication fork stabilization
FAN1
FANCM-mediated regression of both replication forks
HR-mediated replication fork stabilization
Second end capture and replication completion
Pol θ
Branch migration and decatenation
BLM

which is repaired through a HR dependent manner [218, 221]. Although this model implies every step leading up to HR is identical, different protein complexes are involved, influenced by the phase of the cell cycle, but also by the chemical nature of the ICL [219].

At the heart of ICL repair encountered during replication is the Fanconi anaemia (FA) pathway. The blocked replication fork is recognized by the FANCM and FAAP24 heterodimer, which is constitutively bound to chromatin through an interaction with the histone-fold-containing proteins MHF1 and MHF2 [225-228]. FANCM then enables access, through branch migration activity, and recruits the core FA complex [229-231]. The core FA complex, consists of seven additional FA proteins FANCA, FANCB, FANCC, FANCE, FANCF, FANCG, and FANCL, in addition to FANCM, as well as two additional FA accessory proteins, FAAP100 and FAAP20, in addition to FAAP24 [216, 218, 224, 232, 233]. The activity of the core complex is the monoubiquitination of two additional FA proteins, FANCI and FANCD2, leading to their retention on chromatin [234, 235]. The ubiquitin ligase activity of the complex is through the E3 ligase FANCL, with UBE2T functioning as the E2 ligase [236-238]. Loss of any component of the core complex leads to failure of ubiquitination, even in the case of FANCM or FAAP24 depletion, when the rest of the core complex forms, suggesting monoubiquitination of FANCI and FANCD2 may only occur on chromatin [230, 239, 240].

Downstream of FANCI and FANCD2 monoubiquitination is the coordination of multiple nuclease, polymerases, and helicases to remove the ICL and restore DNA integrity. A key scaffold, and cofactor is FANCP, also known as SLX4, that functions

with the structure-specific nucleases XPF-ERCC1, MUS81-EME1, and SLX1, which are endonucleases with a preference for 3'-flap structures involved in unhooking the lesion and other downstream events such as HR [241-247]. Two proteins specifically interacting with the ubiquitinated forms of FANCD2 and FANC1 are the nuclease, FAN1, and the TLS polymerase, POLN [248-252]. While the exact function of these proteins is not clear, the requirement of multiple nucleases and polymerases are necessary for resolution of the ICL. Another recently identified exonuclease, SNM1A, works in concert with XPF-ERCC1 after the initial incision during unhooking to remove ssDNA past the lesion, thus creating a potential substrate for TLS polymerases [253]. In addition to the recruitment of POLN, several other TLS polymerases have also been implicated in ICL repair [216, 218].

Following unhooking of the lesion and TLS, a DSB must form for HR to occur. There are multiple models of how this process might occur. The main difference between these models is whether one fork encounters the ICL or if two forks converge on the lesion. If one fork encounters the ICL, this can lead to a collapsed fork if the unhooking occurs before the fork encounters the lesion, or a stalled fork if, as described above, the FA core complex recognizes the lesion and stabilizes the fork [216]. The one-sided DSB undergoes end resection, strand invasion, and following extension the replication fork would be regenerated [221]. There is also evidence that certain HR proteins, specifically RAD51C, also known as FANCO, which has a more specific role in one-sided opposed to two-sided DSBs [254, 255]. If two forks converge on the ICL, which might occur in late S phase, then second end capture and synthesis would lead to the formation of

Holliday junctions [216]. The resolution of these structures is dependent on BLM, through an interaction with the FA core complex [256, 257]. However, in the absence of BLM, other nucleases resolve Holiday junctions, such as MUS81-EME1, SLX1-SLX4, and the resolvase GEN1 [257]. Although the mechanistic details of HR during ICL is still poorly understood, there appears to be unique features compared to HR occurring during repair of DSB formed from other sources. For example, RAD51 appears to be recruited to ICL stalled forks prior to DSB formation, which inhibits the MRN complex most likely to prevent extensive end resection and to promote strand invasion as soon as possible [223, 258]. Also, the MCM8 and MCM9 helicase appears to be necessary for HR in the context of ICLs, performing a function in the recruitment of RAD51 [259-261].

DNA Damage Response and Human Disease

While most of our knowledge of the DDR has come from studies in yeast, the study of human genetic diseases has led to not only an understanding of the underlying cause of the disease, but also a greater understanding of DNA damage signaling and repair. The disorders range from neurodegenerative and neuromuscular diseases, to immune deficiencies, stem cell dysfunction, and in many cases predisposition to cancer [262, 263]. In many cases a single mutated gene causes the disease, while others result from more global defects in the DDR, such as DNA repeat instability and increased ROS [262].

The accumulation of DNA lesions through an impairment of the DDR and defective DNA repair results in many types of human diseases. The accumulation of lesions, possible through increased ROS, in neurons is associated with many neurodegenerative disorders, such as Alzheimer's, Parkinson's, and Huntington's [264, 265]. Similarly, the accumulation of DNA repeats, typically a trinucleotide motif is involved in many diseases, such as myotonic dystrophy and Fragile X syndrome [262, 266]. While increased ROS may have a role in these processes, this also suggests BER and SSB repair might be involved, and as shown to be the case for diseases such as spinocerebellar ataxia with axonal neuropathy (SCAN1) and ataxia with oculomotor apraxia 1 (AOA1) [262, 263].

There are many human disorders resulting from defective DNA damage signaling resulting from mutations in key molecules. An example of this is ataxia telangiectasia (AT), which is caused by a mutation in ATM, as the name indicates [267]. AT is an autosomal recessive neurological disorder with cerebellar degeneration, predisposition to cancer, radiation sensitivity, and immunodeficiency [262, 263, 267]. Similarly, defects in ATR, or ATRIP, cause Seckel syndrome, also an autosomal recessive disease, characterized by microcephaly, growth retardation and developmental delays [268]. As mentioned above, the MRN complex is involved in detecting DSBs and defects in these proteins give rise to AT-like disorder, Nijmegen breakage syndrome (NBS), and NBS-like syndrome, caused by mutations in the *MRE11*, *NBS1*, and *RAD50* genes, respectively [263]. While these disorders are characterized by many symptoms in addition to cancer predisposition, many DDR components, when mutated, are characterized by early onset

to many tumors. These include p53 and Chk2, which are mutated in Li-Fraumeni syndrome, BRCA1 and BRCA2, which give rise to familial breast cancer went mutated, and Chk2, ATM, the MRN complex, PALB2, and other genes, which when mutated give rise to non-familial breast cancer [262, 263]. In addition, Lynch syndrome is caused by defects in the MMR pathway, which leads to microsatellite instability and predisposes individuals to colon, gastric and endometrial carcinomas [269].

Defects in DNA repair pathways also lead to human diseases. As already mentioned, defects in MMR, BER, SSB repair and DSB, specifically HR, through other repair proteins, such as BRCA1, lead to human disease. This is also true for the other repair pathways. Defects in NHEJ, such as hypomorphic mutations in DNA ligase IV, cause LIG4 syndrome [270]. Mutations in the NER pathway lead to Xeroderma pigmentosum (XP), Cockayne syndrome (CS), and tricothiodystrophy (TTD), all characterized by hypersensitivity to UV light [271]. XP was the first human disorder characterized by a defect in DNA repair [272]. There are seven complementation groups plus one variant form, which have lead to the identification of the appropriately named proteins XPA to XPG and XPV, also known as DNA Pol η [273]. Similarly, many of the proteins involved in ICL repair have been named after the complementation groups within the disease FA. FA is a rare recessive chromosomal instability disorder characterized by bone-marrow failure, congenital abnormalities, infertility and increased susceptibility to haematological and solid tumors [216, 224, 274]. There are 14 complementation groups involving 15 genes identified to date, although there are still some patients who have not had a mutated gene identified [224]. As mentioned above,

ICL repair utilizes proteins from other repair pathways, and thus defects in ICL repair not only lead to FA, but other diseases such as XP, karyomegalic interstitial nephritis (KIN), which has been linked to mutations in FAN1, and Blooms's syndrome, which results from a mutation in BLM [91, 275]. Knowledge gained from studying this non-exhaustive list of human diseases caused by defects in the DDR leads to an increase in the basic understanding of how these conditions occur, the pathways involved, and eventually a better understanding and treatment of these and other human diseases.

Research Objectives

The functions of mammalian septins are still being defined and recent advances point to their role in multiple biological processes. One such function that septins have been implicated in, but not well defined, is the DDR. It is surprising that septins, a cytoskeletal element, might play a role in this nuclear event, but not entirely unexpected considering recent proteomic screens have suggested septins, as well as other proteins involved in various cellular processes, could be involved in the DDR. These screens, among other advances, highlight how complex the DDR is. Understanding how these seemingly different cellular pathways intersect and coordinate is important to fully elucidating this response mechanism, as well as potentially shed light on various diseases and treatment options.

The objectives of this research were to expound upon the previous data of mammalian septins in the DDR and to explore the possibility of other factors involved in

this connection. Previous data in the lab demonstrated an involvement of septins in the DDR, through the adaptor proteins NCK and SOCS7, but the function of this pathway was not clearly defined. As such, the first objective of this research was to further explore the role of the septin associated adaptor proteins, NCK and SOCS7, in the DDR. This work led to a role of the adaptor protein NCK in UV-induced p53 phosphorylation and apoptosis. The other goal of this research was to explore the possibility that other septin associated proteins might be involved in the cellular response to DNA damage. This objective led to the discovery of a novel septin associated nuclease and the implication of septins in a DNA repair process. These discoveries have further defined and revealed novel pathways connecting septins to the DDR, the identification and characterization of a new nuclease involved in ICL repair, and demonstrating the importance of interconnectivity and coordination of various proteins and pathways during this cellular response to DNA damage.

Chapter 2: Depletion of the Adaptor Protein NCK Increases UV-Induced p53 Phosphorylation and Promotes Apoptosis

Errington TM, Macara IG

PloS ONE. 2013 Sep 23;8(9):e76204.

doi: 10.1371/journal.pone.0076204

Abstract

The cellular response to DNA damage requires the coordination of many proteins involved in diverse molecular processes. Discrete molecular pathways are becoming increasingly well understood, but the interconnectivity and coordination of multiple pathways remains less clear. We now show that NCK, an adapter protein involved in cytoskeletal responses to tyrosine kinase receptor signaling, accumulates in the nucleus in response to DNA damage and this translocation can be blocked by specific inhibition of the ATR protein kinase. Strikingly, HeLa cells depleted of NCK undergo apoptosis shortly after UV irradiation, as monitored by caspase-3 cleavage and PARP cleavage. This rapid, hyperactive apoptosis in NCK depleted cells might be p53 dependent, because loss of NCK also increased UV-induced p53 phosphorylation. Importantly, depletion of SOCS7, which is necessary for NCK nuclear translocation, phenocopies NCK depletion, indicating the nuclear accumulation of NCK is responsible for these molecular events. There are two NCK isoforms that have mostly redundant functions, and although NCK2 appears to have a greater contribution, depletion of NCK1 or NCK2, led to increased p53 phosphorylation and early apoptosis after UV exposure. These data reveal a novel function for NCK in regulating p53 phosphorylation and apoptosis, and provide evidence for interconnectedness of growth factor signaling proteins and the DNA damage response.

Introduction

Damage to DNA can occur from endogenous sources, such as reactive oxygen species and short telomeres, or exogenous sources, such as ultraviolet light (UV) and ionizing radiation (IR) [79]. The cellular response to DNA damage involves the recognition of damage, resulting in the initiation of a signal that is transmitted to mediator and signaling kinases, which then act upon different target proteins to mount an appropriate response, such as cell cycle arrest and DNA repair, or apoptosis [82]. Failure to mount an effective DNA damage response (DDR) leads to genetic instability, with impacts on aging, development, and cancer [262]. Three key protein kinases in the DDR pathway are ATM, ATR, and DNAPK, members of the phosphoinositide-3-kinases related kinase (PIKK) family, which phosphorylate multiple proteins, including the histone variant H2AX, the checkpoint protein CHK2, and the tumor suppressor p53, to initiate a signaling cascade [98, 99, 118, 128, 276]. A proteomic screen for substrates of ATM and ATR revealed over 700 proteins phosphorylated in response to IR or UV, a surprising number of which are associated with signaling pathways quite distinct from the DDR, illustrating the broad potential for intersection of multiple cellular processes [277].

NCK (non-catalytic (region of) tyrosine kinase adaptor protein) is part of a family of Src homology domain containing adaptor proteins, which are composed almost entirely of protein-protein interaction domains with no known catalytic activity [278]. Similar to other members of this family, NCK has been shown to couple signals from activated receptor tyrosine kinases to downstream effectors through its various SH

domains [279]. In mammals there are two isoforms of NCK, NCK1 and NCK2, which share 68% amino acid identity and have been considered functionally redundant [280-282]. NCK is predominantly cytoplasmic but, unexpectedly, continually shuttles in and out of the nucleus, as determined by the nuclear accumulation of NCK in cells treated with leptomycin B [76]. A binding partner of NCK, SOCS7 (suppressor of cytokine signaling 7) has been identified as the carrier protein that mediates the nucleo-cytoplasmic translocation of NCK [76, 283]. An earlier study from our group identified an unexpected link between NCK, SOCS7, and the DDR, through the nuclear accumulation of NCK following UV damage [76].

In this study we address the functional significance of UV-induced nuclear accumulation of NCK. We discovered that depletion of NCK in HeLa cells leads to apoptosis shortly after UV damage, possibly by increased phosphorylation of p53.

Materials and Methods

Cell Culture, Constructs, and Transfections

HeLa, MCF7 and 293T cells were purchased from ATCC and grown in DMEM supplemented with 10% fetal calf serum. pK-GFP-NCK1, pK-GFP-NCK2, pK-myc-NCK1, and pK-myc-NCK2 constructs were generated by cloning NCK1 and NCK2 into BamHI/EcoI sites of pKGFP or pKmyc vectors. siRNAs were purchased from Thermo scientific: siControl (custom, described previously [38], siNCK1 (M-006354-01), siNCK2 (M-0197547-01), siCHK2 (M-003256-06), siSOCS7 (M-027197-00), siNCK2#2 (GGAAGUGGCGCUCGUGCAU). Knockdown transfections with siRNA were performed with Lipofectamine RNAiMAX (Invitrogen) and transfected 16 hr after plating then transfected a second time 48 hr after the first transfection following the manufacturer suggested amount of reagent, siRNA and media. Overexpression transfections were performed with Lipofectamine 2000 (Invitrogen) as described previously [284]. Cells were treated, as indicated, 24 hr after transfections. Unless indicated otherwise, siNCK indicates equal amounts of siNCK1 and siNCK2 siRNA were transfected and GFP-NCK indicates equal amounts of GFP-NCK1 and GFP-NCK2 were transfected.

Immunofluorescence

Cells were grown on Lab-Tek II chambers (Nunc) and, when indicated, treated with 50 J/m^2 UV, 10 μM etoposide (Sigma) or 10 Gy IR and allowed to recover for 2 hr or 1 hr

before being fixed in 3.7% paraformaldehyde in PBS. Cells were permeabilized and blocked in 0.3% saponin with 0.5% BSA in PBS for 1 hr before incubation with antibodies. Antibody incubations and washes were carried out in 0.3% saponin with 0.5% BSA in PBS. Where indicated cells were pretreated with 50 μM wortmannin (Sigma), 5 μM ATR inhibitor, VE-821 (3-amino-6-(4methylsulfonyl_phenyl-N-phenylpyrazine-2-carboxamide), (described previously [285]), (a gift from David Cortez (Vanderbilt Univ.)), or vehicle (DMSO) for 30 min prior to UV treatment and then allowed to recover 2 hr in the presence of wortmannin, ATR inhibitor, or vehicle. Primary antibodies used were: mouse anti-NCK (1:250) (BD Biosciences), rabbit anti-CHK2-pT68 (1:100) (Cell Signaling), rabbit anti-γH2AX (pS139) (1:750) (Novus Biologicals), rabbit anti-cleaved CASP3 (1:100) (Cell Signaling), mouse-anti-γH2AX (pS139) (1:250) (Millipore). Alexa Fluor-conjugated secondary antibodies (Invitrogen) were used at a dilution of 1:1,000. Nuclei were counterstained with DRAQ5 (1:500) (Cell Signaling) and mounted in Fluormount-G (Southern Biotech). Images were captured using a LSM510 Meta confocal microscope (Carl Zeiss, Thornwood, NY) using a 100x oil immersion lens (NA 1.3). Images were converted to TIFF format using ImageJ and processed using Adobe Photoshop CS4 Levels tool (Adobe Systems, Mountain View, CA) to enhance contrast. Nuclear and cytoplasmic flurorescence signal was quantified using ImageJ.

Immunoblotting

Immunoblotting was performed as described previously [286]. When indicated cells were treated with 50 J/m^2 UV and allowed to recover for 2 hr before being harvested. Primary

antibodies used were: rabbit anti-NCK (a gift from Tony Pawson (Univ. of Toronto, Canada)), rabbit anti-cleaved CASP3 (Cell Signaling), rabbit anti-CASP3 (Cell Signaling), rabbit anti-PARP (detects total and cleaved forms) (Cell Signaling), rabbit anti-RAN (described previously [287]), rabbit anti-p53-pS15 (Cell Signaling), rabbit anti-CHK2-pT68 (Cell Signaling), sheep anti-p53 (Millipore), rabbit anti-NCK2 (a gift from Louise Larose (McGill Univ., Canada)), rabbit anti-CHK2 (Santa Cruz), rabbit anti-γH2AX (pS139) (Novus Biologicals). HRP-conjugated secondary antibodies (IgG, Jackson ImmunoResearch Laboratories; Protein-A, Millipore) were used at a dilution of 1:5,000. Band intensities were quantified using ImageJ.

Cell Survival Assay

HeLa cells were plated and then transfected in a 96 well plate. Cells were treated with UV at 50 J/m^2 and allowed to recover for the indicated time. Wells were assayed with CellTiter 96 AQ_{ueous} One Solution (Promega) following the manufacturer protocol.

Reverse-Transcription (RT)-PCR

RNA was harvested with TRIzol Reagent (Invitrogen) and then treated with RQ1 RNase-free DNase (Promega) supplemented with RNasin (Promega) before a reverse transcription reaction was performed with random hexamers (Invitrogen) and SuperScript II Reverse Transcriptase (Invitrogen) supplemented with RNasin. PCR of the reverse transcribed cDNA was performed with p53, GAPDH, NCK1, NCK2, and SOCS7 primers as described previously [288] [289] [290].

Immunoprecipitation

HeLa cells were lysed and clarified as described previously [286]. Lysates were incubated with rabbit anti-NCK or rabbit IgG antibodies overnight, rocking, at 4°C before incubation with GammaBind plus sepharose (GE Healthcare) for 4 hr. Beads were washed 3X with lysis buffer before 2X sample buffer was added and samples heated at 95°C for 5 min. All subsequent immunoblots were performed with Protein A-conjugated HRP secondary antibody to prevent detection of denatured antibody chains as described previously [291].

Statistical analysis

Two-tailed Student's *t*-tests were used in the statistical analysis. All graphs and statistical analysis were performed with GraphPad Prism, Version 4.0a (GraphPad Software, Inc.).

Results

NCK Accumulates in the Nucleus Following DNA Damage

Previously, we had discovered that NCK, which constitutively shuttles between the cytoplasm and nucleus and is primarily cytoplasmic in undamaged cells, accumulates in the nucleus in response to UV irradiation [76]. We sought to confirm this observation and expand it to other types of DNA damage. HeLa cells were irradiated with UV or IR, or treated with the topoisomerase inhibitor etoposide, and then stained to determine NCK localization with a specific NCK antibody (Fig. 2.2A). Phosphorylated CHK2 (pT68) was used to monitor whether the treatments had triggered an appropriate DDR [113]. In all cases, NCK accumulated in the nuclei of damaged cells, versus a primarily cytoplasmic staining in untreated, or vehicle-treated, cells (Fig. 2.1A). This result is further supported by a similar relocalization of ectopically expressed GFP-NCK after UV treatment (Fig. 2.1B). Moreover, similar results were obtained using MCF7 cells, with NCK accumulating in the nucleus following UV treatment (Fig. 2.2B). These data show that nuclear relocalization of NCK occurs in response to multiple types of DNA damage, occurs in different cell types, and correlates with CHK2 phosphorylation. Therefore, we focused on HeLa cells and UV irradiation to further study the significance of nuclear accumulation of NCK in response to DNA damage.

Figure 2.1: DNA damage induces the nuclear accumulation of NCK. (A) HeLa cells were treated with 50 J/m^2 UV, 10 μM Etoposide, or 10 Gy IR and allowed to recover for 2 hr, 1 hr, and 1 hr, respectively, before being fixed and stained with the indicated antibodies and DRAQ5 to visualize nuclei. Scale bars are 20 μm. All images are confocal sections. (B) HeLa cells transfected with GFP-NCK1 and GFP-NCK2 were treated with 50 J/m^2 UV and allowed to recover for 2 hr before being fixed and stained with indicated antibodies and DRAQ5. Bar graphs below each panel are ratio of nuclear to cytoplasmic fluorescence of endogenous NCK, A, or GFP-NCK, B, with no treat, or vehicle, defined as 1. n = 19-82; error bars represent SE; (*) $P < 0.0001$.

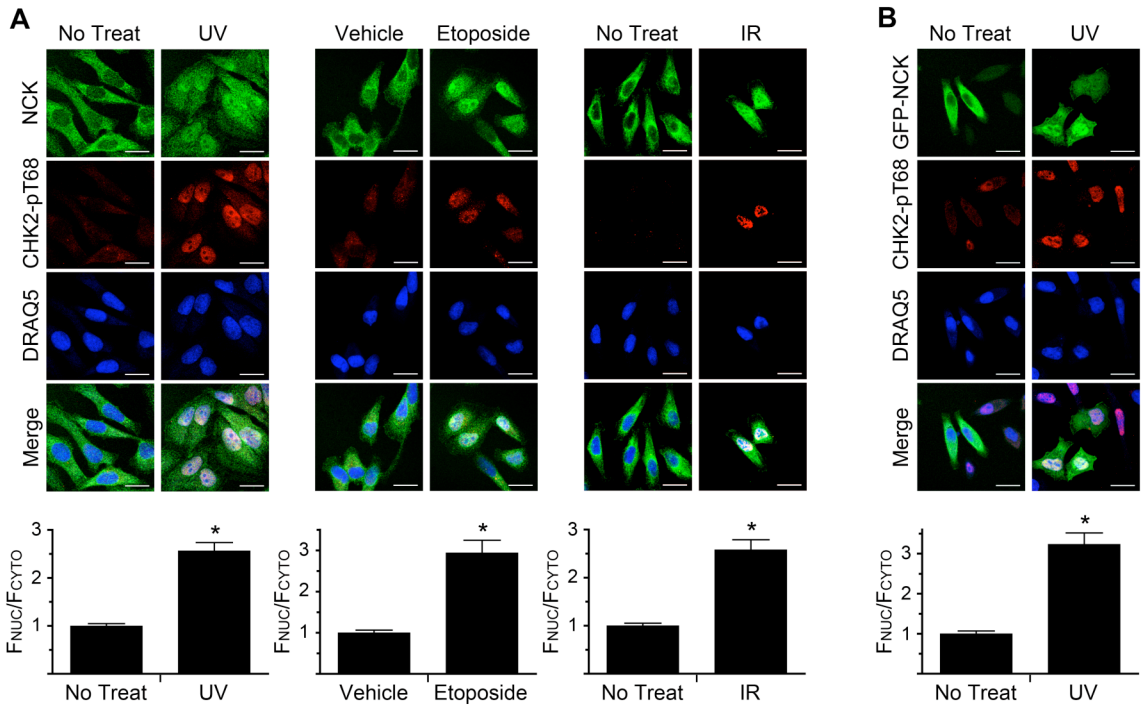
A
No Treat
UV
Vehicle
Etoposide
No Treat
IR
NCK
CHK2-pT68
DRAQ5
Merge
FNUC/FCYTO
3
2
1
*
No Treat
UV
Vehicle
Etoposide
No Treat
IR
B
No Treat
UV
GFP-NCK
CHK2-pT68
DRAQ5
Merge
FNUC/FCYTO
3
2
1
*
No Treat
UV

Figure 2.2: NCK antibody is specific and UV-induced nuclear accumulation of NCK occurs in other cell lines. (A) HeLa cells transfected with control or NCK1 and NCK2 siRNA were fixed and stained with the indicated antibody and DRAQ5. Scale bars are 20 μm. All images are confocal sections. n = 4. (B) MCF7 cells were treated with 50 J/m^2 UV and allowed to recover for 2 hr before being fixed and stained with indicated antibodies and DRAQ5. Scale bars are 20 μm. All images are confocal sections. Bar graph below is ratio of nuclear to cytoplasmic fluorescence of NCK with no treat defined as 1. n = 20-27; error bars represent SE; (*) $P < 0.0001$.

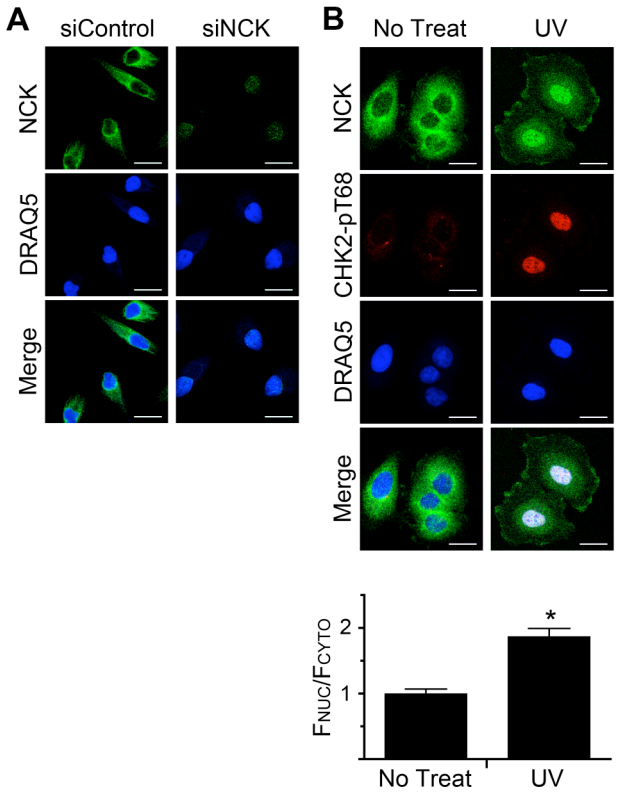
A
siControl
siNCK
NCK
DRAQ5
Merge
B
No Treat
UV
NCK
CHK2-pT68
DRAQ5
Merge
FNUC/FCYTO
2
1
*
No Treat
UV

NCK Nuclear Accumulation Requires the Activity of the PIKK Family Member ATR

We next sought to determine the upstream signaling requirements for NCK nuclear accumulation. An early event in response to DNA damage is the activation of the PIKK family of protein kinases, which phosphorylate multiple downstream targets including histone H2AX, p53, and the checkpoint kinase, CHK2 [99]. Because CHK2 phosphorylation correlates with NCK nuclear accumulation after UV irradiation, we first tested the requirement for CHK2 in this process by RNAi. However, despite efficient knockdown of the kinase, NCK still accumulated in the nucleus following UV irradiation, indicating that CHK2 is not required for NCK relocalization and that NCK acts upstream, or parallel, to the checkpoint kinase (Fig. 2.3A,B). Phosphorylation of the histone variant H2AX on serine 139 (γH2AX) was, as expected, also unaffected by depletion of CHK2 (Fig. 2.3B,C).

We next asked if NCK nuclear accumulation is dependent on PIKK kinase activity. To first test the general requirement for these kinases in UV-induced NCK nuclear accumulation we used the PIKK inhibitor wortmannin [292]. Treatment of cells with wortmannin did not affect the untreated cytoplasmic localization of NCK, but did prevent the UV-induced nuclear accumulation of NCK, compared to vehicle treatment (Fig. 2.4A). This result indicates that NCK nuclear accumulation is likely dependent on the activity of the PIKK family. To further elucidate which PIKK family member was responsible for UV-induced NCK nuclear translocation, specific inhibitors were tested. Treatment of cells with a potent and specific ATR kinase inhibitor, VE-821 [285],

Figure 2.3: Loss of CHK2 does not alter nuclear accumulation of NCK. (A) HeLa cells transfected with control or CHK2 siRNA were treated with 50 J/m^2 UV and allowed to recover for 2 hr before being fixed and stained with the indicated antibodies and DRAQ5. Scale bars are 20 μm. All images are confocal sections. Bar graph below is ratio of nuclear to cytoplasmic fluorescence of NCK with siControl, no treat, defined as 1. n = 8-73; error bars represent SE. (B) Cells were treated as in A, and equal amounts of lysates were immunoblotted for CHK2 and γH2AX. RAN was used as a loading control. * indicates non-specific band. n =3 (C) HeLa cells transfected with control or CHK2 siRNA were treated with 50 J/m^2 UV and allowed to recover for 2 hr before being fixed and stained with the indicated antibodies. Scale bars are 20 μm. All images are confocal sections. n = 3.

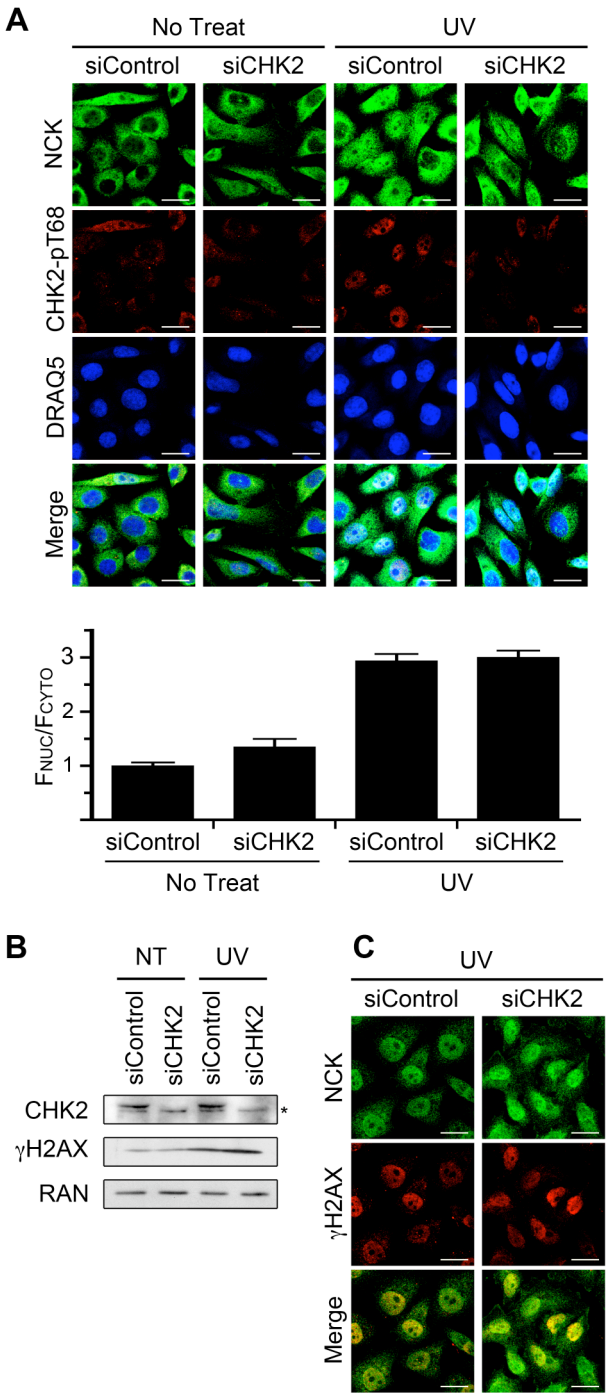
A
No Treat
UV
siControl
siCHK2
siControl
siCHK2
NCK
CHK2-pT68
DRAQ5
Merge
FNUC/FCYTO
3
2
1
siControl
siCHK2
siControl
siCHK2
No Treat
UV
B
NT
UV
siControl
siCHK2
siControl
siCHK2
CHK2
γH2AX
RAN
*
C
UV
siControl
siCHK2
NCK
γH2AX
Merge

Figure 2.4: ATR activity is necessary for nuclear accumulation of NCK. (A) HeLa cells were pretreated for 30 min with 50 μM wortmannin and then treated with 50 J/m^2 UV and allowed to recover for 2 hr in the presence of wortmannin before being fixed and stained with the indicated antibodies and DRAQ5. Scale bars are 20 μm. All images are confocal sections. Bar graph below is ratio of nuclear to cytoplasmic fluorescence of NCK with vehicle pretreated, no treat, defined as 1. n = 125-174; error bars represent SE; (*) $P < 0.0001$. (B) Same as in A, except 5 μM ATR inhibitor (VE-821) was used, and n = 79-117.

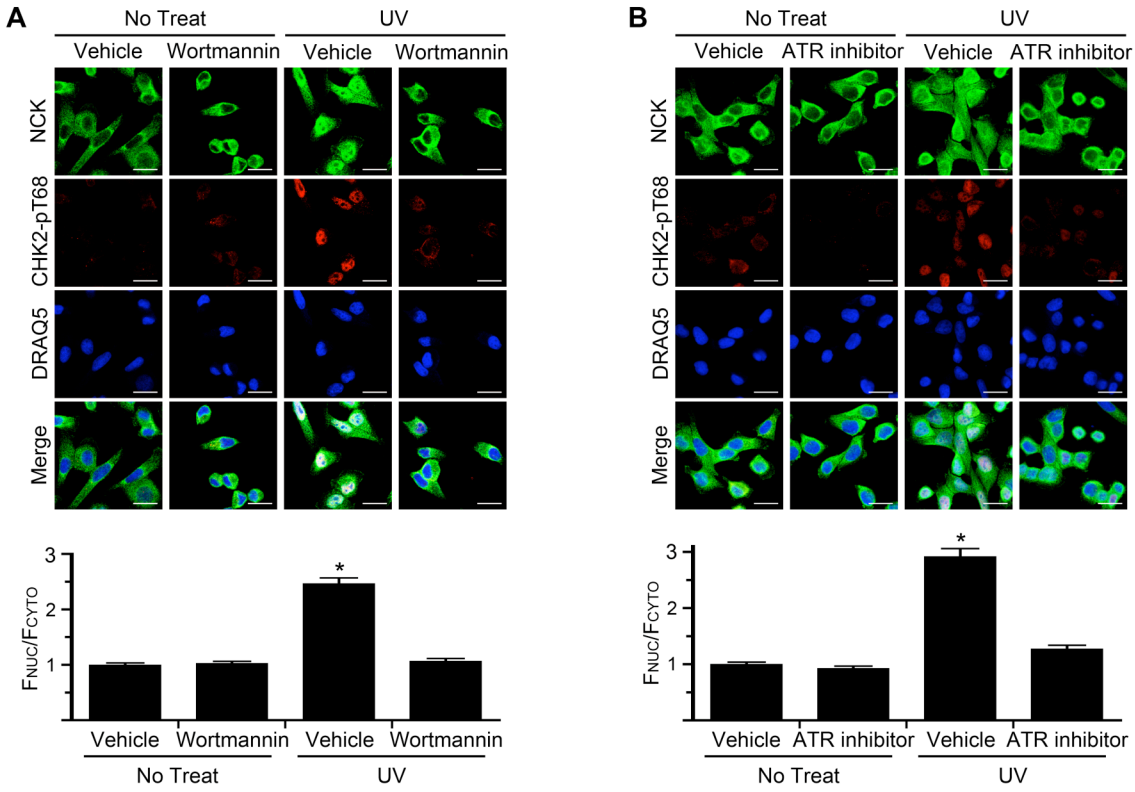
A
No Treat
UV
Vehicle
Wortmannin
Vehicle
Wortmannin
NCK
CHK2-pT68
DRAQ5
Merge
FNUC/FCYTO
3
2
1
*
Vehicle
Wortmannin
Vehicle
Wortmannin
No Treat
UV
B
No Treat
UV
Vehicle
ATR inhibitor
Vehicle
ATR inhibitor
NCK
CHK2-pT68
DRAQ5
Merge
FNUC/FCYTO
3
2
1
*
Vehicle
ATR inhibitor
Vehicle
ATR inhibitor
No Treat
UV

prevented the nuclear accumulation of NCK compared to vehicle treatment (Fig. 2.4B). This result indicates that NCK nuclear accumulation in response to UV damage is dependent on ATR activity.

Depletion of NCK Results in the Hyper-activation of DNA Damage-induced Apoptosis

We next examined if NCK is required for the cellular response to DNA damage. Remarkably, when HeLa cells were depleted of NCK (both isoforms) and irradiated with UV, cell death appeared to occur within 2 hrs after treatment, as opposed to UV-irradiated control cells, all of which showed no change in morphology over this period (Fig. 2.5). There are various forms of cell death, but a hallmark of cells undergoing apoptosis is the induction of the caspase cascade, leading to cleavage, and thus activation of downstream caspases, specifically caspase-3 (cleaved CASP3) [136]. Strikingly, cells depleted of NCK were positive for cleaved caspase-3 staining within 2 hr after UV treatment (Fig. 2.6A). As determined by immunoblotting, both cleaved CASP-3 and cleaved PARP, a downstream target of the caspases, were increased in UV-irradiated NCK-depleted cells compared to control (Fig. 2.6B). To further examine the effects of NCK-depletion on apoptosis, cell viability was monitored following UV irradiation. While control cells showed a modest decrease in cell viability 12 hr after UV irradiation, depletion of NCK resulted in a significant decrease in cell viability as early as 2 hr after UV treatment that further decreased to less than 50% after 12 hr (Fig. 2.6C). These data show that loss of NCK results in unusually rapid UV-induced apoptosis.

Figure 2.5: Loss of NCK causes early UV-induced cell death in HeLa cells. HeLa cells transfected with control or NCK1 and NCK2 siRNA were treated with 50 J/m^2 UV and allowed to recover for 2 hr before being fixed and stained with the indicated antibodies and DRAQ5. Scale bars are 20 μm. All images are confocal sections. n = 3.

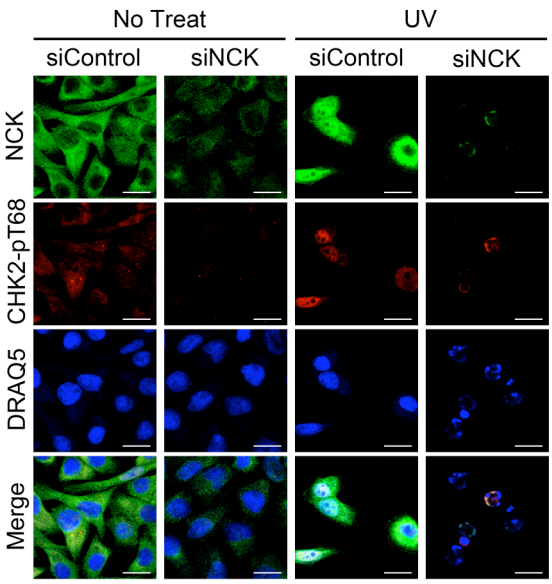
No Treat
UV
siControl
siNCK
siControl
siNCK
NCK
CHK2-pT68
DRAQ5
Merge

Figure 2.6: Loss of NCK causes early UV-induced apoptosis in HeLa cells. (A) HeLa cells transfected with control or NCK1 and NCK2 siRNA were treated with 50 J/m^2 UV and allowed to recover for 2 hr before being fixed and stained with the indicated antibody and DRAQ5. Scale bars are 20 μm. All images are confocal sections. n = 3. (B) Cells were treated as in A, and equal amounts of lysates were immunoblotted for cleaved CASP3, total CASP3, cleaved PARP, total PARP, and NCK. RAN was used as a loading control. n = 4. (C) HeLa cells transfected with control or NCK1 and NCK2 siRNA were treated with 50 J/m^2 UV and allowed to recover for the indicated amount of time before cell viability was assayed. Percent cell viability for each siRNA at time 0 hr (no treat), is defined as 100%. n = 8; error bars represent SE; (*) $P < 0.05$, (**) $P < 0.01$, (#) $P < 0.001$, (##) $P < 0.0001$.

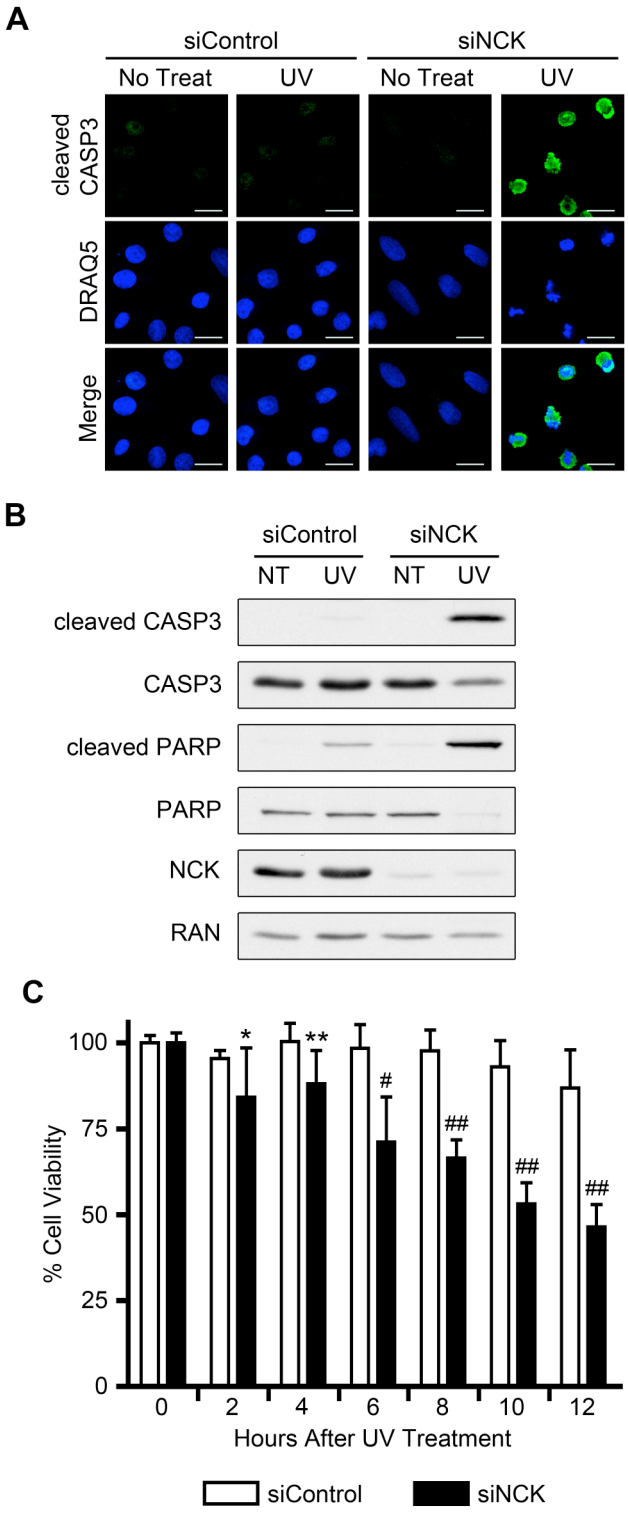
A
siControl
siNCK
No Treat
UV
No Treat
UV
cleaved CASP3
DRAQ5
Merge
B
siControl
siNCK
NT
UV
NT
UV
cleaved CASP3
CASP3
cleaved PARP
PARP
NCK
RAN
C
% Cell Viability
100
75
50
25
0
*
**
#
##
##
##
0
2
4
6
8
10
12
Hours After UV Treatment
siControl
siNCK

Depletion of SOCS7 Blocks UV-Induced Nuclear Accumulation of NCK, and Hyper-Activates DNA Damage-Induced Apoptosis

Previously, we had discovered that SOCS7 is necessary for the nuclear translocation of NCK [76]. Thus, through depletion of SOCS7, we could test specifically the requirement for nuclear accumulation of NCK during DNA damage. We first sought to confirm that SOCS7 is necessary for NCK translocation in response to UV irradiation. Depletion of SOCS7 from HeLa cells did not affect the untreated cytoplasmic localization of NCK, but did prevent the nuclear accumulation of NCK, compared to control, following UV (Fig. 2.7A). This result confirms our previous data that NCK nuclear accumulation is dependent on SOCS7. Importantly, however, loss of SOCS7 also resulted in early UV-induced apoptosis as assessed by immunoblots of lysates from SOCS7 depleted cells, which showed increased cleaved CASP3 and cleaved PARP compared to control cells (Fig. 2.7B). Because of the low expression of SOCS7 at the protein level and the lack of a suitable antibody, we were unable to detect SOCS7 by immunoblot, but confirmed silencing at the mRNA level (Fig. 2.7C). These data show that blocking NCK nuclear accumulation, through the knockdown of SOCS7, phenocopies NCK depletion, causing rapid UV-induced apoptosis.

UV-induced p53 Phosphorylation is Elevated in NCK, or SOCS7, Depleted Cells

In our previous study, mouse embryonic fibroblasts cell lines null for NCK1 and NCK2 were used to examine the effect of NCK on p53 phosphorylation following DNA damage. These cells were unable to induce PIKK-dependent phosphorylation of p53 on

Figure 2.7: Loss of SOCS7 prevents nuclear accumulation of NCK and results in early UV-induced apoptosis and elevated p53 phosphorylation. (A) HeLa cells transfected with control or SOCS7 siRNA were treated with 50 J/m^2 UV and allowed to recover for 1 hr before being fixed and stained with the indicated antibodies and DRAQ5. Scale bars are 20 μm. All images are confocal sections. Bar graphs below are ratio of nuclear to cytoplasmic fluorescence of NCK with siControl, no treat, defined as 1. n = 43-67; error bars represent SE; (**) $P < 0.0001$. (B) HeLa cells were treated as in A, and equal amounts of lysates were immunoblotted for cleaved CASP3, total CASP3, cleaved PARP, total PARP, and NCK. RAN was used as a loading control. n = 3. (C) RT-PCR of SOCS7 mRNA from HeLa cells transfected with control or SOCS7 siRNA. GAPDH was used as an internal control. RT = reverse transcriptase. n = 3. (D) HeLa cells transfected with control, NCK1 and NCK2, or SOCS7 siRNA were treated with 50 J/m^2 UV and allowed to recover for 2 hr before lysates were prepared. Equal amounts of lysates were immunoblotted for p53-pS15 (phospho-specific), CHK2-pT68 (phospho-specific), and NCK. RAN was used as a loading control. Band intensities were measured with ImageJ. Bar graph is ratio of p53-pS15 band intensity to RAN band intensity with siControl, no treat (NT), defined as 1. n = 4; error bars represent SE; (*) $P < 0.005$. (E) RT-PCR of p53 mRNA from HeLa cells transfected with control, NCK1 and NCK2, or SOCS7 siRNA. GAPDH was used as an internal control. Bar graph is ratio of p53 mRNA to GAPDH mRNA with siControl ratio defined as 1. n = 4; error bars represent SE. (F) 293T cells transfected with control, NCK1 and NCK2, or SOCS7 siRNA were treated with 50 J/m^2 UV and allowed to recover for 2 hr before lysates were prepared. Equal amounts of

lysates were immunoblotted for p53-pS15, p53 (total protein), and NCK. RAN was used as a loading control. n = 3. (G) RT-PCR of SOCS7 mRNA from 293T cells transfected with control or SOCS7 siRNA. GAPDH was used as an internal control. n = 3.

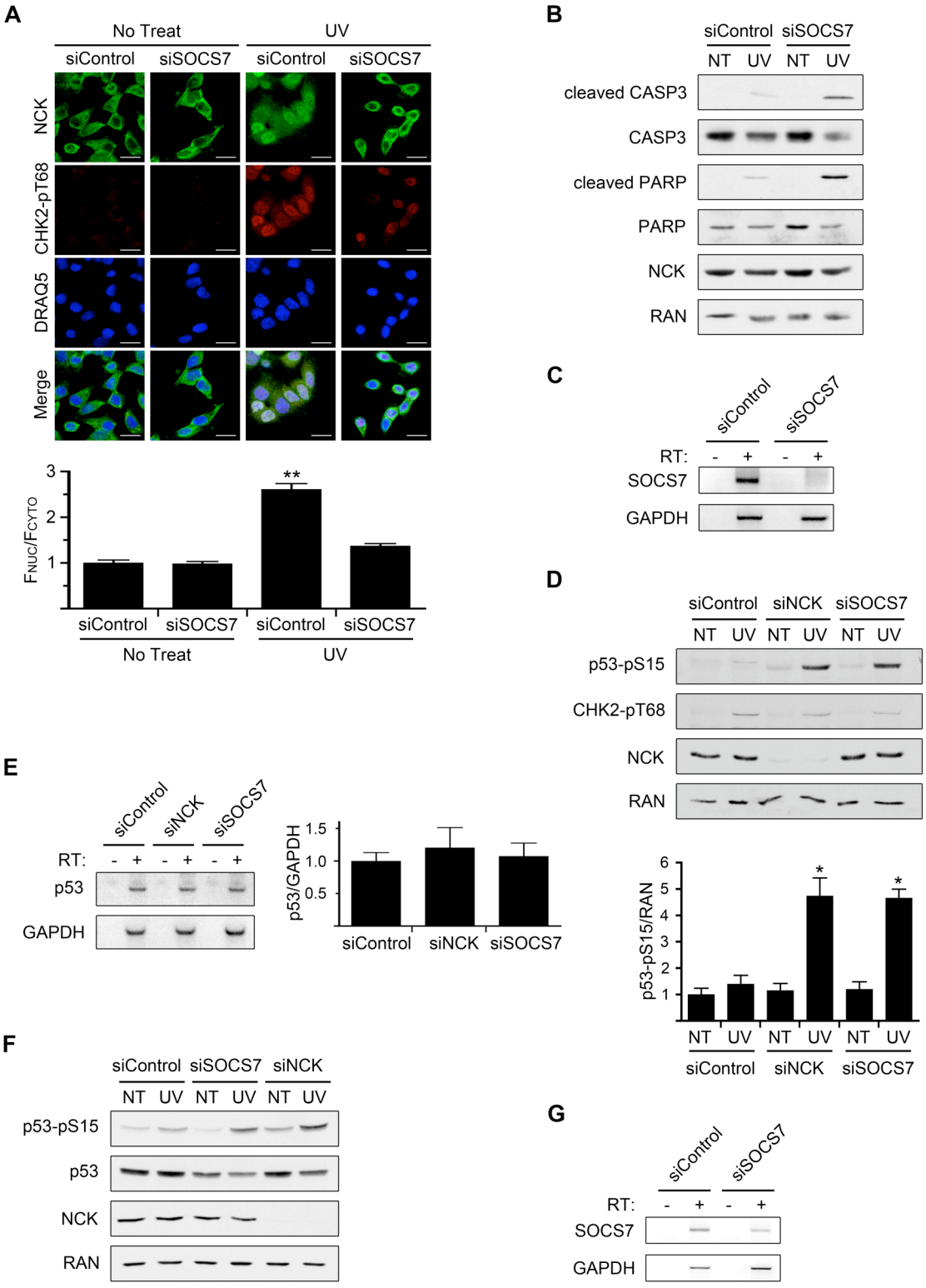
A
No Treat
UV
siControl
siSOCS7
siControl
siSOCS7
NCK
CHK2-pT68
DRAQ5
Merge
FNUC/FCYTO
3
2
1
**
siControl
siSOCS7
siControl
siSOCS7
No Treat
UV
B
siControl
siSOCS7
NT
UV
NT
UV
cleaved CASP3
CASP3
cleaved PARP
PARP
NCK
RAN
C
siControl
siSOCS7
RT:
- + - +
SOCS7
GAPDH
D
siControl
siNCK
siSOCS7
NT UV NT UV NT UV
p53-pS15
CHK2-pT68
NCK
RAN
p53-pS15/RAN
6
5
4
3
2
1
*
*
NT UV NT UV NT UV
siControl
siNCK
siSOCS7
E
siControl
siNCK
siSOCS7
RT:
- + - + - +
p53
GAPDH
p53/GAPDH
1.5
1.0
0.5
siControl
siNCK
siSOCS7
F
siControl
siSOCS7
siNCK
NT UV NT UV NT UV
p53-pS15
p53
NCK
RAN
G
siControl
siSOCS7
RT:
- + - +
SOCS7
GAPDH

serine 18 (mouse homolog to human serine 15) following UV irradiation [76]. In contrast, however, HeLa cells depleted of either NCK, or SOCS7, exhibited a dramatic increase in p53 phosphorylation on serine 15 after UV treatment, as compared to control cells (Fig. 2.7D). We asked if this increase was due to an increase in p53 transcript levels in NCK, or SOCS7, depleted cells, but as determined by RT-PCR, there was no difference with control cells (Fig. 2.7E). Since HeLa cells have a low level of p53 protein due to the human papillomavirus E6 oncoprotein, we tested another cell line to confirm this result [293]. Using 293T cells we observed the same UV-induced increase in p53 phosphorylation in NCK, or SOCS7, depleted cells compared to control cells (Fig. 2.7F,G). However, there was no effect on total p53 levels, indicating that the increased phosphorylation was not due to increased protein levels (Fig. 2.7F). Taken together, these data strongly suggest that elevated UV-induced p53 phosphorylation is correlated with a loss of nuclear NCK.

Contributions of NCK Isoforms on UV-Induced p53 Phosphorylation and Apoptosis

Two isoforms of NCK exist and are expressed in human cells [294]. However, the antibodies used in the above experiments are not selective for either isoform (Fig. 2.9A), and knockdowns were performed with siRNAs against both transcripts. Therefore, we next asked if the UV damage response phenotype might be specific to one or the other isoform. First, HeLa cells transfected with either GFP-NCK1 or GFP-NCK2 showed mostly cytoplasmic fluorescence, and nuclear accumulation occurred to similar extents for both constructs following UV irradiation (Fig. 2.8A). The loss of each NCK isoform

Figure 2.8: Specific contributions of the NCK isoforms. (A) HeLa cells transfected with GFP-NCK1 or GFP-NCK2 were treated with 50 J/m^2 UV and allowed to recover for 2 hr before being fixed and stained with indicated antibodies and DRAQ5. Scale bars are 20 μm. All images are confocal sections. Bar graphs below each panel are ratio of nuclear to cytoplasmic fluorescence of GFP-NCK with no treat defined as 1. n = 14-28; error bars represent SE; (*) $P < 0.001$, (**) $P < 0.0001$. (B) HeLa cells transfected with control, NCK1, or NCK2 siRNA were treated with 50 J/m^2 UV and allowed to recover for 2 hr before lysates were prepared. Equal amounts of lysates were immunoblotted for p53-pS15 (phospho-specific) and NCK. RAN was used as a loading control. n = 3. (C) RT-PCR of p53 mRNA from HeLa cells transfected with control, NCK1, or NCK2 siRNA. GAPDH was used as an internal control. RT = reverse transcriptase. n = 4. (D) HeLa cells transfected with control, NCK1, or NCK2 siRNA were treated with 50 J/m^2 UV and allowed to recover for 2 hr before lysates were prepared. Equal amounts of lysates were immunoblotted for cleaved CASP3, total CASP3, cleaved PARP, total PARP, and NCK. RAN was used as a loading control. n = 3. (E) RT-PCR of NCK1 and NCK2 mRNA from HeLa cells transfected with control, NCK1, or NCK2 siRNA. GAPDH was used as an internal control. n = 3. (F) Cell lysates from HeLa cells transfected with control, NCK1, or NCK2 siRNA were immunoprecipitated with a NCK antibody, which detects NCK 1 and NCK2, or IgG control, and immunoblotted for NCK or NCK2. n = 4.

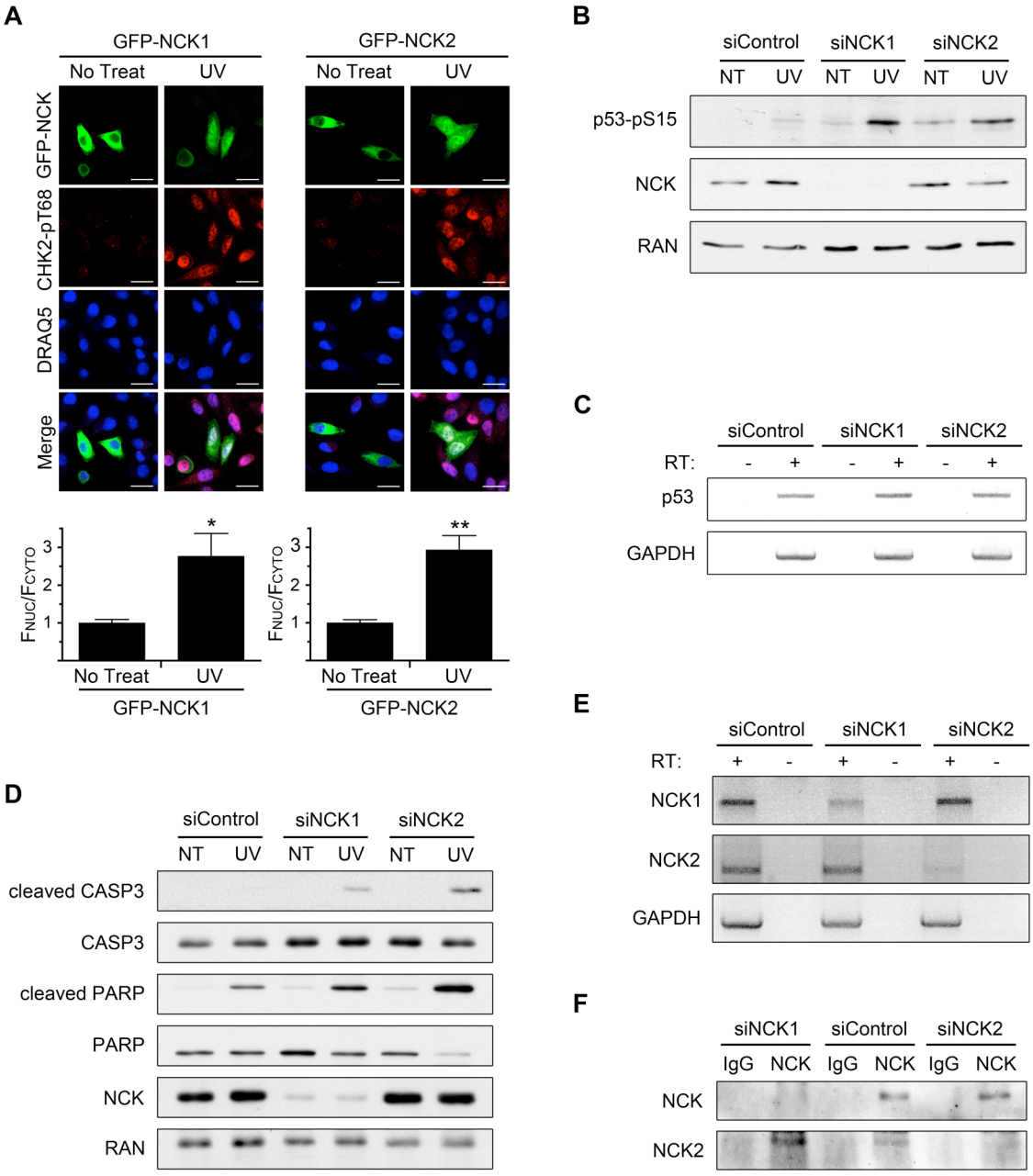
A
GFP-NCK1
GFP-NCK2
No Treat
UV
GFP-NCK
CHK2-pT68
DRAQ5
Merge
FNUC/FCYTO
*
**
B
siControl
siNCK1
siNCK2
NT
UV
p53-pS15
NCK
RAN
C
RT:
p53
GAPDH
D
cleaved CASP3
CASP3
cleaved PARP
PARP
E
NCK1
NCK2
F
IgG
NCK

Figure 2.9: Isoform specificity of NCK antibodies used and experiments with additional NCK2 siRNA. (A) Equal amounts of lysates from 293T cells transfected with myc-vector, myc-NCK1, or myc-NCK2 were immunoblotted with indicated NCK antibodies and Myc. IB indicates antibody was used for immunoblots. IP indicates antibody was used for immunoprecipitations. IF indicates antibody was used for immunofluorescence. ^ indicates endogenous NCK. * indicates non-specific band. n = 3. (B) HeLa cells transfected with control, or NCK2 siRNA#2 were treated with 50 J/m^2 UV and allowed to recover for 2 hr before lysates were prepared. Equal amounts of lysates were immunoblotted for p53-pS15 (phospho-specific). RAN was used as a loading control. n = 3. (C) Cells were treated the same as in B, and equal amounts of lysates were immunoblotted for cleaved CASP3, total CASP3, cleaved PARP, and total PARP. RAN was used as a loading control. n = 3. (D) RT-PCR of NCK2 mRNA from HeLa cells transfected with control, or NCK2 siRNA#2. GAPDH was used as an internal control. RT = reverse transcriptase. n = 3. (E) Cell lysates from HeLa cells transfected with control, or NCK2 siRNA#2 were immunoprecipitated with a NCK antibody, which detects NCK1 and NCK2, or IgG control, and immunoblotted for NCK or NCK2. n = 3.

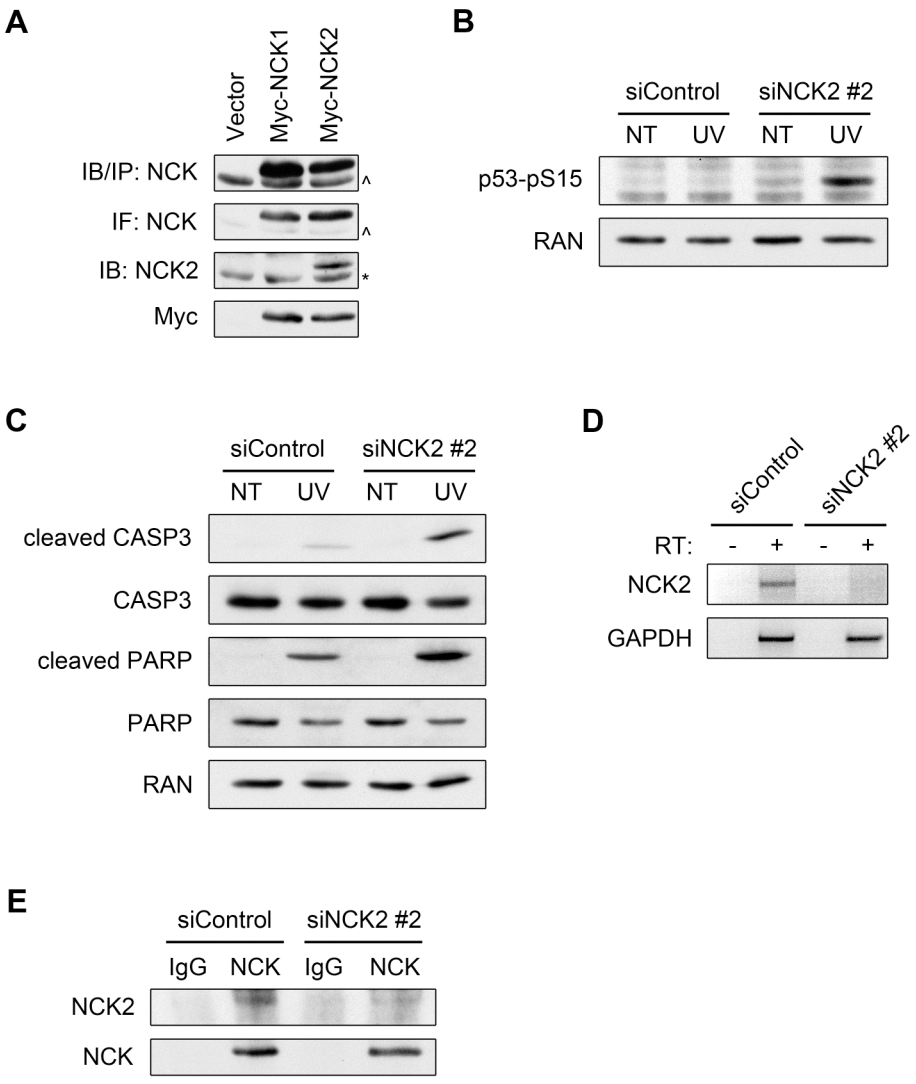
A
Vector
Myc-NCK1
Myc-NCK2
IB/IP: NCK
IF: NCK
IB: NCK2
Myc
^
^
*
B
siControl
siNCK2 #2
NT
UV
NT
UV
p53-pS15
RAN
C
siControl
siNCK2 #2
NT
UV
NT
UV
cleaved CASP3
CASP3
cleaved PARP
PARP
RAN
D
siControl
siNCK2 #2
RT:
-
+
-
+
NCK2
GAPDH
E
siControl
siNCK2 #2
IgG
NCK
IgG
NCK
NCK2
NCK

was then tested to determine the effect on p53 phosphorylation. Increased UV-induced p53 phosphorylation was observed after knockdown of either isoform (Fig. 2.8B), an effect that was not due to any change of the p53 transcript (Fig. 2.8C).

We next asked if there is a differential effect of silencing NCK1 versus NCK2 on apoptosis. While the depletion of either isoform resulted in an increase in cleaved CASP3 and cleaved PARP compared to control, the loss of the NCK2 isoform caused a greater increase compared to NCK1-depleted cells (Fig. 2.8D). This result is particularly striking because NCK2 is expressed at a much lower level than NCK1 in these cells. We base this conclusion on the observation that although the NCK antibody used in the immunoblots detects both NCK isoforms (Fig. 2.9A), depletion of NCK2 did not cause a significant decrease of the total NCK detected (Fig. 2.8B,D). We confirmed the knockdown of each isoform at the mRNA level with isoform-specific primers (Fig. 2.8E). Using a NCK2-specific antibody (Fig. 2.9A) we were also able to detect the loss of NCK2 at the protein level, although only after immunoprecipitation (IP) of total NCK from cells (Fig. 2.8F). NCK2-specific silencing reduced the level of NCK2 detected in the pan-NCK IP. As would be expected, NCK1-specific silencing decreased the amount of total NCK in the IP; interestingly, however, NCK1 depletion increased the amount of immunoprecipitated NCK2 compared to control, probably because of reduced competition for binding to the pan-NCK antibody (Fig. 2.8F).

Finally, we also further confirmed the effect of NCK2 depletion on UV-induced p53 phosphorylation and apoptosis by performing the experiments with another NCK2 specific siRNA (Fig. 2.9B-E). Taken together, these data indicate both NCK isoforms

undergo UV-induced nuclear accumulation, their loss is correlated with an increase in p53 phosphorylation, and they contribute to post-UV viability, although it appears that loss of NCK2 might have a more prominent role in the apoptotic response.

Discussion

The cellular response to DNA damage involves a cascade of signaling events initiated by the members of the PIKK family [82]. This network of phosphorylation events has been demonstrated to encompass proteins involved in multiple cellular pathways, but little is understood about which proteins are involved and how they intersect with the core DNA signaling pathway [277]. The adaptor protein NCK, and SOCS7, a binding partner required for its nuclear-cytoplasmic shuttling, were previously shown to accumulate in the nucleus following UV damage [76]. We found that the nuclear accumulation of NCK occurs in response to different types of DNA damage and requires PIKK signaling. Based on the use of a specific ATR inhibitor, the nuclear accumulation of NCK in response to UV irradiation appears to be dependent on ATR kinase activity, consistent with previous studies identifying ATR as the primary PIKK family member activated in response to UV damage [81].

Cells exposed to UV damage can survive through DNA repair; however, if damage is too severe, or there are defects in repair or other protective mechanisms, cell death usually occurs via p53-dependent apoptosis [80]. In our experiments we used a UV dose shown to induce apoptosis, but not until 12-16 hr after exposure to UV [295, 296]. Remarkably, in NCK-depleted cells, this apoptosis event started to occur within 2 hr, indicating that NCK plays a key anti-apoptotic role following UV treatment. Importantly, depletion of SOCS7, which blocks the UV-induced nuclear accumulation of NCK, also induced rapid apoptosis. This result suggests that the anti-apoptotic role of NCK is

dependent on its nuclear translocation during the DDR. However, it is possible nuclear accumulation of SOCS7 during the DDR could also contribute to this result if there is impaired UV-induced SOCS7 nuclear translocation in NCK depleted cells. Additionally, the data indicates nuclear accumulation of NCK is required during the DDR, but does not address if it is sufficient. A possible way to determine the sufficiency of nuclear NCK during the DDR would be to perform rescue experiments in NCK depleted cells with variants of NCK that are only nuclear, such as with a nuclear localization signal added.

NCK depletion resulted in early UV-induced apoptosis, however the role of NCK is still unclear. It is possible NCK depletion affects the balance between cell cycle arrest and apoptosis. The response of NCK depleted cells to undergo rapid UV-induced apoptosis could be a consequence of the cells failure to undergo cell cycle arrest and/or attempt DNA repair. NCK might repress the cellular response to apoptosis during DNA damage by promoting cell cycle arrest and DNA repair. To examine this possibility a dose curve of UV irradiation could be tested in control and NCK depleted cells. Examining the cells for apoptosis and cell cycle arrest might elucidate if NCK has a role in this decision process.

Our data suggest that the early apoptotic events that occur in NCK, or SOCS7, depleted cells might be mediated by p53. Phosphorylation of p53 on serine 15 occurs rapidly in response to DNA damage and has been proposed as a priming event for other modifications to occur [128, 129]. Once activated, p53 can cause cell cycle arrest or induce cells to undergo apoptosis [80, 126]. Since NCK does not possess intrinsic enzyme activity, it ability to suppress p53 phosphorylation and apoptosis is likely

mediated through an associated protein, perhaps recruiting a phosphatase to p53, or activating a negative regulator of p53 S15 phosphorylation. Although numerous proteins bind NCK, interaction studies have not yet been investigated in the context of DNA damage [297]. Since the nuclear accumulation of NCK is only correlated with the increase in p53 phosphorylation and apoptosis in NCK depleted cells, identification of a NCK binding partner during the DDR would aid in the elucidation of the mechanism. Proteomics on immunoprecipitated NCK following DNA damage would be a possible way to examine this. Additionally, performing rescue experiments in NCK depleted cells with variants of NCK lacking each of the SH2/SH3 protein interacting domains could test the importance of these domains in the protective function of NCK.

It is also possible that the negative inhibition of p53 phosphorylation by NCK is only correlated with the protection from apoptosis. Apoptosis can occur through p53-dependent and p53-independent mechanisms [134]. This could be tested with p53 null cells to examine if depleting cells of NCK, or SOCS7, results in an increase in apoptosis compared to wild-type p53 cells. Another avenue to explore would be the examination of p53 transcriptional targets, such as BAX and PUMA. This would test if the increase in p53 phosphorylation has a direct effect on known targets genes that have a role in apoptosis [134, 135]. Also, the acetylation of the C-terminus of p53 is necessary for the transcriptional activity of p53 [126, 127]. Thus, it would be interest to examine the status of p53 acetylation in NCK, or SOCS7, depleted cells following DNA damage.

In our earlier work, mouse embryonic fibroblasts (MEFs) null for NCK showed a decrease in UV-induced p53 phosphorylation compared to wild-type cells [76], in

contrast to the effects described here for HeLa and 293T cells depleted of NCK (Fig. 2.7D,F). However, these MEFs were cell lines that might have undergone additional genetic changes during culture, or in response to long-term loss of NCK. With this in mind, we attempted to rescue the NCK knockout mouse embryonic fibroblasts with human NCK, but despite expression of the proteins, the defect in p53 phosphorylation was not reversed (data not shown). Moreover, we found that siRNA mediated knockdown of NCK, or SOCS7, in wild-type primary mouse embryonic fibroblasts also increased p53 phosphorylation compared to control siRNA, similar to the observations reported in this study (data not shown). We conclude, therefore, that the lack of response to UV irradiation in the NCK knockout MEFs was an artifact of the MEF cell lines, and that for multiple mouse and human cell types the loss of NCK causes an increase in p53 phosphorylation in response to DNA damage.

The two NCK isoforms are considered to be functionally redundant, because the knockout of either isoform in mice has no detectable effect, but the double knockout mouse is embryonic lethal [282]. In our study, we sought to determine if the NCK isoforms are functionally redundant in their response to DNA damage. Both NCK isoforms translocate to the nucleus following UV irradiation and their loss correlates with an increase in p53 phosphorylation, and results in early apoptosis. This suggests the two isoforms are able to compensate for each other. However, NCK2 might have a more prominent role in the protection from an apoptotic response since it displayed greater caspase activation when depleted compared to the loss of NCK1, despite being expressed at lower levels. Important questions for the future concern whether there are different

binding partners of NCK1 and NCK2 following DNA damage, whether the UV-induced increase in p53 phosphorylation and increase in apoptosis are causative or correlative, and whether NCK is involved in other types of cellular stress or if it is specific to DNA damage.

Chapter 3: Septins and SAN1, a Novel Septin-Associated Nuclease that Functions in DNA Interstrand Crosslink Repair

Abstract

Septins are cytoskeletal elements that function as signaling platforms and diffusion barriers. Additionally, circumstantial evidence suggests a role in the DNA damage response, through unknown mechanisms. Here, we show that septin depletion sensitizes cells to multiple DNA damaging agents. Distinct mechanisms detect and repair damaged DNA depending on the nature of the lesions. Proteomic analysis revealed an uncharacterized septin-interacting protein, which possesses 5' exonuclease activity mediated by a FEN1-related nuclease domain. Cells depleted of SAN1 (Septin-Associated Nuclease 1) are sensitized to interstrand crosslink (ICL)-inducing agents. Additionally, SAN1, which becomes mislocalized by the loss of septins, translocates to the nucleus during ICL repair. SAN1 and septins are each required for efficient homologous recombination by participating in the resection of double-strand breaks generated during ICL repair. Our results identify SAN1 as a new nuclease required for repair of ICLs and suggest a novel and unexpected role for septins in this repair process.

Introduction

Septins are abundant filamentous GTP-binding proteins that have multiple cellular functions. They were discovered in budding yeast, where they form a ring at the bud neck during cytokinesis, but are also expressed throughout the animal kingdom [298]. There are 13 genes encoding septins in vertebrates, which can form hetero-oligomers in various combinations, the most common of which is a hexamer consisting of septins 2, 6, and 7, which can associate into filaments [7, 11]. Septins can act as scaffolds and diffusion barriers, regulate actin filament structure and microtubule stability, and are necessary for efficient cytokinesis [298]. Unexpectedly, septins have also been implicated in the DNA damage response (DDR), although through unknown mechanism [76-78].

DNA damage occurs in many forms and each type elicits different mechanisms and protein complexes to detect and repair the lesions so as to ensure genomic integrity. An especially toxic form of DNA damage is DNA interstrand crosslinks (ICLs), which disrupt transcription and replication by covalently joining the two strands of DNA. Repair of ICLs involves the collective effort of multiple repair pathways and proteins to sense the damage, remove the lesion, undergo translesion synthesis (TLS), and regenerate the DNA through homologous recombination (HR) [299]. ICLs are detected after a transcription or replication fork stalls at the site of the damage, mainly during S phase of the cell cycle [222]. After fork stalling, the Fanconi anemia (FA) complex is activated, which leads to unhooking of the lesion on one strand, filling of the resulting gap by TLS polymerases, and removal of the unhooked lesion by excision repair [300]. The resulting

double strand break (DSB) undergoes 5'-3' resection of the DNA ends to generate long, 3' single-stranded DNA (ssDNA) tails, which are coated with replication protein A (RPA) [173, 174]. RPA is displaced by RAD51, which initiates homology search and strand invasion [223].

We now report the discovery of a septin-binding protein that possesses a sequence related to the catalytic domains of the FEN1 family of structure-specific nucleases. This protein, which we named SAN1 (Septin Associated Nuclease 1), has not previously been characterized, other than a single report that it can act as a transcriptional co-activator of PPAR-gamma [301]. FEN1 and related nucleases are essential for many aspects of DNA replication, recombination, transcription, and repair [302]. We now report that SAN1 is a novel exonuclease involved in DNA end resection, and is important for the resolution of ICLs. These data highlight a novel, unexpected link between cytoskeletal elements and the DNA repair machinery.

Materials and Methods

Cell culture

HeLa (ATCC), 293T (ATCC) and HeLa-DR (provided by R. Fishel) cells were grown in DMEM supplemented with 10% FCS, 100 U/ml penicillin and 100 U/ml streptomycin (GIBCO). Transfection of plasmids or siRNA was performed with calcium phosphate, Lipofectamine 2000 (Invitrogen), or Lipofectamine RNAiMAX (Invitrogen). Virus was made, collected and titered as described previously [303].

Plasmids and siRNA

SAN1 cDNA (FLJ56631) was purchased from the NBRC, Japan and cloned into the pRK7 expression vector with a C-terminal FLAG tag. SAN1 (D90A) and SAN1 rescue constructs were made by QuikChange site-directed mutagenesis (Agilent Technologies). I-SceI expressing plasmid (pCBASce) was provided by R. Fishel. Firefly luciferase cDNA from pBESTluc (Promega) was cloned into pRK7 expression vector to make pK-Firefly. pRL-TK was purchased from Promega. shRNA constructs targeting SEPT2 (sense sequence: GCAGGAAAGTGGAGA ATGA), SEPT7 (sense sequence: GGACTTAAACCATTGGATA), RAD51 (sense sequence: GGGAATTAGTGAAGCCAAA), and KU70 (sense sequence: GAGTGAAGATGAGTTGACA) were cloned into the pLVTHM vector as described previously [303]. The human SAN1 (sense sequence: AGGCGAGAAGTTCCCGTGT) lentiviral shRNAmir pGIPZ and control (described previously (Tooley et al., 2010)

constructs were obtained from Open Biosystems and grown and purified according to their protocol. siRNA targeting SAN1 (sense sequence: UAUUAUGGCUGAACCAAGA), SAN1 pool (M-014898-00), control (described previously [38]), and SEPT7 (described previously [38]) were obtained from Thermo Scientific.

Antibodies

The following antibodies were used: rabbit anti-SAN1 (polyclonal antisera produced by Cocalico and purified), mouse anti-SEPT6, rabbit anti-SEPT2, and rabbit anti-SEPT7 (all septin antibodies described previously [38]), mouse anti-γH2AX (pS139) (Millipore), mouse anti-FLAG (Sigma), rabbit anti-γH2AX (pS139) (Novus Biologicals), rabbit anti-RAN (described previously [287]), rabbit anti-RPA70 (Cell Signaling), mouse anti-SAN1 (Novus Biologicals), mouse anti-alpha Tubulin (Sigma), mouse anti-FLAG-HRP (Sigma), rabbit anti-RAD51 (Santa Cruz, H-92), mouse anti-KU70 (Transduction Laboratories).

Immunodetection

Immunoblotting and immunoprecipitation (IP) was performed as described previously [286] with anti-SEPT6 or control antibody (mouse anti-GST, described previously [38]) on protein A-sepharose beads (Sigma) or with anti-SAN1 or control antibody (rabbit IgG, Santa Cruz) on GammaBind plus sepharose (GE Healthcare). When indicated cells were treated with 5μM cisplatin for 2 hrs, replaced with fresh media and harvested 24 hrs later.

Cell viability assay

HeLa cells transduced with control or SEPT2 shRNA were plated in a 96 well plate at 100 cells/well and allowed to adhere overnight. Media was then replaced with vehicle or the following concentration of DNA damage agents for the following time: 2.5 μM cisplatin (Biovision) for 2 hrs; 800 nM mitomycin-C (MMC) (Sigma) for 2 hrs; 40 μg/mL methyl methanesulfonate (MMS) (Sigma) for 2 hrs; 50 μM hydrogen peroxide (H_2O_2) (Sigma) for 2 hrs; 25 μM etoposide (Sigma) for 16 hrs; 250 nM camptothecin (CPT) (Sigma) for 16 hrs; 4 μM 6-thioguanine (C-TG) (Sigma) for 16 hrs. Growth media was replaced after treatment time. After 10 days, the wells were assayed with CellTiter 96 AQ_{ueous} One Solution (Promega). Percent cell viability was determined by dividing DNA damage agents by vehicle for each shRNA and then defining the control hairpin as 100% for each agent.

Clonogenic survival assay

The assay was performed as described previously [249] with the following changes. Sixteen hrs after plating, HeLa cells were treated with the indicated concentrations of cisplatin, MMC, MMS, ionizing radiation (IR), or carmustine (Sigma). Growth medium was replaced 2 hrs (cisplatin, MMC, MMS, and carmustine), or directly (IR) after treatment. After 10 days, the cells were fixed, stained and counted.

Protein Digestion and Mass Spectrometry

Visible bands were excised from the gel and cut into 1mm x 1mm pieces. These were washed x3 with water, x2 with 1:1 acetonitrile: 100mM ammonium bicarbonate, and dehydrated in 100% acetonitrile. After removing all acetonitrile, 30µl of porcine trypsin (Promega) at a concentration of 20 µg/ml was added. After incubation on ice for 1 hr the gel pieces were incubated at 37°C for 12-16 hrs. The supernatant was transferred to a second tube, and peptides were further extracted from the gel with acetonitrile. The two supernatants were mixed then frozen and lyophilized. The peptides were redissolved in 5 µl of 1:1 acetonitrile: 0.25% trifluoroacetic acid immediately prior to spotting on the MALDI target.

The matrix solution consisted of alpha-cyano-4-hydroxycinnamic acid (Sigma) saturating a solution of 1:1:0.02 acetonitrile: 25mM ammonium citrate in water:trifluoroacetic acid. Peptide (0.15 µl) was spotted on the MALDI target immediately followed by 0.15 µl matrix solution and allowed to dry. MALDI MS and MS/MS data were then acquired using a AB 4700 TOFTOF Mass Spectrometer (Applied Biosystems Inc.). Resultant peptide mass fingerprint and peptide sequence data were submitted to the NCBI database using the Mascot search engine.

Purification of SAN1-FLAG

293T cells were transfected with pK-SAN1-FLAG, pK-SAN1 (D90A)-FLAG or pK-FLAG vector and 24 hrs later pelleted by centrifugation, washed in PBS, and lysed in HLB (25 mM HEPES (pH 7.4), 10% glycerol, 1mM EDTA, 1 mM DTT, 20 nM

calyculin A (Sigma) and protease inhibitors). Cells swelled for 5 min on ice before being subjected to three freeze thaws (liquid nitrogen and 37°C) before NaCl was added to 300 mM. The lysates were spun at 16,100*g* at 4°C for 15 min and the supernatant was added to an equal amount of HLB with 0.2% NP-40 before another spin at 16,100*g* at 4°C for 5 min. Clarified lysates were incubated with mouse anti-FLAG M2-Agarose (Sigma) for 2 hrs at 4°C. Beads were washed x2 for 15 min with HLB with 0.1% NP-40 and 150 mM NaCl, then x2 for 15 min with elution buffer (62.5 mM HEPES (pH 7.4), 62.5 KCl, 5% glycerol, 1mM DTT, 50 μg/ml BSA). Bound proteins were eluted with FLAG-peptide (150 ng/μl) for 30 min at 4°C in a shaker (600 rpm).

Nuclease assay

Oligonucleotide (IDT) X1 (TGGGTCAACGTGGGCAAAGATGTCCTAGCAATGTAATCGT CTATGACGTT) and oligonucleotide X2 (TGCCGAATTCTACTGGGTCAACGTGGGC AAAGATGTCCTAGCAATGTAATCGTCTATGACGTT) were 5' end-labeled with T4 polynucleotide kinase (NEB) and [γ-^{32}P]ATP (MP Biomedicals). Oligonucleotides X1, X3 (GTCGGATCCTCTAGACAGCTCCATG), X4 (CAACGTCATAGACGATTACATTGCTACA TGGAGCTGTCTAGAGGATCCGA), and X5 (TTTTTTTTTTTTTTTTTTTTTTTTTTTTTTT TTTTTTTTTTTTTTTTT) were 3' end-labeled with terminal transferase (NEB) and [α-^{32}P] cordycepin 5'-triphosphate (Perkin Elmer). To make splayed arm DNA structure, 5' end-labeled X2 and unlabeled X4 were annealed. To make 5' flap DNA structure, 5' end-labeled X2,

unlabeled X4, and unlabeled X6 (GGACATCTTTGCCCACGTTGACCCAGTAGAATTCGGC) were annealed. To make dsDNA, 3' end-labeled X1 and unlabeled X7 (AACGTCATAGACGA TTACATTGCTAGGACATCTTTGCCCACGTTGACC CA) were annealed. All substrates were PAGE-purified and eluted. Nuclease reactions (10 µl) contained radiolabeled DNA substrates (5 nM) and 4 µl of the indicated IP in reaction buffer (25 mM HEPES (pH 7.4), 25 mM KCl, 2% glycerol, 50 µg/ml BSA, 1 mM β-ME). Reactions were started by the addition of 3 mM $MgCl_2$ and allowed to proceed for 2 hrs at 37°C. The reaction was stopped by the addition of 3 mM EDTA, the samples were boiled at 95°C for 5 min, and analyzed by denaturing PAGE (15% polyacrylamide, 7 M urea, 1X TBE). Gels were exposed to film at 4°C. The purine-specific chemically digested ladder (oligo X1) was performed as previously described [102].

Immunofluorescence

HeLa cells were grown on Lab-Tek II chambers (Nunc) and, when indicated, treated with vehicle, 5 µM cisplatin, or 1 µM MMC for 2 hrs, replaced with fresh media and 24 hrs later fixed in 3.7% paraformaldehyde and quenched in 2% H_2O_2 (for endogenous SAN1 detection). Cells were permeabilized and blocked in 0.3% saponin with 1x blocking reagent (Roche), except for RPA foci formation when cells were permeabilized in 0.5% Trition X-100 and blocked in 3% BSA. Nuclei were counterstained with DRAQ5 (Cell Signaling). For endogenous SAN1 detection, rabbit-anti-HRP was used as secondary antibody, and tyramide signal amplification plus fluorphore cyanine 3 (PerkinElmer) was

added for 10 min. Imaging was on a Zeiss LSM510 Meta confocal microscope using a x100 oil immersion lens (NA 1.3).

GFP-based HR assay

The assay was performed as described previously [304], with the following changes. For transfections of control, SAN1 pool, or SEPT7 siRNA, Lipofectamine RNAiMAX was used and the second siRNA transfection was performed separately and 6 hrs before transfection with pCBASce or vector plasmid (pK-myc). After 60 hrs, cells were analyzed by flow cytometry to detect GFP-positive cells, with viable cells determined as propidium iodine (Sigma) negative.

Luciferase-based HR assay

For the luciferase-based HR assay, pK-Firefly was digested with KpnI and XcmI and gel purified to produce one fragment (long) or digested with BstBI and NaeI and gel purified to produce the other fragment (short) (Fig. 3.10C,D). Long contains the promoter and the 5' region of firefly gene. Short contains the remaining part of the firefly gene and lacks the start codon. The long and short fragments contain two complimentary regions between the BstB1 and Xcm1 sites in the firefly gene, and between the Kpn1 and Nae1 sites in the vector backbone 3' of the gene. 293T cells were transfected with equal molar concentrations of long and short fragments, as well as pRL-TK, which expresses renilla luciferase, as a transfection control. After 24 hrs cells were harvested and assayed with

the Dual-Luciferase Reporter Assay (Promega) and assayed using a 20/20^{n} luminometer (Promega).

Proliferation assay

HeLa cells transduced with shRNA were plated in a 96 well plate at 100 cells/well and allowed to adhere. Every day a number of the wells were assayed with CellTiter 96 AQ_{ueous} One Solution (Promega). Relative cell growth was determined by dividing each time point by day 1.

Cell cycle analysis

HeLa cells were transfected with indicated siRNA and then treated with vehicle or 5 μM cisplatin for 2 hrs, replaced with fresh media and 24 hrs later harvested for flow cytometric analysis. Cells were washed in PBS and then fixed in ice-cold 70% ethanol for at least 2 hrs. The cells were washed in PBS and resuspended in propidium iodide staining solution (PBS, 0.1% Triton X-100, 0.2 mg/mL DNase-free Rnase A (Sigma), 20 μg/mL PI (Sigma)) and analyzed using a FACSCalibur machine (BD).

Statistical analysis

Two-tailed Student's *t*-tests were used in the statistical analysis when comparing two samples. A two-way ANOVA test was used for colony survival assays and proliferation assays. All graphs and statistical analysis was performed with GraphPad Prism, Version 4.0a (GraphPad Software, Inc.).

Results and Discussion

Depletion of septins and a novel septin-associated protein, SAN1, decreases cellular survival to ICLs

To test the requirement for septins in the DDR, we assayed cellular viability against different DNA damage agents in cells depleted of septins. Individual septin subunits are unstable, but form stable heteromeric complexes, so that a reduction in any one septin type causes a parallel decrease in the expression of the others [38]. We designed a short-hairpin sequence against SEPT2, which decreased not only SEPT2 expression, but also SEPT6 and SEPT7, three septins known to form a hexameric complex *in vivo* and *in vitro* (Fig. 3.1A) [16, 46]. Using a range of DNA-damaging agents we measured the viability of control and SEPT2 shRNA expressing cells. Compared to control, cells depleted of septins were more sensitive to the ICL-inducing agents, cisplatin and mitomycin-C (MMC), the alkylating agent, methyl methanesulfonate (MMS), oxidative stress induced by hydrogen peroxide (H_2O_2), and the topoisomerase inhibitors, etoposide and camptothecin (CPT) (Fig. 3.1B). However, loss of septins had no effect when cells were treated with 6-thioguanine (6-TG) (Fig. 3.1B), a compound that is toxic to cells defective in mismatch repair [305]. Therefore, it is unlikely that septins are involved in this pathway, but seem to be required for the response of a broad array of other types of DNA damage. For the current study we focus on damage involving ICL.

Figure 3.1: Cells depleted of septins are hypersensitive to DNA damage agents. (A) Immunoblot for septins from cells transduced with indicated shRNA. RAN was used as a loading control. (B) Cell viability assay in cells transduced with indicated shRNA. Cells were treated with vehicle or indicated DNA damage agents. Percent cell viability was determined by dividing cell number of each DNA damage agent by vehicle with survival of cells transduced with control hairpin defined as 100% for each condition. n = 6-12; error bars represent SD; (*) $P < 0.001$; (**) $P < 0.0001$. (C) Proliferation assay of cells transduced with indicated shRNA. For each shRNA, day 1 is set to 1. n = 6; error bars represent SD. (D) Clonogenic survival assay of cells transduced with indicated shRNA. For each shRNA, colony number of untreated cells is defined as 100%. n = 4-9; error bars represent SE; (#) $P < 0.05$; (##) $P < 0.01$.

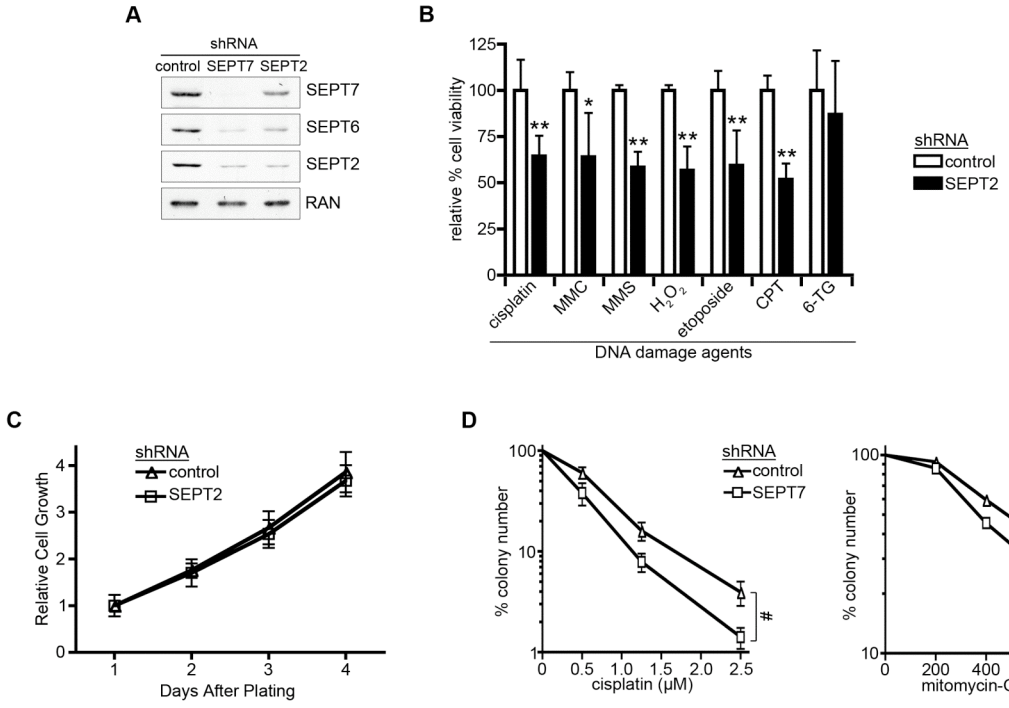
A
shRNA
control SEPT7 SEPT2
SEPT7
SEPT6
SEPT2
RAN
B
relative % cell viability
125
100
75
50
25
0
**
*
**
**
**
**
cisplatin
MMC
MMS
H2O2
etoposide
CPT
6-TG
DNA damage agents
shRNA
control
SEPT2
C
Relative Cell Growth
4
3
2
1
0
shRNA
control
SEPT2
1
2
3
4
Days After Plating
D
% colony number
100
10
1
shRNA
control
SEPT7
#
0
0.5
1.0
1.5
2.0
2.5
cisplatin (μM)
% colony number
100
10
##
0
200
400
600
800
mitomycin-C (nM)

Since loss of septins can sometimes cause cytokinetic defects, which might result in reduced growth rates, we performed a proliferation assay, but could detect no difference between control and septin-depleted cells (Fig. 3.1C). To exclude off-target effects we performed clonogenic survival assays (CSAs) with cells expressing an shRNA targeting a different septin, SEPT7. As expected, loss of SEPT7 resulted in the co-depletion of SEPT2 and SEPT6 (Fig. 3.1A). Importantly, however, cells expressing the SEPT7 shRNA were hypersensitive to cisplatin and MMC compared with control (Fig. 3.1D). This result confirms septin depletion sensitizes cells to ICL-inducing agents.

We next sought to determine the mechanism through which septins might potentiate this response to DNA damage. Notably, we identified by mass spectrometry a novel septin-binding protein, FAM120B, which possesses a putative nuclease domain related to FEN1 (Fig. 3.2A). First, we confirmed that endogenous FAM120B, which we have renamed SAN1, binds to the endogenous septins and *vice versa* (Fig. 3.2B). Next, we tested if SAN1 might be involved in the DDR by performing CSAs. Strikingly, cells depleted of SAN1 by expression of an shRNA became hypersensitive to the ICL-inducing agents, cisplatin, MMC, and carmustine, compared to control, but not to other DNA damage agents (Fig. 3.2C). The response to ICL agents was not due to any difference in growth rates as determined by a proliferation assay and cell cycle analysis (Fig. 3.2D,E). Additionally, SAN1 levels were not reduced by septin depletion (Fig. 3.2F). Taken together, these data suggest septins are involved in the response to ICLs through a novel associated protein, SAN1.

Figure 3.2: Loss of the septin-associated protein SAN1 sensitizes cells to ICL-inducing agents. (A) Mass spectrometric analysis revealed 12 unique peptides that correspond to FAM120B/ SAN1. (B) Cell lysates were immunoprecipitated (IP) with the indicated antibodies and analyzed by immunoblot to detect SAN1 and septins. (C) Clonogenic survival assays performed with cells transduced with indicated shRNA. Immunoblot shows knockdown of SAN1 compared to control shRNA. For each shRNA, colony number of untreated cells is defined as 100%. n = 2-11; error bars represent SE; (*) $P < 0.05$; (**) $P < 0.01$; (***) $P < 0.001$. (D) Proliferation assay of cells transduced with indicated shRNA. For each shRNA, day 1 is set to 1. n = 6; error bars represent SD. (E) Cell cycle analysis of control or SAN1-depleted cells, treated with vehicle or cisplatin. (F) Immunoblot for SAN1 from cells depleted of septins with indicated shRNA. RAN was used as a loading control.

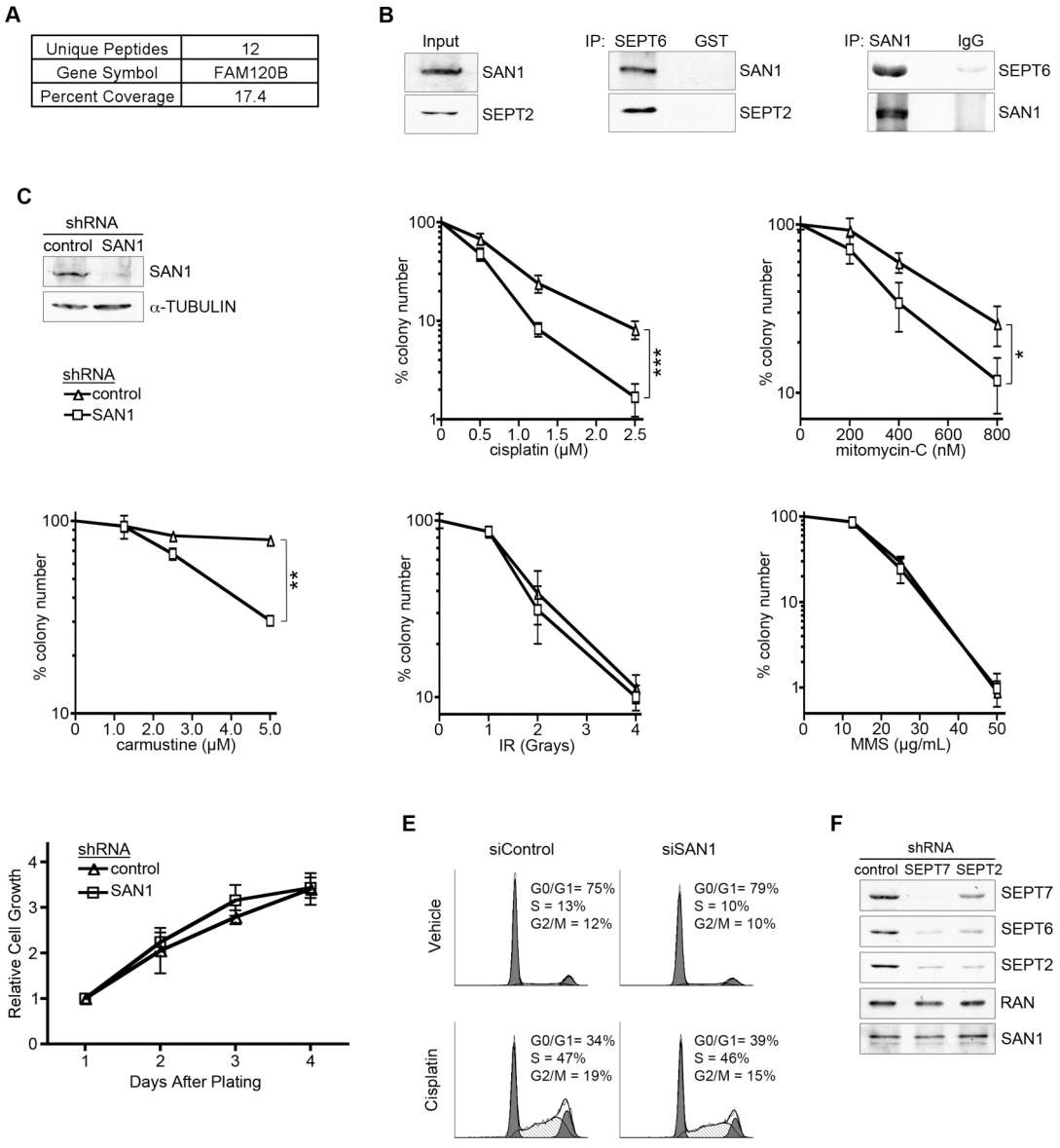
A
Unique Peptides 12
Gene Symbol FAM120B
Percent Coverage 17.4
B
Input
IP: SEPT6 GST
IP: SAN1 IgG
SAN1
SEPT2
SEPT6
C
shRNA
control SAN1
SAN1
α-TUBULIN
shRNA
control
SAN1
% colony number
cisplatin (μM)
mitomycin-C (nM)
carmustine (μM)
IR (Grays)
MMS (μg/mL)
D
Relative Cell Growth
Days After Plating
E
siControl
siSAN1
Vehicle
Cisplatin
G0/G1= 75%
S = 13%
G2/M = 12%
G0/G1= 79%
S = 10%
G2/M = 10%
G0/G1= 34%
S = 47%
G2/M = 19%
G0/G1= 39%
S = 46%
G2/M = 15%
F
shRNA
control SEPT7 SEPT2
SEPT7
SEPT6
SEPT2
RAN
SAN1

SAN1 is a FEN1-related nuclease, which possess 5' ssDNA exonuclease activity

SAN1 contains a putative FEN1-related nuclease domain, which raised the interesting possibility that it might function as a novel repair nuclease. The FEN1 family is involved in DNA replication and a variety of repair pathways [302]. These nucleases possess distinct features that are conserved among family members, including two regions, N and I, which together form a domain containing seven acidic residues essential for enzymatic activity [302]. A sequence alignment of the nuclease domain of human SAN1 with the other family members, FEN1, EXO1, XPG, and GEN1, shows the location of the conserved residues (Fig. 3.3A). Moreover, the Robetta server found a confident match between the nuclease domain of SAN1 and the crystal structure of *A. fulgidus* FEN1, which allowed for comparative modeling (Fig. 3.3B). The locations of the active site carboxylates in the SAN1 model correspond very closely with those of FEN1 (Fig. 3.3C).

In addition to the N-terminal nuclease-like domain, SAN1 also possesses a central region of unusual repeated motifs containing the consensus sequence TDPESRQEVPMC (Fig. 3.3D and Fig. 3.4A). While absent from *Drosophila* or *C. elegans* genomes, orthologs of SAN1 were identified in other insects and the lower Metazoa, including the sea anemone and Hydra (Fig. 3.4B).

Based on this concordance we asked if SAN1 has nuclease activity. As a control, we created a mutant version of SAN1 in which the conserved Aspartate-90 residue was mutated to Alanine (D90A). We expressed FLAG-tagged wild-type (WT) SAN1, SAN1(D90A), or vector in 293T cells, purified the proteins on M2 beads, and eluted with

Figure 3.3: Alignment and modeling of SAN1 nuclease domain to FEN1 family members. (A) Sequence alignment of nuclease domains of human SAN1, EXO1, FEN1, GEN1 and XPG. Identical and similar residues are in bold. Conserved acidic residues in the active site are highlighted in red. (B) The nuclease domain sequence of SAN1 was submitted to the Robetta server (http://robetta.bakerlab.org) and the server found a confident match to the *A. fulgidus* FEN1 protein, whose structure was used as a template for comparative modeling. SAN1 model (light blue) and FEN1 template (PDB 1RXW) (green) were aligned and visualized with the PyMol Molecular Graphics System, Version 1.3 Schrödinger, LLC. (C) Modeling of conserved carboxylates in active site of SAN1 (light blue) using *A. fulgidus* FEN1 structure (green) as template. (D) Schematic of the domain architecture of SAN1. N-terminal nuclease domain (N), internal nuclease domain (I), central repeats (R).

A

```
                                10        20        30        40        50
hSAN1      1  MGVRGLQGFVGSTCPHICTVVNFKELAEHHRSKYPGCTPTIVVDAMCCLRYWYTPESW--
hEXO1      1  MGIQGLLQFIKEA----SEPIHVRK--------YKG--QVVAVDTYCWLHKGAIACAEKL
hFEN1      1  MGIQGLAKLIADVAPSAIRENDIKS--------YFG--RKVAIDASMSIYQFLIAVRQGG
hGEN1      1  MGVNDLWQILEPVK---QHIP-LRN--------LGG--KTIAVDLSLWVCEAQTVKKMM-
hXPG       1  MGVQGLWKLLECSG--RQVSPEA----------LEG--KILAVDISIWLNQALKGVRDRH

                   60        70        80        90       100       110
hSAN1     59  ----ICGGQWREYFSALRDFVKTFTAAGIKLIFFFDGMVEQDKRDEWVKRRLKNNREISR
hEXO1     47  AK----GEPTDRYVGFCMKFVNMLLSHGIKPILVFDGCTLPSKKEVERSRRERRQANLLK
hFEN1     51  DVLQNEEGETTSHLMGMFYRTIRMMENGIKPVYVFDGKPPQLKSGELAKRSERRAEAEKQ
hGEN1     46  ------GSVMKPHLRNLFFRISYLTQMDVKLVFVMDGEPPKLKADVISKRNQSRYGSS--
hXPG      47  -----GNSIENPHLLTLFHRLCKLLFFRIRPIFVFDGDAPLLKKQTLVKRRQRKDLASS.

                  120       130       140       150       160       170
hSAN1    115  IFHYIKSHKEQPGRNMF----FIPSGLAVFTRFALKTLGQETLCSLQEADYEVASYGLQH
hEXO1    103  GKQLLREGKVSEARECFTRSINITHAMAHKVIKAARSQGVDCLVAPYEADAQLAYLNKAG
hFEN1    111  LQQAQAAGAEQEVEKFTKRLVKVTKQHNDECKHLLSLMGIPYLDAPSEAEASCAALVKAG
hGEN1     98  -------GKSWSQK--TGRSHF--KSVLRECLHMLECLGIPWVQAAGEAEAMCAYLNAGG
hXPG     763  ......[insert].......TVTGQMFLESQELLRLFGIPYIQAPMEAEAQCAILDLTD

                  180       190       200       210       220
hSAN1    171  NCLGILGEDTDYLIYDTCPYFSISELCLESLDTVMLCRE-KLCESLGL----CVADLPLL
hEXO1    163  IVQAIITEDSDLLAFGCKKVILKMD----QFGNGLEIDQARLGMCRQLGDVFTEEKFRYM
hFEN1    171  KVYAAATEDMDCLTFGSPVLMRHLTASEAKKLPIQEFHLSRILQELGL----NQEQFVDL
hGEN1    147  HVDGCLTNDGDTFLYGAQTVYRNFTM-NTKDPHVDCYTMSSIKSKLGL----DRDALVGL
hXPG     802  QTSGTITDDSDIWLFGARHVYRNF---FNKNKFVEYYQYVDFHNQLGL----DRNKLINL

                  230       240       250       260       270
hSAN1    226  ACLLGNDIIPEGMFESFRYKCLSSYTSVKENFD----KKG-NIILAVSDHISK-VLYLYQ
hEXO1    219  CILSGCDYL-SSLRGIGLAKACKVLRLANNPDIVKVIKKIGHYL-----KMNITVPEDYI
hFEN1    227  CILLGSDYC-ESIRGIGPKRAVDLIQKHK--SIEEIVRRL--------DPNKYPVPENW-
hGEN1    202  AILLGCDYLPKGVPGVGKEQALKLIQILK--GQSLLQRFNRWNE-----TSCNSSPQLLV
hXPG     855  AYLLGSDYT-EGIPTVGCVTAMEILNEFPGHGLEPLLKFSEWWHEAQKNPKIRPNPHDTK

                  280       290       300       310       320
hSAN1    280  GEKKLEEIL---PLG--PNKALFYKGMAS--------YLLPGQKSPWFF-----QKPKGV
hEXO1    273  NGFIRANNTFLYQLVFDPIKRKLIPLNAYEDD------VDPETLSYAG------QYVDDS
hFEN1    275  -LHKEAHQLFLEPEVLDPESVELK------------WSEPNEEELIKFMCGEKQFSEER
hGEN1    255  TKKLAHCSVCSHPGSPKDHERNGCRLCKSDK------YCEPHDYEYCCPCE----WHRTE
hXPG     914  VKKKLRTLQLT-PGFPNPAVAEAYLKPVVDDSKGSFLWGKPDLDKIREFCQRYFGWNRTK

                  330
hSAN1    322  ITLDKQVISTSSDAES
hEXO1    321  IALQIALGNKDINTFE
hFEN1    321  IRSGVKRLSKSRQGST
hGEN1    305  HDRQLSEVENNIKKKA
hXPG     973  TDESLFPVLKQLDAQQ
```

B

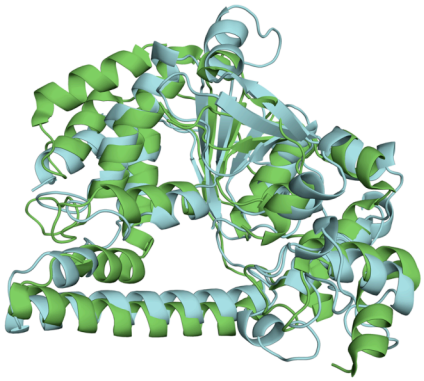

C

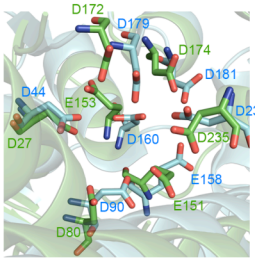

D

Figure 3.4: Central repeats of SAN1 protein and phylogenetic analysis of SAN1 gene in metazoa. (A) Dot plot analysis of SAN1 against SAN1. Parallel diagonals offset from the main diagonal indicate repetitive regions in the central repeats region. MacVector was used to generate the plot. (B) Phylogenetic analysis of SAN1 gene in metazoa. MacVector was used to generate the tree.

A

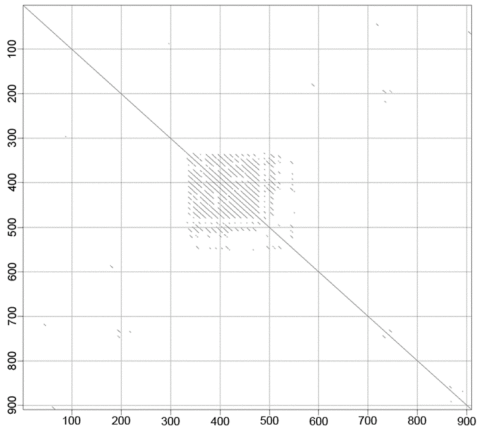
100
200
300
400
500
600
700
800
900
100
200
300
400
500
600
700
800
900

B

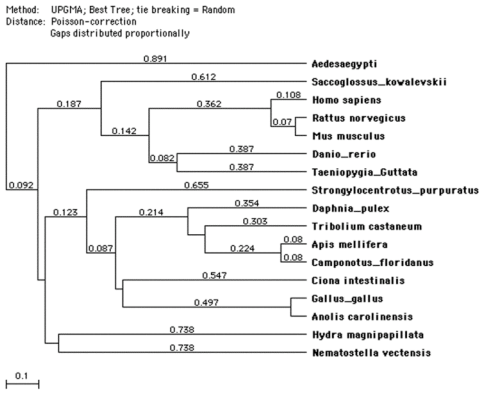
Method: UPGMA; Best Tree; tie breaking = Random
Distance: Poisson-correction
Gaps distributed proportionally
0.891
0.612
0.187
0.108
0.362
0.07
0.142
0.387
0.082
0.387
0.092
0.655
0.123
0.354
0.214
0.303
0.087
0.08
0.224
0.08
0.547
0.497
0.738
0.738
Aedesaegypti
Saccoglossus_kovalevskii
Homo sapiens
Rattus norvegicus
Mus musculus
Danio_rerio
Taeniopygia_Guttata
Strongylocentrotus_purpuratus
Daphnia_pulex
Tribolium castaneum
Apis mellifera
Camponotus_floridanus
Ciona intestinalis
Gallus_gallus
Anolis carolinensis
Hydra magnipapillata
Nematostella vectensis
0.1

FLAG peptide (Fig. 3.5A). Given the specificities of the FEN1 family as structure-specific nucleases, we tested the ability of the purified SAN1 to cleave splayed arm and 5' flap oligonucleotide structures, and detected cleavage only with the splayed arm structure in a region where the labeled oligo was single-stranded (Fig. 3.5B). We then tested ssDNA, labeling the oligonucleotide at the 5' or 3'-end with ^{32}P. After incubation with SAN1, the reaction products were visualized by denaturing PAGE and autoradiography. SAN1 displayed nuclease activity towards the 5'-end of the substrates, to generate two cleaved products (~3 and 7 nt) when detected using a 5' label and five cleaved products when observed with a 3' label (Fig. 3.5C). Importantly, the nuclease activity of SAN1(D90A) was severely reduced compared with WT SAN1 (Fig. 3.5C). The unusual pattern of cleaved products prompted us to examine another oligonucleotide with a different sequence. The cleaved products of the second 3'-labeled ssDNA also produced multiple cleaved products, but with different sized products (Fig. 3.5D), suggesting that SAN1 shows sequence specificity. However, from comparisons of the sizes and sequences of the oligonucleotide cleavage products we have been unable to decipher the recognition code (Fig. 3.5E). An oligonucleotide composed of all thymidines was only inefficiently cleaved by SAN1, and produced a smear rather than discrete bands (Fig. 3.5F).

One unexpected feature of SAN1-mediated cleavage is that no products shorter than 25 nt were generated from the 3' labeled oligonucleotides. We speculated that SAN1 requires ~25 nt for binding, and cuts 5' to its binding site, a model which predicts that an oligonucleotide of 25 nt or less would not be a SAN1 substrate. Indeed, a 25 nt

Figure 3.5: SAN1 possesses a unique type of 5' exonuclease activity. (A) Immunoblot (top) and silver stain (bottom) of wild-type (WT) SAN1, D90A SAN1, and vector (V) eluates used in nuclease assays. L denotes protein molecular weight ladder. (B) Cleavage of splayed arm or 3' flap DNA structures. * denotes oligonucleotide with 5' ^{32}P-label. (C) Cleavage of ssDNA (X1 oligo) radioactively 5' (left panel) or 3' (middle and right panels) ^{32}P-labeled. The position of the fragments from a purine-specific chemical digestion of X1 oligo is indicated on the right. (D) Cleavage of different ssDNA sequences 3' ^{32}P-labeled. The position of the fragments from a purine-specific chemical digestion of the X1 oligo is indicated on the left. (E) Size and sequence of cleavage products from nuclease reactions with X1 or X4 oligo. (F) Cleavage of 3' ^{32}P-labeled ssDNA composed of all thymidines (X5 oligo).

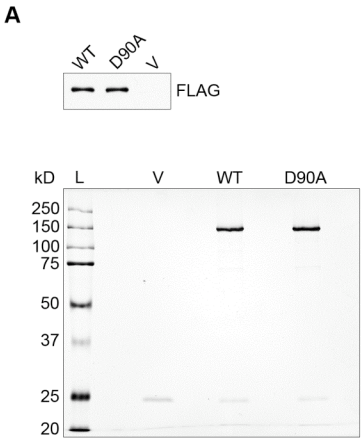

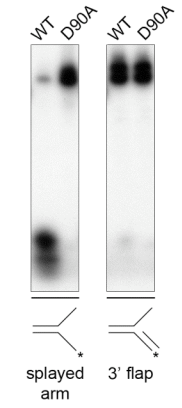

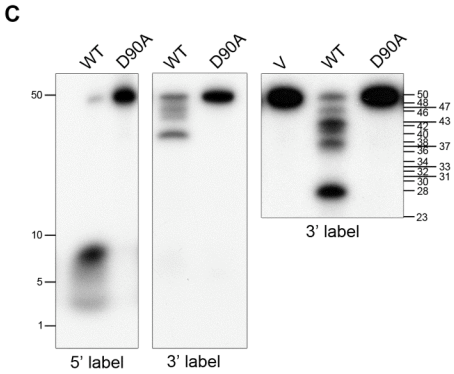

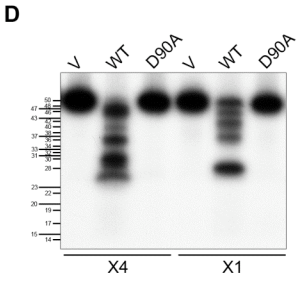

E

X1

Nucleotides	5' of cut site	3' of cut site	Nucleotides
3	TGG	GTCAACGTGGGCAAAGATGTCCTAGCAATGTAATCGTCTATGACGTT	47
7	TGGGTCA	ACGTGGGCAAAGATGTCCTAGCAATGTAATCGTCTATGACGTT	43
9	TGGGTCAAC	GTGGGCAAAGATGTCCTAGCAATGTAATCGTCTATGACGTT	41
13	TGGGTCAACGTGG	GCAAAGATGTCCTAGCAATGTAATCGTCTATGACGTT	37
22	TGGGTCAACGTGGGCAAAGATG	TCCTAGCAATGTAATCGTCTATGACGTT	28

X4

Nucleotides	5' of cut site	3' of cut site	Nucleotides
2	CA	ACGTCATAGACGATTACATTGCTACATGGAGCTGTCTAGAGGATCCGA	48
5	CAACG	TCATAGACGATTACATTGCTACATGGAGCTGTCTAGAGGATCCGA	45
10	CAACGTCATA	GACGATTACATTGCTACATGGAGCTGTCTAGAGGATCCGA	40
14	CAACGTCATAGACG	ATTACATTGCTACATGGAGCTGTCTAGAGGATCCGA	36
20	CAACGTCATAGACGATTACA	TTGCTACATGGAGCTGTCTAGAGGATCCGA	30
21	CAACGTCATAGACGATTACAT	TGCTACATGGAGCTGTCTAGAGGATCCGA	29
24	CAACGTCATAGACGATTACATTGC	TACATGGAGCTGTCTAGAGGATCCGA	26

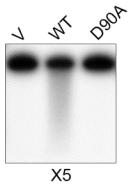

oligonucleotide did not generate any detectable products (Fig. 3.6A). To further investigate the substrate preference of SAN1, we tested double-stranded DNA (dsDNA). Unlike ssDNA substrates, a dsDNA substrate with one of the strands 3' labeled was not cleaved by SAN1 (Fig. 3.6B). We conclude that SAN1 has highly unusual 5' to 3' exonuclease activity that requires the DNA to be single-stranded and more than 25 nt in length. The data are consistent with a model in which the enzyme slides down the ssDNA and cuts 5' to its binding site at intervals, in a sequence-specific manner.

To determine if the nuclease activity of SAN1 is required for repair of ICLs we generated cDNAs of SAN1-FLAG containing silent mutations, which made the transcribed mRNA resistant to knockdown by a SAN1 siRNA. The siRNA decreased endogenous SAN1, but the WT and D90A variants expressed to similar levels in the presence or absence of the siRNA (Fig. 3.6C). Treatment of cells with SAN1 siRNA increased their sensitivity to cisplatin compared to control, but when the SAN1 knockdown cells expressed WT SAN1, the sensitivity was significantly decreased, whereas SAN1 (D90A) remained sensitized to cisplatin treatment (Fig. 3.6D). The level of rescue was consistent with the cell transfection efficiency (~50%). This result confirms that the phenotype of SAN1 knockdown is not due to an off-target effect and, most importantly, demonstrates that the nuclease activity is indispensable for the role of SAN1 in ICL repair.

Figure 3.6: ssDNA exonuclease activity of SAN1 is necessary for survival to ICLs.

(A) Cleavage of 3' ^{32}P-labeled ssDNA of either 50 (X1 oligo) or 25 (X3 oligo) nucleotides (nt) in length. (B) Cleavage of 3' ^{32}P-labeled ssDNA (X1 oligo) or dsDNA. (C) Immunoblot of cells transfected with indicated siRNA and rescue plasmid. (D) Clonogenic survival assay of cells transfected with indicated siRNA and rescue plasmid. For each transfection, colony number of untreated cells is defined as 100%. n = 4; error bars represent SD; (*) $P < 0.0001$.

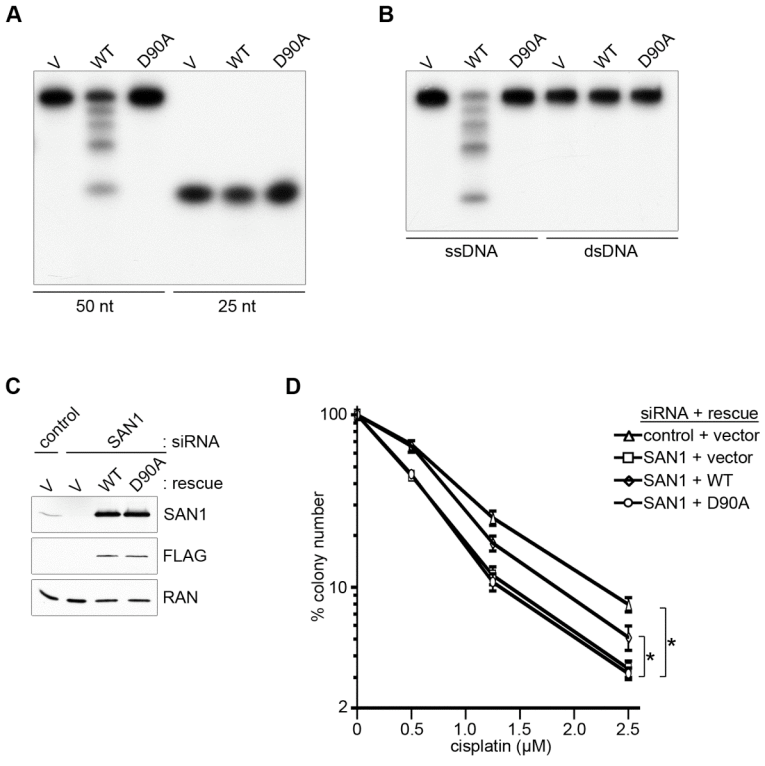
A
V
WT
D90A
V
WT
D90A
50 nt
25 nt
B
V
WT
D90A
V
WT
D90A
ssDNA
dsDNA
C
control
SAN1
: siRNA
V
V
WT
D90A
: rescue
SAN1
FLAG
RAN
D
siRNA + rescue
control + vector
SAN1 + vector
SAN1 + WT
SAN1 + D90A
% colony number
100
10
2
0
0.5
1.0
1.5
2.0
2.5
cisplatin (μM)
*
*

SAN1 translocates to the nucleus during ICL repair and requires septins for proper localization in the absence of damage.

Septins are exclusively cytoplasmic proteins, but DNA repair enzymes must access the nucleus, therefore, it was of interest to determine the subcellular distribution of SAN1. Expression of the nuclease was too low to detect by standard immunofluorescence, but tyramide amplification permitted the specific detection of endogenous SAN1, which was abolished by knockdown of SAN1 expression (Fig. 3.7). Staining was cytoplasmic, as predicted from its interaction with septins; however, when cells were damaged with either cisplatin or MMC, SAN1 partially re-localized and accumulated in the nucleus (Fig. 3.8A). To further test the subcellular distribution, we expressed SAN1-FLAG, which was also mostly cytoplasmic in control cells and seen as filaments, detected under the nucleus, which co-localized with septins (Fig. 3.8B). Also, SAN1-FLAG moved partially into the nucleus following damage by ICL-inducing agents, consistent with endogenous SAN1 staining (Fig. 3.8C). Considering that septins have diverse roles as signaling scaffolds, we tested if loss of septins might affect SAN1 localization. As a note, septins play multiple additional roles in cytokinesis and cytoskeletal organization, so silencing of SEPT7 causes changes in cell shape and cytokinetic defects that can result in multi-nucleation [38]. Strikingly, depletion of septins caused a partial redistribution of endogenous and SAN1-FLAG into the nucleus, even in the absence of DNA damage (Fig. 3.8D,E and Fig. 3.9). Thus, septins are necessary for the proper subcellular localization of SAN1 in the absence of damage.

Figure 3.7: Specificity of SAN1 antibody. Confocal images of cells transduced with indicated shRNA and treated as indicated (left) and stained with anti-SAN1 antibody. DRAQ5 was used to visualize nuclei.

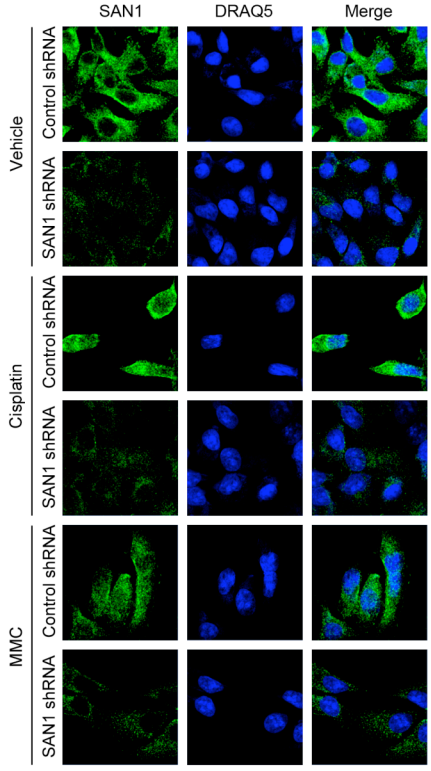
SAN1
DRAQ5
Merge
Vehicle
Control shRNA
SAN1 shRNA
Cisplatin
Control shRNA
SAN1 shRNA
MMC
Control shRNA
SAN1 shRNA

Figure 3.8: DNA ICLs increase nuclear accumulation of SAN1 and depletion of septins cause mislocalization of SAN1. (A) Confocal images of HeLa cells treated and stained with antibodies as indicated. DRAQ5 used to visualize nuclei. Images are confocal sections through the middle of cells. (B) Confocal images of HeLa cells expressing SAN1-FLAG stained with antibodies as indicated. DRAQ5 used to visualize nuclei. Images are confocal sections taken in different locations in z-axis, either through the middle of cells (Middle) or under the nucleus (Under). (C) Same as A, but with HeLa cells expressing SAN1-FLAG. (D) Confocal images of HeLa cells transfected with indicated siRNA and stained with antibodies as indicated. (E) Same as D, but with HeLa cells expressing SAN1-FLAG. Bar graphs are ratio of nuclear (F_{NUC}) to cytoplasmic (F_{CYTO}) fluorescence of endogenous SAN1 (A,D), or SAN1-FLAG (C,E), with vehicle (A,C), or siControl (D,E) defined as 1. n = 15-93; error bars represent SE; (*) $P < 0.05$; (**) $P < 0.001$; (***) $P < 0.0001$.

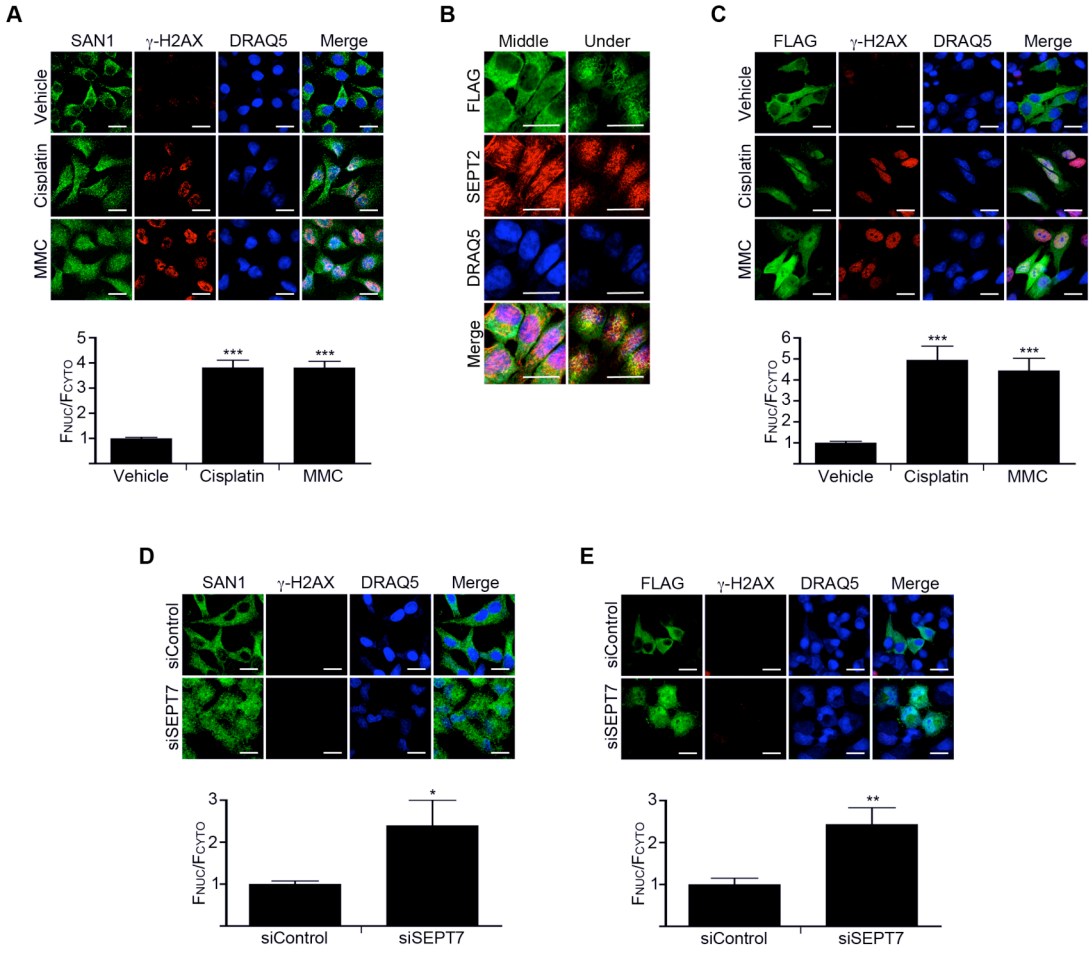
A
SAN1
γ-H2AX
DRAQ5
Merge
Vehicle
Cisplatin
MMC
FNUC/FCYTO
***
***
Vehicle
Cisplatin
MMC
B
Middle
Under
FLAG
SEPT2
DRAQ5
Merge
C
FLAG
γ-H2AX
DRAQ5
Merge
Vehicle
Cisplatin
MMC
FNUC/FCYTO
***
***
Vehicle
Cisplatin
MMC
D
SAN1
γ-H2AX
DRAQ5
Merge
siControl
siSEPT7
FNUC/FCYTO
*
siControl
siSEPT7
E
FLAG
γ-H2AX
DRAQ5
Merge
siControl
siSEPT7
FNUC/FCYTO
**
siControl
siSEPT7

Figure 3.9: Effect of SEPT7 knockdown on SEPT2. Confocal images of cells transfect with indicated siRNA (left) and stained with anti-SEPT2 antibody. DRAQ5 was used to visualize nuclei.

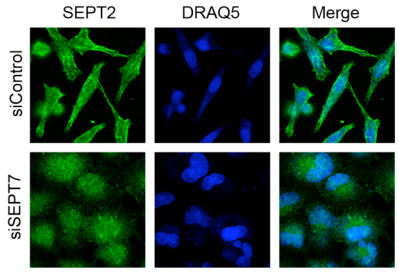
SEPT2
DRAQ5
Merge
siControl
siSEPT7

Septins and SAN1 are necessary for efficient HR

We next sought to determine at what stage of ICL repair SAN1 and septins act. Resolution of ICLs is a complicated process involving numerous repair proteins, but two major steps involving nucleases are unhooking of the lesion and HR. We initially measured HR efficiency, using a reporter system induced by I-Sce1, which generates a double-stranded break between tandem mutant copies of GFP [306]. HR at the break generates functional wild-type GFP, detectable by flow cytometry. Depletion of SAN1 or septins significantly reduced the frequency of HR compared to control (Fig. 3.10A,B). Although significant, the HR defect was modest (50 – 70% reduction), similar to that previously found for FA proteins, which have a relatively minor defect in HR when assayed in the context of this reporter system [220, 249].

To further test the involvement of SAN1 and septins in HR, we used a new, quantitative luciferase-based HR assay. The assay uses two overlapping fragments of the firefly luciferase plasmid, one containing the promoter and the 5' region of luciferase and the other containing the remaining 3' part of the gene, lacking a start codon (Fig. 3.10C,D). Formation of a functional firefly luciferase open reading frame requires in-frame recombination of the two fragments, and indeed, only when both plasmids are co-transfected is a substantial signal produced (Fig. 3.10E). One advantage of this assay is the renilla internal control, which will correct for nonspecific toxic effects of gene silencing. To validate the luciferase assay, we tested the effects of silencing RAD51, a recombinase known to be necessary for HR [171], and KU70, a component of non-homologous end-joining, the depletion of which has been shown previously to increase

Figure 3.10: SAN1 and septins are required for efficient HR. (A) GFP-based HR assay. Cells were transfected with indicated siRNA and following depletion, cells were transfected with a plasmid expressing I-Sce1 or vector. GFP expression was determined by flow cytometry and cells transfected with control siRNA is defined as 100%. n = 6; error bars represent SE. Immunoblot of cells transfected with control or SAN1 siRNA shows knockdown efficiency. (B) Same as A, except cells were transfected with control or SEPT7 siRNA. n = 4-5; error bars represent SE. (C) Diagram of plasmids used in luciferase-based HR assay. pK-Firefly-luciferase is digested with the indicated restriction enzymes to produce two fragments, long and short. (D) Ethidium bromide-stained DNA agarose gel of pK-Firefly luciferase plasmid cut with single-cutting restriction enzyme (linear), uncut, or digested as described in C. bp = basepairs. (E) Cells were transfected with indicated plasmids (bottom) and renilla normalization plasmid. Firefly to renilla ratio for long + short is defined as 100%. n = 9; error bars represent SD. (F) Cells were transduced with control or RAD51 shRNA and were transfected with firefly long and short plasmids and renilla normalization plasmid. Immunoblot shows knockdown efficiency. For graph firefly to renilla ratio for control is defined as 100%. n = 9-12; error bars represent SD. (G) Same as E, except cells were transduced with control or KU70 shRNA. n = 7-9; error bars represent SD. (H) Cells were transduced with indicated shRNA and were transfected with firefly long and short plasmids and renilla normalization plasmid. Firefly to renilla ratio for control is defined as 100%. n = 6-35; error bars represent SD. (*) $P < 0.01$; (**) $P < 0.001$ (***) $P < 0.0001$.

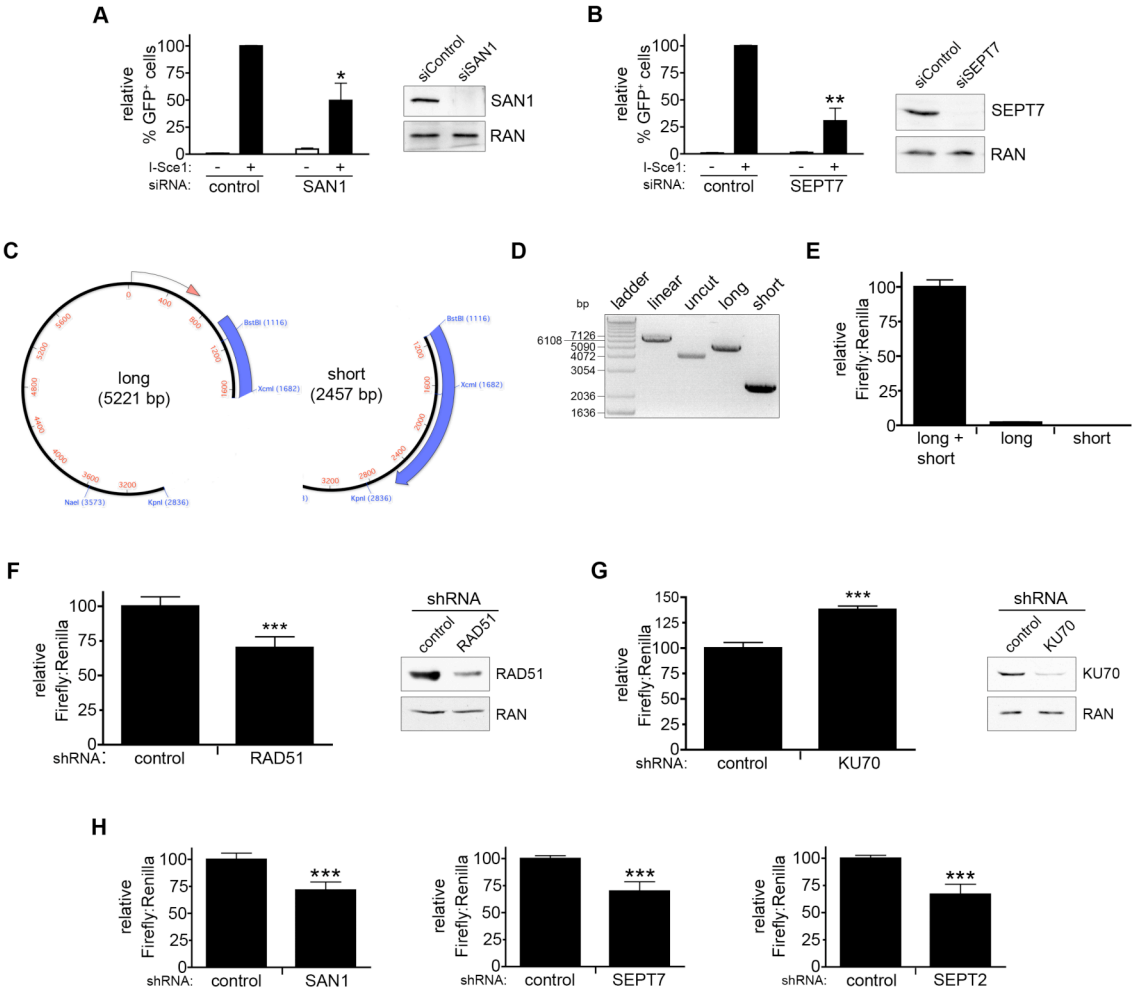
A
relative % GFP+ cells
100
75
50
25
0
*
I-Sce1: - + - +
siRNA: control SAN1
siControl
siSAN1
SAN1
RAN
B
relative % GFP+ cells
**
I-Sce1: - + - +
siRNA: control SEPT7
siControl
siSEPT7
SEPT7
RAN
C
long
(5221 bp)
short
(2457 bp)
BstBI (1116)
XcmI (1682)
NaeI (3573)
KpnI (2836)
D
bp
ladder
linear
uncut
long
short
6108
7126
5090
4072
3054
2036
1636
E
relative Firefly:Renilla
long + short
long
short
F
relative Firefly:Renilla
***
shRNA: control RAD51
shRNA
control
RAD51
RAD51
RAN
G
relative Firefly:Renilla
150
125
100
75
50
25
0
***
shRNA: control KU70
shRNA
control
KU70
KU70
RAN
H
relative Firefly:Renilla
***
shRNA: control SAN1
shRNA: control SEPT7
shRNA: control SEPT2

HR efficiency [307]. Consistent with these functions, cells expressing shRNA against RAD51 exhibited a significant decrease in luciferase activity, while silencing of KU70 increased luciferase activity compared to control cells (Fig. 3.10F,G). While basal luciferase activity is quite high, the assay is extremely sensitive and quantitative, enabling precise measurements of extra-chromosomal HR efficiency. Using this reporter system in cells depleted of SAN1 or septins we observed a significant decrease in the efficiencies of HR compared to a control knockdown (Fig. 3.10H). Taken together, these data demonstrate that both SAN1 and septins are involved in HR.

Septins and SAN1 are necessary for DNA end resection during ICL repair

Unhooking of the DNA lesion creates DSBs, which initiate HR during ICL repair [221]. To test whether the decreased HR efficiency in cells depleted of SAN1 or septins results from a decrease in DSB formation we looked at γ-H2AX, a marker of DSBs [98]. Cells treated with cisplatin, and depleted of SAN1 or septins, did not show any difference in γ-H2AX phosphorylation compared to control (Fig. 3.11A). This result indicates that SAN1 and septins do not affect the detection and unhooking of ICLs, but participates in a downstream process.

After generation of DSBs, HR is initiated by 5'-3' resection, generating ssDNA that is coated by RPA [173, 174]. We hypothesized that the exonuclease activity of SAN1 could affect HR by controlling the end resection of DSBs. To test this mechanism, we analyzed RPA foci after exposure of cells to cisplatin. Depletion of either SAN1 or septins caused a significant decrease in both the average number of RPA foci per cell,

Figure 3.11: SAN1 and septins are required for formation of RPA foci. (A) Immunoblot of cisplatin treated cells transfected with indicated siRNA. RAN was used as a loading control. (B) Representative confocal images of cisplatin treated cells transfected with indicated siRNA and stained with anti-RPA antibody. (C) Average number of cisplatin-induced RPA foci per cell transfected with indicated siRNA. n = 3-5, > 100 cells/n; error bars represent SD. (D) Percent of indicated siRNA transfected cells with > 9 cisplatin-induced RPA foci per cell. n = 3-5, > 100 cells/n; error bars represent SD. (**) $P < 0.001$; (***) $P < 0.0001$. (E) Cells transfected with SAN1 siRNA and indicated SAN1 rescue plasmid. Representative confocal images of cisplatin treated cells stained with anti-RPA antibody, FLAG antibody to detect rescue plasmid, and DRAQ5 used to visualize nuclei. Graphs show average number of cisplatin-induced RPA foci per cell and percent of cells with > 9 cisplatin-induced RPA foci per cell. n = 18-21.

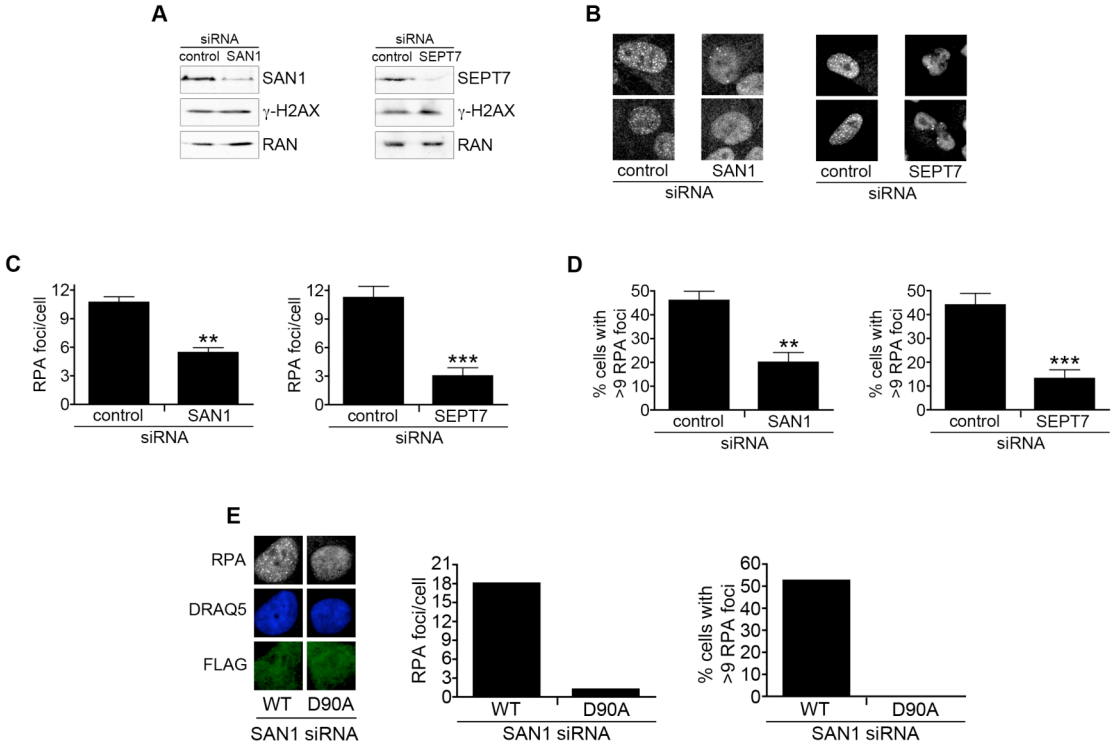
A
siRNA
control SAN1
SAN1
γ-H2AX
RAN
siRNA
control SEPT7
SEPT7
γ-H2AX
RAN
B
control
SAN1
siRNA
control
SEPT7
siRNA
C
RPA foci/cell
12
9
6
3
0
**
control
SAN1
siRNA
RPA foci/cell
12
9
6
3
0
***
control
SEPT7
siRNA
D
% cells with >9 RPA foci
50
40
30
20
10
0
**
control
SAN1
siRNA
% cells with >9 RPA foci
50
40
30
20
10
0
***
control
SEPT7
siRNA
E
RPA
DRAQ5
FLAG
WT
D90A
SAN1 siRNA
RPA foci/cell
21
18
15
12
9
6
3
0
WT
D90A
SAN1 siRNA
% cells with >9 RPA foci
60
50
40
30
20
10
0
WT
D90A
SAN1 siRNA

and in the average number of cells with more than nine RPA foci (Fig. 3.11B-D). To determine if the nuclease activity of SAN1 is required for end resection we expressed WT and D90A variants of siRNA resistant cDNA in cells transfected with SAN1 siRNA. We then analyzed RPA foci after exposure of cells to cisplatin. Expression of WT SAN1 rescued the decrease in RPA foci, while SAN1 (D90A) remained decreased in both the average of RPA foci per cell, and in the average number of cells with more than nine RPA foci. These data strongly suggest that SAN1 and septins are involved in the end resection of DSBs during ICL repair.

Conclusions

While circumstantial evidence has linked septins to DDR signaling, mechanisms have remained unclear and it was unknown whether these cytoskeletal proteins might also be engaged in DNA repair. We were surprised, therefore, to discover that silencing of the septin 2,6,7 complex compromises the survival of cells exposed to several different types of DNA damaging agents. However, these observations are supported by the results of previous genome-wide screens for genes involved in the DDR, which uncovered several septins as candidates [248, 277, 308, 309].

Our investigation of potential mechanisms through which septins might interface with the DDR unexpectedly revealed an association with an uncharacterized protein that possesses nuclease activity, and which we have named Septin-Associated Nuclease 1, SAN1. While these data demonstrate the involvement of septins in the response to ICL-inducing agents through the actions of SAN1, the mechanism of septins in response to

other DNA damage agents remains to be determined. SAN1 is a FEN1-related exonuclease, necessary for the efficient repair of ICLs by resecting DSBs formed from the unhooking of the lesion, which leads to the initiation of HR and resolution of the damaged DNA. SAN1 is unusual in that it specifically cleaves from the 5' end of ssDNA at apparently random intervals of 2 – 10 nts. The cleavages appear to be sequence-specific, but we have been unable, thus far, to decipher the code that governs cleavage site identity. Since SAN1 will not cut oligonucleotides shorter than ~25 nt, we speculate that it binds 3' to the cleavage sites, and that these sites are ~25 nt 5' to binding. Interestingly, SAN1 re-localizes from the cytoplasm to the nucleus during DNA damage.

Functionally, septins prevent the inappropriate nuclear accumulation of SAN1 in the absence of DNA damage. Additionally, however, septins must somehow convey an activating signal to SAN1, because nuclear accumulation of SAN1 caused by depletion of septins is insufficient in itself to enable efficient repair of ICLs. This suggests that retention of SAN1 in the cytoplasm by septins is necessary for the activation of SAN1, indicating that septins might be acting as a signaling platform during the DDR. To test this possibility, the SAN1 and septin interaction should be examined. The region in SAN1 necessary for septin binding would need to be identified and then exploited to determine if the effects of SAN1 knockdown and septin knockdown are correlated or causative. Rescue experiments with SAN1 variants lacking the septin binding domain could be examined for their localization, which would test if septins are necessary for their cytoplasmic retention.

It is also possible SAN1 and septins are functioning independently of each other. Rescue experiments for any of the functional assays, such as colony survival with ICLs, HR and RPA foci formation with a SAN1 variant that is unable to bind to septins would test if the interaction of SAN1 with septins is necessary for SAN1 function. However, these tests would still not identify the underlying mechanism of this interaction. The model presented here suggests septins relay a signal to SAN1 during the DDR. To test this, post-translational modifications, such as phosphorylation and mono-ubiquitination on SAN1 or septins, which have been demonstrated to be important for the function of other DDR proteins, could be explored. Further studies would then be necessary to determine if these modifications lead to a change in binding partners, or a change in protein structure.

SAN1 is a new exonuclease involved in HR, specifically during end resection of ICL repair. Because of the potential involvement of other exonucleases, such as EXO1 and DNA2 in HR during ICL repair, it would be important to test for the expression levels of these nucleases in SAN1 knockdown cells. It would also be of interest to identify other SAN1 interacting proteins during ICL repair. Proteomic analysis of SAN1 in cells treated with ICL agents should identify associated proteins, specifically the nuclear fraction of SAN1. It is possible SAN1 could interact with components of the FA complex, other nucleases, and helicases. Overall, these data identify a new member of the FEN1 family of nucleases, reveal its role in the resolution of ICLs, and highlight a novel and unexpected link between cytoskeletal elements and the DNA repair machinery.

Chapter 4: Discussion

Every day, the approximately 10^{13} cells in the human body receives tens of thousands of DNA lesions, that if left unrepaired, or repaired incorrectly, can lead to mutations, genomic instability, cell death, disease, premature aging, and cancer [262]. The DDR has evolved to cope with these insults, coordinating multiple proteins and pathways to ensure DNA integrity and cellular survival. The breadth of this response is becoming increasingly understood as multiple screens have been performed to look for proteins involved in multiple aspects of the cellular response to DNA damage. While these screens reinforce the involvement of key proteins in the DDR, they also discover the potential involvement of proteins involved in other cellular processes. A screen that highlights the complexity of the DDR was one designed to look for phosphorylation substrates of the PIKK family, particularly ATM and ATR [277]. The screen identified over 900 sites on more than 700 proteins, with functional analysis performed on 421 candidate substrates revealing many biological processes potentially involved in the DDR [277]. While many known proteins and pathways were identified, there were also proteins involved in cellular processes such as insulin signaling, cell structure and motility, intracellular protein traffic, as well as many others that were previously unconnected, or only hinted at in previous studies [277]. Although this screen was designed to find only ATM and ATR substrates, based on the kinases substrate preference for a glutamine C-terminally adjacent to a serine, or threonine, other kinases could have phosphorylated these sites, although the response would still have been

activated in response to DNA damage [310, 311]. Of particular interest to the work presented here, SEPT6 was identified in this screen with potential phosphorylations on three serine residues, all present in the coiled-coil domain [277]. Although, these phosphorylations have not been confirmed, the identification of SEPT6 in a screen for phosphorylation targets during the DDR suggests septins might play a role during this process.

Septins have been implicated in the DDR in both yeast and human cells. In yeast, septins were reported to bind the CHK2 homolog Rad53, where, through unknown mechanisms, septins participate in the response to DNA damage, in particular DNA replication stress [77, 78]. Interestingly, Rad53 was shown to directly phosphorylate the septin Shs1 using recombinant proteins, which, at least in the context of DNA damage induced by the alkylating agent MMS, was confirmed *in vivo* [78, 312]. However, to date, there is no evidence of CHK2 phosphorylation of a human septin. In human cells, though, previous work in our lab also indicated the involvement of septins in the DDR. This was through septins involvement in mediating the localization of SOCS7 and NCK [76]. Septins appear to be necessary for regulating the predominantly cytoplasmic localization of these adaptor proteins, which, through an unknown mechanism, become mostly nuclear upon DNA damage [76]. The nuclear accumulation of NCK only occurs in cells mounting a proper DDR and although it is not dependent on CHK2, it does require PIKK family activity, specifically ATR during UV damage. NCK negatively regulates the phosphorylation, and activation, of p53, because depletion of NCK, or SOCS7, results in hyper-phosphorylation of p53 on serine 15, a residue that is

phosporylated by PIKK family members, in addition to CHK1 and CHK2 [118, 120, 128, 129, 313]. Furthermore, loss of NCK, or SOCS7, results in cells undergoing early DNA damage-induced apoptosis.

Several questions remain to be answered about the mechanism of NCK nuclear accumulation in response to DNA damage, as well as how NCK negatively regulates p53 phosphorylation and apoptosis. Although, an ATR specific inhibitor blocked the nuclear accumulation of NCK following UV irradiation, determining how this signal is relayed to retain NCK in the nucleus will be important to elucidate. Since NCK is cycling between the nucleus and cytoplasm, it is possible NCK and/or SOCS7, or another unidentified binding partner could be modified and thus retained in the nucleus during the DDR. Possible candidates might be c-Abl and EGF receptor, which have been shown to interact with NCK and have been shown to relocalize to the nucleus upon DNA damage where they interact with the PIKK family [314-319]. It is also possible NCK is acting as an adaptor in the nucleus during the DDR and it is only when a nuclear binding partner of NCK in the nucleus becomes modified does NCK remain nuclear. Similarly, identifying how NCK negatively regulates p53 phosphorylation and how it specifically protects against apoptosis would be of interest. Identifying NCK1 and NCK2 specific binding partners during the DDR might help elucidate the mechanism. NCK might transport proteins into the nucleus during the DDR, or act as a scaffold in the nucleus. The phosphorylation of p53 on serine 15 prevents its interaction with MDM2, thus preventing its degradation, and resulting in nuclear accumulation of p53 [125]. It could be possible that NCK might somehow foster this interaction, either directly, or indirectly by blocking

p53 phosphorylation, to keep p53 levels low during the DDR and in the absence of nuclear NCK, p53 phosphorylation and protein levels increase above what they normally would during the DDR. Indeed, p53 protein levels have been shown to oscillate during the DNA damage response, and only when they are sustained at a high level do cells undergo apoptosis [320]. Interestingly, p53, besides having a function as a nuclear transcription factor for genes involved in cellular responses such as apoptosis and cell cycle control, also has additional roles in the cytoplasm, where it has been shown to induce apoptosis via mitochondrial outer membrane permeabilization by directly activating Bax [321-323]. Thus, NCK might perform an inhibitory role during this process separate from the function of NCK negatively regulating p53 phosphorylation. More study should determine how the NCK proteins mediate their effects during the DDR.

Mammalian septins are also involved in the DDR through the interaction with a new DNA repair exonuclease, SAN1. The central region of SAN1, composed of unusual repeated motifs, is necessary for this interaction, although further study will determine if the repeats are sufficient and if this interaction is direct. In addition to the redistribution of NCK and SOCS7, depletion of septins also mislocalize SAN1. This suggests there is an underlying mechanism of how septins are involved in the DDR. In both situations, septins are necessary to prevent the inappropriate nuclear accumulation of the associated proteins in the absence of DNA damage. It is possible septins are binding and sequestering these proteins in the cytoplasm until they are released through some mechanism. However, in the case of NCK and SOCS7, this is probably not occurring

since these proteins still accumulated in the nucleus after cells were treated with the Crm1 inhibitor leptomycin B, in the presence of intact septins, indicating septins are not preventing the cycling of these proteins [76].

Whether SAN1 is also cycling in the absence of DNA damage has yet to be determined, but additionally, septins must somehow convey an activating signal to SAN1, because nuclear accumulation of SAN1, caused by depletion of septins, is insufficient in itself to enable efficient repair. Septins roles in maintaining the correct localization of SAN1 in the absence of damage and transmission of an activating signal are not necessarily mutually exclusive. If SAN1 is cycling between the nucleus and cytoplasm in the absence of damage, it is possible SAN1 is activated and recruited in the nucleus upon DNA damage recognition. It is also possible that DNA damage could lead to the activation of a nuclear protein, thus triggering its relocalization to the cytoplasm where it could release SAN1 from septins and also possible activate SAN1. Indeed, this is similar to how the transcription factor NF-κB, which is kept inactive in the cytoplasm through an interaction with inhibitor of κB (IκB), is activated in response to DNA damage [324, 325]. DNA damage induces ATM phosphorylation of NF-κB essential modulator (NEMO), which results in ubiquitination and then nuclear export of NEMO [326, 327]. Cytoplasmic NEMO activates the IκB kinase, which phosphorylates and degrades IκB and thus activates NF-κB, which then translocates into the nucleus to regulate gene transciption [326-328]. While NEMO might not be a candidate to perform this function with septins and SAN1, the checkpoint kinase MK2 could perform this function. Following DNA damage, MK2 translocates from the nucleus to the cytoplasm,

where it phosphorylates downstream effector proteins [329]. Interestingly, a recent phospho-proteomic screen for CHK1 identified SEPT7 as a potential substrate [330]. CHK1, CHK2 and/or MK2 could be responsible for this phosphorylation since these three kinases share similar consensus motifs, and MK2 has been shown to phosphorylate CHK1 substrates in cells [104, 329].

The activating signal septins somehow convey to SAN1 to enable efficient ICL repair might be to facilitate the phosphorylation of SAN1, or an associated protein. This phosphorylation event may be necessary for the retention of SAN1 in the nucleus during DNA damage possibly through an interaction with a BRCT domain-containing protein. Septins are required for SAN1 binding to BRCT domains following DNA damage, which could be explained by SAN1, or an associated protein, not being phosphorylated. Thus, even though loss of septins leads to mislocalization of SAN1, SAN1 is unable to be activated and/or properly localized to sites of DNA damage. Further studies to identify the BRCT domain-containing protein, as well as the phosphorylation of SAN1, or an associated protein, should elucidate the mechanism of SAN1 activation and nuclear retention. An important step will be determining if the phosphorylation occurs in the nucleus or the cytoplasm, and if septins are required.

The models presented here suggest septins play a role as a cytoplasmic scaffold in the regulation of associated proteins. This function of septins has been demonstrated for other proteins and pathways, but the involvement of septins in the nucleus during DNA damage cannot be ruled out. While endogenous septins seem to exist only as hetero-oligomers, overexpression of septins in mammalian cells, as well as purification of

recombinant septins, have shown septins can exist as dimers or monomers [11, 16, 19, 331]. However, no physiological functions of septin monomers or dimers have been described. Although the abundance of septins in the cytoplasm and that septin stability is dependent on other septins complicates studies, it would be interesting to investigate the potential role of septins in the nucleus during the DDR.

Our data identify SAN1 as a novel exonuclease necessary for ICL repair. The nuclease domain of SAN1 is related to other members of the FEN1 family of structure-specific nucleases. The conserved acidic residues are important for the activity of SAN1 and other members of the FEN1 family [332-336]. These residues coordinate two metal ions (Mg^{2+}or Mn^{2+}) to create the nuclease active site [337]. Recently the structure of FEN1 and EXO1 bound to DNA substrates was determined, which have defined other important and conserved features of the FEN1 family, including a K^{+}-binding site, a hydrophobic wedge, and a helical gateway formed by alpha helices [333, 334]. Additional studies should determine the importance of these features for substrate binding and SAN1 activity. Interestingly, we show SAN1 possesses exonuclease activity towards ssDNA that might be sequence dependent, although ssDNA secondary structure is more likely. This activity is unique compared to FEN1 family members, which appear to recognize the junction between dsDNA and ssDNA of a variety of substrates [302]. It is possible SAN1 also recognizes other substrates besides ssDNA and further studies would need to be done to determine this. Another interesting feature is the unique cleavage pattern of SAN1. Although the recognition sequence, or secondary structure, recognized by SAN1 should be determined with further studies, the current model

predicts SAN1 requires 25 nucleotides 3' of where the cleavage occurs. This would indicate SAN1 is binding these 25 nucleotides because nuclease activity is not recognized with a substrate of this length, nor are products produced smaller than ~25 nucleotides when a 50 nucleotide substrate is used. The nuclease domain of EXO1 was determined to bind 10 base pairs, which is in agreement with the crystal structure of EXO1 with DNA [334, 338]. Since it is likely the nuclease domain of SAN1 would bind the same length, the additional length must be through the remaining C-terminal portion of the protein. Future studies, such as a DNA footprinting assay, should be able to determine if this model is correct.

The 5' to 3' nuclease activity towards ssDNA, but not dsDNA, is consistent with a role of SAN1 in DNA end resection during ICL repair. However, because SAN1 appears unable to resect one strand of dsDNA, there must be a mechanism in which a displaced ssDNA is exposed for SAN1 to cleave. This is performed by helicases, which unwind the DNA at the DSB. The BLM helicase, which plays a role in end resection during DSB repair, has been implicated in ICL repair, but is postulated to function in the resolution of Holliday junctions [216, 256, 257]. The related RecQ homolog, WRN, has also been implicated in ICL repair, through interactions with HR proteins, including BRCA1, RAD51, RAD54, and RAD54B, however it is not clear where in the repair process WRN functions [339, 340]. The helicase, HEL308, has also been shown to be involved in ICL repair, through an interaction with the TLS polymerase, POLN, although it is suggested HEL308 functions in a late step of HR [251, 341]. Also, the MCM8/MCM9 helicase has recently been shown to be necessary for HR during ICL

repair, through the recruitment of RAD51, although similar to BLM, WRN, and HEL308, a role in end resection during ICL repair has not be determined [259-261]. Finally, the helicase FANCJ, one of the genes mutated in FA, functions in HR during ICL repair, although the precise nature remains unclear [342]. Interestingly, FANCJ was recently shown to participate in end resection with MRE11, but only during DSB repair, not ICL repair [343]. During ICL repair, FANCJ cooperates with components of the MMR machinery, such as interacting with MLH1, which is necessary for proper localization of FANCJ to sites of ICLs [343, 344]. The involvement of these, and other unidentified, helicases, in ICL repair illustrates the complexity of this repair process. Further studies should determine which helicase, or helicases, are working in cooperation with SAN1 during end resection of ICL repair.

Similar to the potential involvement of multiple helicases in end resection during ICL repair, multiple nucleases could also be involved. While the identification of FAN1, provided a mechanistic link between FANCD2 monoubiquitination and ICL repair, the exact step of where FAN1 acts to promote ICL repair remains unclear [248-250, 252]. While FAN1 possesses 5' to 3' exonuclease activity, it is unlikely to participate in end resection since RPA foci formation was not decreased following ICL formation, but instead persisted consistent with a downstream defect in the repair pathway [249, 250]. The endonuclease DNA2 and the exonuclease EXO1 were recently implicated in end resection during ICL repair [345]. DNA2 and EXO1 have been shown to be important in end resection during DSB repair [195, 197]. Interestingly, although DNA2 and EXO1, working in concert, are necessary for DNA end resection, their depletion results in a

defect in SSA and an increase in HR [345]. Thus, it appears the role of these nucleases during end resection alters the balance between which repair pathway is utilized. It is also likely that these nucleases are acting during a part of the cell cycle when a homologous region is not present, which would promote the use of the error-prone SSA pathway. Unlike DNA2 and EXO1, the role of SAN1 during end resection appears to promote a HR pathway, since loss of SAN1 results in a decrease in HR. Further studies should further elucidate the role of SAN1 in ICL repair and determine the possible coordination with other components of the FA and HR pathway.

It now appears mammalian septins are involved in the DDR, through the interaction of NCK and SAN1. There is also the possibility septins, through other interacting proteins, could have other connections to the DDR. Interestingly, a yeast two-hybrid screen of human septins found a number of novel septin-interacting proteins, some of which have a demonstrated role in the DDR, such as CASP8AP2, an associated protein of CASP8 necessary for apoptosis, the SUMO-conjugating enzyme UBC9 involved in the SUMOylation of BRCA1 during DNA damage, and thymine DNA glycosylase a BER enzyme which excises thymine when mispaired with guanine [346-349]. In addition, multiple septins were identified in a screen for proteins ubiquitinated in response to UV damage [350]. Intriguingly, a recent study demonstrated the ubiquitin ligase RNF8 monoubiquitinates septins [351]. Although this modification was not in response to DNA damage, RNF8 has an established role in recruiting repair proteins to DNA damage sites [352]. More studies should determine the importance of these interactions and

modifications and potentially expand, and further clarify, the role of septins during the DDR.

Our findings, summarized in Fig. 4.1A, demonstrate septins have multiple roles in the DDR. Septins through the adaptor protein NCK, regulate DNA damage induced p53 phosphorylation and apoptosis. This interaction is mediated by SOCS7, which is necessary for the nucleo-cytoplasmic translocation of NCK. Septins also mediate DNA repair, through the interaction with the novel DNA repair nuclease, SAN1. Following DNA damage, NCK and SAN1 accumulate in the nucleus where they appear to function. In addition to maintaining proper cellular localization, at least in the case of SAN1, septins are also necessary for relaying an activating signal. SAN1 localization to sites of damage appears to be dependent on an interaction with a BRCT domain containing protein, possibly mediated by SMC1. The interaction of SAN1 at the site of the ICL might also be facilitated by an interaction with PCNA. SAN1 is necessary for DNA end resection, a necessary step for HR and for proper resolution of ICLs (Fig. 4.1B). Further study should shed light on the exact mechanisms of SAN1 in ICL repair, as well as explore the possible involvement of septins in other aspects of the DDR.

Figure 4.1: Model of our findings. (A) Septins are involved in the DDR through interaction and regulation of the adaptor protein NCK, mediated by SOCS7, and SAN1. See text for more details. (B) SAN1 is necessary for DNA end resection during ICL repair. After unhooking and translesion synthesis past the flipped out lesion occurs, HR is completed, along with removal of the lesion, and replication is re-established. A necessary step during the HR step of ICL repair, where SAN1 acts, involves 5' – 3' end resection at the site of the DSB generated during removal of the lesion. The involvement of SAN1, and the necessity of DNA end resection, would occur whether one replication fork, or a second replication fork from the opposite direction, encounters the lesion.

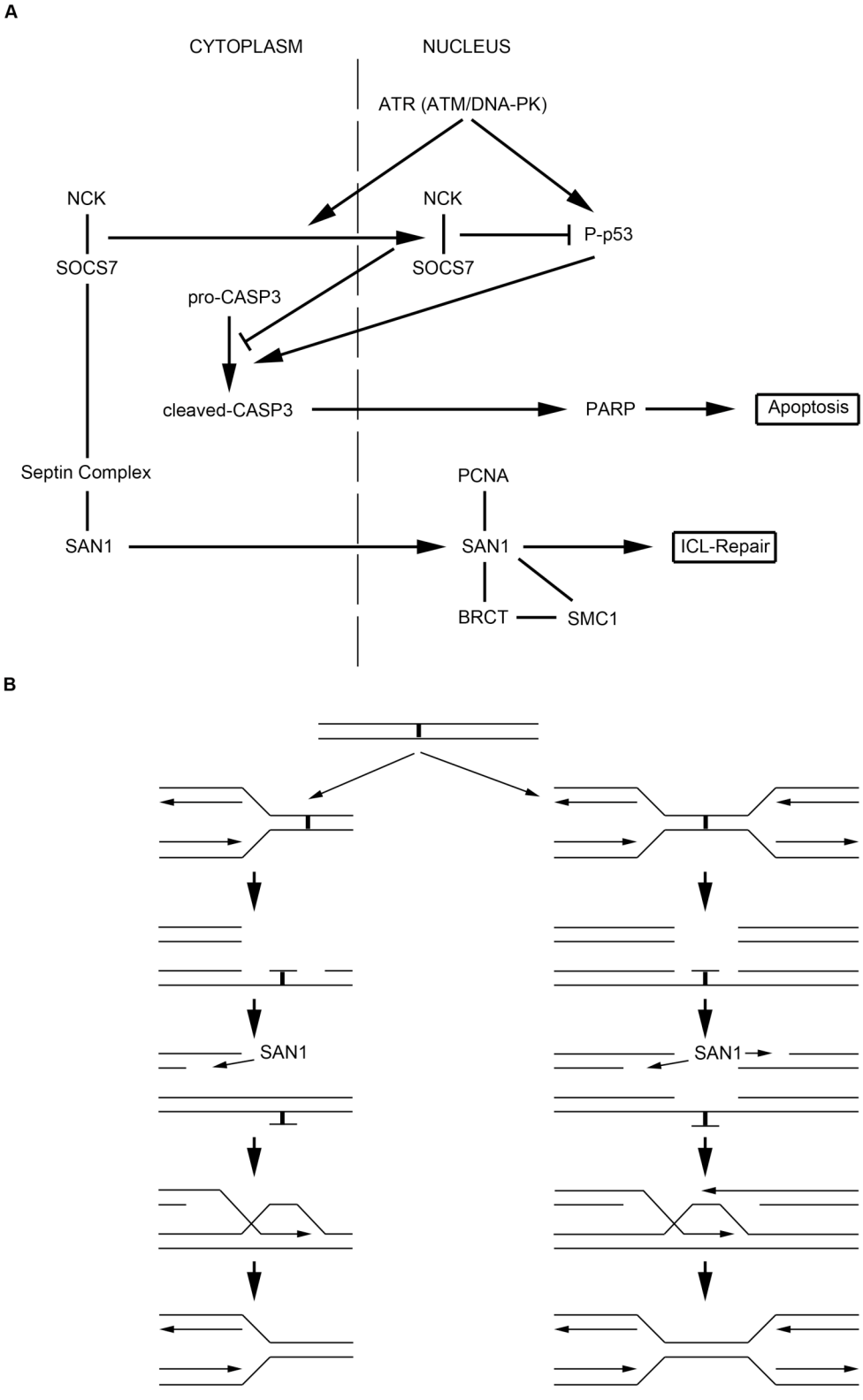
A
CYTOPLASM
NUCLEUS
ATR (ATM/DNA-PK)
NCK
SOCS7
NCK
SOCS7
P-p53
pro-CASP3
cleaved-CASP3
PARP
Apoptosis
Septin Complex
SAN1
PCNA
SAN1
ICL-Repair
BRCT
SMC1
B
SAN1
SAN1

Appendix I: Additional Data

Central repeats of SAN1 bind septins

In addition to the N-terminal FEN-1-related nuclease domain, composed of the two regions N and I, SAN1 also possesses a central region of unusual repeated motifs (Fig. 5.1A). Dot plot analysis of the amino acid sequence of SAN1 against itself revealed the repetitive region, which contains 15 repeats, of 12 amino acids each (Fig. 3.4A and Fig. 5.1B). A sequence alignment of the repeats was generated and reveals some conserved features[353]. At position four and eight there is a glutamic acid residue, and in between these residues, at position six, is a basic residue (Fig. 5.1C). This is interesting because at physiological pH, these would generate a positively charged residue in between two negatively charged residues. This might form a salt bridge between the oppositely charged residues either within a repeat, or more likely between repeats. Salt bridges have important roles in the stability and function of proteins, such as affecting oligomerization, flexibility, and affecting interaction specificity with other proteins and molecules that may be involved in allosteric regulation [354].

To test the requirement of the central repeats of SAN1 for binding to septins we expressed a variant of SAN1 expressing just the central region of SAN1 (255-700) that contains the repeats, or a variant of SAN1 that lacked all of the repeats (Δrepeat) (Fig. 5.1D). While Δrepeat expressed to a high level, 255-700 was undetected by immunoblot (Fig. 5.1D). This may be due the repetitive nature of the repeats, which might be

Figure 5.1: Characterization of septin binding region of SAN1. Repeat sequence of SAN1 is necessary for binding to septins. (A) Schematic of the domain architecture of SAN1. N-terminal nuclease domain (N), internal nuclease domain (I), central repeats (R). (B) Sequence of SAN1 with 15 central repeats highlighted in blue. (C) Graphical representation of an amino acid sequence alignment of the 15 central repeats generated by WebLogo [353]. (D) FLAG-tagged SAN1 variants 255-700 or Δrepeat were transfected into cells. Input lysates were analyzed by immunoblot to detect the indicted proteins. (E) Lysates from D were immunoprecipitated (IP) with anti-SEPT6 antibody or mouse IgG (mIgG) and analyzed by immunoblot to detect the indicated proteins. (F) Confocal images of HeLa cells expressing SAN1-FLAG-Δrepeat treated and stained with antibodies as indicated. DRAQ5 used to visualize nuclei. Images are confocal sections through the middle of cells.

A

B

```
1     MGVRGLQGFVGSTCPHICTVVNFKELAEHHRSKYPGCTPTIVVDAMCCLRYWYTPESWIC
61    GGQWREYFSALRDFVKTFTAAGIKLIFFFDGMVEQDKRDEWVKRRLKNNREISRIFHYIK
121   SHKEQPGRNMFFIPSGLAVFTRFALKTLGQETLCSLQEADYEVASYGLQHNCLGILGEDT
181   DYLIYDTCPYFSISELCLESLDTVMLCREKLCESLGLCVADLPLLACLLGNDIIPEGMFE
241   SFRYKCLSSYTSVKENFDKKGNIILAVSDHISKVLYLYQGEKKLEEILPLGPNKALFYKG
301   MASYLLPGQKSPWFFQKPKGVITLDKQVISTSSDAESREEVPMCSDAESRQEVPMCTGPE
361   SRREVPVYTDSEPRQEVPMCSDPEPRQEVPTCTGPESRREVPMCSDPEPRQEVPMCTGPE
421   ARQEVPMYTDSEPRQEVPMYTDSEPRQEVPMYTGSEPRQEVPMYTGPESRQEVPMYTGPE
481   SRQEVLIRTDPESRQEIMCTGHESKQEVPICTDPISKQEDSMCTHAEINQKLPVATDFEF
541   KLEALMCTNPEIKQEDPTNVGPEVKQQVTMVSDTEILKVARTHHVQAESYLVYNIMSSGE
601   IECSNTLEDELDQALPSQAFIYRPIRQRVYSLLLEDCQDVTSTCLAVKEWFVYPGNPLRH
661   PDLVRPLQMTIPGGTPSLKILWLNQEPEIQVRRLDTLLACFNLSSSREELQAVESPFQAL
721   CCLLIYLFVQVDTLCLEDLHAFIAQALCLQGKSTSQLVNLQPDYINPRAVQLGSLLVRGL
781   TTLVLVNSACGFPWKTSDFMPWNVFDGKLFHQKYLQSEKGYAVEVLLEQNRSRLTKFHNL
841   KAVVCKACMKENRRITGRAHWGSHHAGRWGRQGSSYHRTGSGYSRSSQGQPWRDQGPGSR
901   QYEHDQWRRY
```

C

D

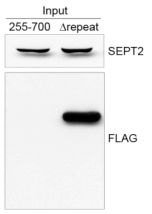

E

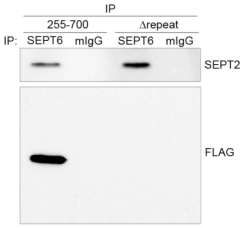

F

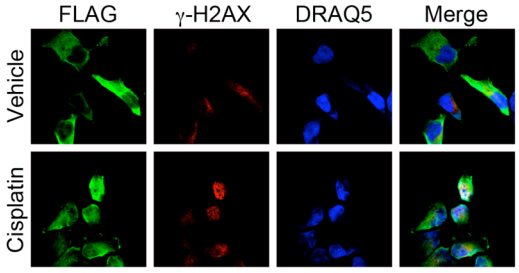

unstructured, and thus vulnerable to degradation or insolubility. When SEPT6 was immunoprecipitated from these lysates, the 255-700 variant interacted specifically with septins and was enriched greatly considering it was undetectable on the input blot, while the Δrepeat was undetectable (Fig. 5.1E). This indicates the central repeats of SAN1 are interacting with septins. However, when the Δrepeat variant was expressed in cells and visualized by immunofluorescence, the SAN1 variant still localized to the cytoplasm and partially relocalized to the nucleus upon cisplatin treatment (Fig. 5.1F). Although the repeats are necessary for a biochemical interaction with septins in soluble cellular extract, this data suggests the region might not be the only interaction SAN1 makes with septins in the context of an intact cellular architecture. Further study should determine the nature of the septin and SAN1 interaction; such as whether it is direct and what other region, or regions, of SAN1 interact with septins. Further insight into how these proteins interact should help elucidate how septins regulate SAN1 function during ICL repair.

SAN1 interacts with PCNA and BRCT domains

Many proteins involved in DNA repair form associations with PCNA, a DNA clamp that functions as a recruiter, organizer, and a cofactor during catalytic steps, and with proteins that contain BRCT domains, which recognize peptide sequences phosphorylated by PIKK family members during the DDR [102, 355-357]. Interestingly, within the SAN1 sequence are candidate motifs for both proteins – the PCNA binding motif in the nuclease domain (RFALK) and the BRCT motif in the C-terminal region

(SQAF). The potential PCNA binding motif is not a classical PIP (PCNA-interacting peptide) sequence, but instead a recently identified APIM (AlkB homologue 2 PCNA-interacting motif) [358]. The potential BRCT binding motif, characterized by an aromatic residue at position +3 of the phosphorylated residue, would be recognized by a type 1 BRCT domain-containing protein since it is not at the carboxyl terminus of SAN1 [102]. Based on this we used the tandem BRCT motifs of BRCA1, which has been shown to bind peptides similar in sequence and location to the potential BRCT motif in SAN1 [100, 101, 359]. To test if SAN1 interacts with these two proteins, we used recombinant GST-fusions on glutathione beads incubated with FLAG-tagged SAN1 from cell extracts. Both PCNA and BRCT domains specifically pulled down SAN1 (Fig. 5.2A). We confirmed that SAN1 binding to BRCT domains are phosphorylation-dependent by treating lysate with lambda phosphatase prior to incubation with bound BRCT domains, which decreased SAN1 binding (Fig. 5.2B,C).

Since BRCT domains are present on proteins involved in the DDR, and in particular DNA repair, and used to recruit proteins to sites of damage we next used this binding assay to determine if SAN1 binding increases upon induction of ICLs. 293T cells expressing FLAG-tagged SAN1 were treated with the ICL-inducing agents cisplatin, MMC, or UV irradiation prior to extract preparation. BRCT association with SAN1 was not altered by UV irradiation, but was significantly enhanced when the cells were treated with ICL-inducing agents (Fig. 5.2D-F). Taken together with the relocalization of SAN1 from the cytoplasm to the nucleus during ICL repair, this suggests SAN1 may be recruited to sites of damage by interacting with a BRCT domain-containing protein.

Figure 5.2: Recombinant PCNA and BRCT domains bind to SAN1. SAN1 binds recombinant PCNA and BRCT domains and increases BRCT binding with ICL-inducing agents, which is dependent on septins. (A) Recombinant GST-tagged BRCT domains, GST-PCNA, or GST vector were used to co-precipitate Flag-tagged SAN1 from cellular extract. Immunoblots show GST-tagged proteins used as bait and amount of Flag-tagged SAN1 protein that co-precipitated. (B-C) SAN1 interaction with BRCT domains are phosphorylation dependent. (B) Flag-tagged SAN1 was transfected into cells and lysates were treated with, or without, lambda phosphatase (λ PPase) prior to binding assay. Input lysates were analyzed by immunoblot to detect Flag-tagged SAN1. (C) Binding assay was performed as described in A with lysates from B. (D-F) ICL-inducing agents increase binding to BRCT domains. (D) Flag-tagged SAN1 was transfected into cells and treated as indicated prior to extract preparation. Input lysates were analyzed by immunoblot to detect indicated proteins. (E) Binding assay was performed as described in A with lysates from D. (F) Quantification of BRCT binding assays. For each set analyzed the IP to input ratio of Flag-tagged SAN1 treated with vehicle was set to 1. Error bars, ± 1 sem, n = 3. Data analyzed by paired, two-tailed *t*-test. (G-I) Depletion of septins block cisplatin-induced SAN1 binding to BRCT domains. (G) Flag-tagged SAN1 was transfected into cells expressing shRNA against SEPT7 or control and treated as indicated prior to extract preparation. Input lysates were analyzed by immunoblot to detect indicated proteins. (H) Binding assay was performed as described in A with lysates from G. (I) Quantification of BRCT binding assays, as described in F. Error bars, ± 1 sem, n = 3. Data were analyzed by 2-way ANOVA. (J) Flag-tagged SAN1, WT or S617A

mutant, were transfected into cells and treated with cisplatin prior to extract preparation. Binding assay was performed as described in A. (*) $P < 0.05$; (**) $P < 0.001$; (***) $P < 0.0001$.

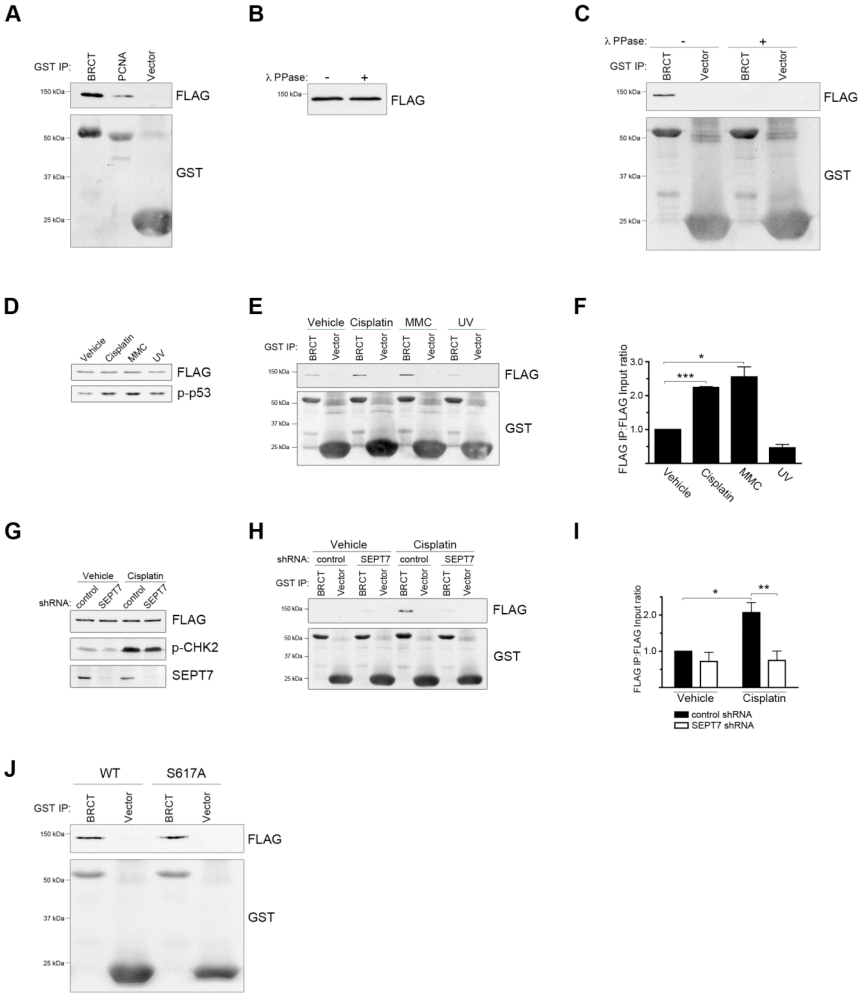
A
GST IP:
BRCT
PCNA
Vector
150 kDa
50 kDa
37 kDa
25 kDa
FLAG
GST
B
λ PPase:
-
+
150 kDa
FLAG
C
λ PPase:
-
+
GST IP:
BRCT
Vector
BRCT
Vector
150 kDa
FLAG
50 kDa
37 kDa
25 kDa
GST
D
Vehicle
Cisplatin
MMC
UV
FLAG
p-p53
E
Vehicle
Cisplatin
MMC
UV
GST IP:
BRCT
Vector
BRCT
Vector
BRCT
Vector
BRCT
Vector
150 kDa
FLAG
50 kDa
37 kDa
25 kDa
GST
F
FLAG IP:FLAG Input ratio
3.0
2.0
1.0
*
***
Vehicle
Cisplatin
MMC
UV
G
Vehicle
Cisplatin
shRNA:
control
SEPT7
control
SEPT7
FLAG
p-CHK2
SEPT7
H
Vehicle
Cisplatin
shRNA:
control
SEPT7
control
SEPT7
GST IP:
BRCT
Vector
BRCT
Vector
BRCT
Vector
BRCT
Vector
150 kDa
FLAG
50 kDa
37 kDa
25 kDa
GST
I
FLAG IP:FLAG Input ratio
2.0
1.0
*
**
Vehicle
Cisplatin
control shRNA
SEPT7 shRNA
J
WT
S617A
GST IP:
BRCT
Vector
BRCT
Vector
150 kDa
FLAG
50 kDa
37 kDa
25 kDa
GST

To further explore the role of septins in regulating SAN1 during ICL repair we asked if septins mediate SAN1 engagement during DNA repair, using the BRCT binding assay. Notably, enhanced BRCT domain binding of SAN1 from cells treated with cisplatin was abolished by silencing expression of septins (Fig. 5.2G-I). This result suggests septins are required for SAN1 binding to BRCT domains following DNA damage, which could explain their involvement in HR and end resection during ICL repair.

Finally, we tested if SAN1 directly binds the BRCT domains. A mutation in the potential BRCT binding motif was made that changed the serine to alanine, which should prevent binding since a phosphorylated serine is essential to binding [100, 101, 359]. However, the S617A mutant still bound as efficiently as wild-type SAN1, indicating binding is not direct (Fig. 5.2J). Thus, although SAN1 interacts with BRCT domains, it is not direct and appears to be mediated by another protein, or proteins. Further study should identify what bridges the interaction of SAN1 with BRCT domains, whether the BRCT domain-containing protein is BRCA1, or another type 1 protein, and how septins are involved during this process, possibly by providing a signaling platform for the essential phosphorylation required during for BRCT binding.

SAN1 interacts with SMC1

We performed a co-precipitation study to identify other proteins that might have a biological link with SAN1 and the DDR. Using cells that expressed SAN1 with a C-

terminal tag containing both the FLAG tag and two copies of the Strep II tag, we performed a previously described tandem affinity purification approach to identify associated proteins [360, 361]. Mass spectrometric analysis identified 22 unique peptides corresponding to 7.8% coverage of the protein SMC1 (Fig. 5.3A). The structural maintenance of chromosomes (SMC) proteins are highly conserved proteins that function in different aspects of chromosome biology with SMC1 part of the cohesin complex necessary for proper chromosome segregation [362]. The cohesin complex is composed of SMC1, SMC3, and two non-SMC proteins, SA1 and SA2, which functions to regulate sister-chromatid cohesion [362]. In response to various forms of DNA damage, SMC1 and SMC3 are phosphorylated by ATM or ATR, which are necessary for the intra-S phase checkpoint [363-366]. However, the role of these phosphorylations is still unknown. In addition to the role in the checkpoint response, SMC1 and the cohesion complex have been implicated in DSB repair, specifically HR. It is proposed that during HR, the cohesion complex maintains sister-chromatid cohesion near the DSB to promote strand invasion and sister-chromatid HR [362]. Consistent with this, the cohesion complex was detected at sites of DSBs and depletion of cohesion subunits led to defects in DNA repair and sister-chromatid exchange (SCE) [367-369].

We verified SMC1 interacts with SAN1, by affinity purifying SAN1-FLAG from transfected cells and analyzing endogenous SMC1 by immunoblot (Fig. 5.3B). While we did not pursue this result further, a number of questions remain. Does endogenous SAN1 and SMC1 interact? Do septins interaction with SMC1? Do SMC1 and SAN1 and/or septins co-localize? Does SMC1 participate with SAN1 during ICL repair? While it

Figure 5.3: SMC1 identified as potential SAN1 binding partner. SAN1 interacts with SMC1. (A) Mass spectrometric analysis revealed 22 peptides (bold/underlined) corresponding to SMC1. (B) FLAG-tagged SAN1 or FLAG vector were transfected into cells, lysed, and incubated with FLAG-M2 agarose beads. Input lysates and FLAG IP were analyzed by immunoblot to detect the indicted proteins.

A

```
1     MGFLKLIEIENFKSYKGRQIIGPFQRFTAIIGPNGSGKSNLMDAISFVLGEKTSNLRVKT
61    LRDLIHGAPVGKPAANRAFVSMVYSEEGAEDRTFARVIVGGSSEYKINNKVVQLHEYSEE
121   LEKLGILIKARNFLVFQGAVESIAMKNPKERTALFEEISRSGELAQEYDKRKKEMVKAEE
181   DTQFNYHRKKNIAAERKEAKQEKEEADRYQRLKDEVVRAQVQLQLFKLYHNEVEIEKLNK
241   ELASKNKEIEKDKKRMDKVEDELKEKKKELGKMMREQQQIEKEIKEKDSELNQKRPQYIK
301   AKENTSHKIKKLEAAKKSLQNAQKHYKKRKGDMDELEKEMLSVEKARQEFEERMEEESQS
361   QGRDLTLEENQVKKYHRLKEEASKRAATLAQELEKFNRDQKADQDRLDLEERKKVETEAK
421   IKQKLREIEENQKRIEKLEEYITTSKQSLEEQKKLEGELTEEVEMAKRRIDEINKELNQV
481   MEQLGDARIDRQESSRQQRKAEIMESIKRLYPGSVYGRLIDLCQPTQKKYQIAVTKVLGK
541   NMDAIIVDSEKTGRDCIQYIKEQRGEPETFLPLDYLEVKPTDEKLRELKGAKLVIDVIRY
601   EPPHIKKALQYACGNALVCDNVEDARRIAFGGHQRHKTVALDGTLFQKSGVISGGASDLK
661   AKARRWDEKAVDKLKEKKERLTEEL
```

B

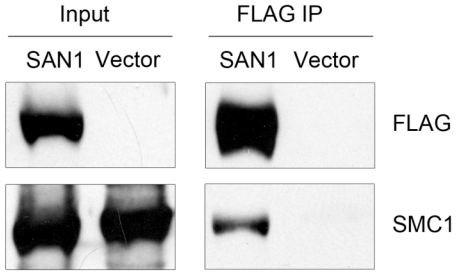

appears SAN1 has a necessary role in the repair of ICL, specifically during end resection, a role for SMC1 in ICL repair is not clear. The phosphorylation of SMC1, at least in response to IR treatment, is not altered in cell lines from FA patients [370]. However, the importance of homologous DNA sequences in ICL repair has been well documented as has the involvement of SMC1, and the cohesion complex, in maintaining sister chromatids in close proximity. Recombination between sister chromatids is not the only method of HR during ICL repair, with recombination between sister chromosomes thought to be more prevalent, especially when repair occurs prior to the completion of DNA replication [371]. Interestingly, Bloom's syndrome and FANCM-deficient cells, but not other FA subtypes, display increased frequency of SCEs, which are further increased by ICL-inducing agents [216, 342]. Thus, even though the exact role of SMC1 and the cohesion complex in ICL repair is not known, there is evidence that suggests the importance of cohesion in ICL repair. Further study should identify the importance of SAN1 interacting with the cohesion complex, if septins are involved in this interaction, and how these proteins mechanistically function during ICL repair.

Appendix II: Protocols

Buffer recipes

Lysis Buffer:

Reagent	Stock	To make 10 mL
25 mM HEPES, pH 7.4	1 M	250 µl
150 mM NaCl	5 M	300 µl
0.5% (v/v) Triton X-100	10 %	500 µl
0.5 mM EDTA	250 mM	20 µl
1 mM $MgCl_2$	4.9 M	2 µl
2 mM DTT	1 M	20 µl
1 mM PMSF	100 mM	100 µl
10 µg/ml leupeptin	25 ng/ml	4 µl
20 µg/ml aprotinin	25 ng/ml	8 µl
dH_2O		Q'sd to 10 ml (~8796 µl)

Wash Buffer:

Reagent	Stock	To make 10 mL
25 mM HEPES, pH 7.4	1 M	250 µl
450 mM NaCl	5 M	900 µl
0.5% (v/v) Triton X-100	10 %	500 µl
0.5 mM EDTA	250 mM	20 µl

1 mM $MgCl_2$	4.9 M	2 µl
2 mM DTT	1 M	20 µl
1 mM PMSF	100 mM	100 µl
10 µg/ml leupeptin	25 ng/ml	4 µl
20 µg/ml aprotinin	25 ng/ml	8 µl
dH_2O		Q'sd to 10 ml (~8196 µl)

TGN Buffer:

Reagent	Stock	To make 10 mL
50 mM Tris (pH 7.4)	500 mM	1000 µl
150 mM NaCl	5 M	300 µl
10% glycerol	100%	1000 µl
1% NP-40	10%	1000 µl
1 mM DTT	1 M	10 µl
1 mM NaF	250 mM	40 µl
1 mM $NaVO_4$	250 mM	40 µl
1 mM PMSF	100 mM	100 µl
5 µg/mL leupeptin	25 mg/mL	2 µl
10 µg/mL aprotinin	25 mg/mL	4 µl
1 nM calyculin A	20 mM	5 µl
dH_2O		6499 µl

Hypotonic Lysis Buffer:

Reagent	Stock	To make 10 mL
25 mM HEPES (pH 7.4)	1 M	250 µl
10% Glycerol	100%	1000 µl
1 mM EDTA	250 mM	40 µl
1 mM DTT	1 M	10 µl
0.1 mM PMSF	100 mM	10 µl
25 µg/ml leupeptin	25 ng/ml	10 µl
25 µg/ml aprotinin	25 ng/ml	10 µl
1 µM microcystin	1 mM	10 µl
dH_2O		Q'sd to 10 ml (~8660 µl)

Nuclease assay Elution Buffer:

Reagent	Stock	To make 10 mL
62.5 mM HEPES (pH 7.4)	1 M	625 µl
62.5 mM KCl	2 M	312.5 µl
5% Glycerol	100%	500 µl
1 mM DTT	1 M	10 µl
50 µg/mL BSA	10 mg/mL	50 µl
dH_2O		Q'sd to 10 ml (~8502 µl)

Substrates for nuclease assay

For 5' end'labeled substrates:

- combine 1 µL (resuspend oligo in 100 picomole/µL) with 2 µL T4 PNK Buffer (10X), 2 µL DTT (100 mM), 5 µL Υ-^{32}P-ATP (specific activity 7,000 Ci/mmol), 8 µL dH_2O
- start reaction with 2 µL T4-PNK (10U/µL)
- incubate @ 37°C for 1 hr
- inactivate PNK @ 70°C for 20 min
- add to cleared G-25 spin column; spin @ 3K for 2 min

For 3' end'labeled substrates:

- combine 1 µL (resuspend oligo in 100 picomole/µL) with 2 µL Terminal Transferase Buffer (10X), 2 µL $CoCl_2$ (10X), 5 µL α-^{32}P-cordycepin 5' triphosphate (specific activity 5,000 Ci/mmol), 8 µL dH_2O
- start reaction with 2 µL Terminal Transferase (10U/µL)
- incubate @ 37°C for 1 hr
- inactivate PNK @ 70°C for 20 min
- add to cleared G-25 spin column; spin @ 3K for 2 min

(note, if you want to make structures, you will then take the labeled oligo and add to unlabeled oligos (always use less of the labeled to ensure complete incorportation)

25 picomol labeled, 50 picomole for one equally long substrate, 100 picomole if a smaller substrate

Add all together with 6X annealing buffer (0.9M NaCl, 90 mM NaCitrate)

Heat 500 mL H_2O in beaker (in microwave) until boiling, add tubes and let cool slowly to room temp 3 hr to O/N

Purify substrates:

- pour 29:1 acrylamid:bis, 1X TAE gel (Check which percentage based on size of substrates, I use 8-10%)
- let polymerize for at least 30 min
- pre-run gel @ 10V/cm for 15 min
- add 10X native DNA loading buffer (50% glycerol, 0.005% BB, pH 8.0)
- load samples, preferable with space between each lane, and run @ 10V/cm till good separation (may take 2 plus hr)
- expose gel to film (30 sec to a few minutes), match up band with gel and cut out bands (reexposure to make sure you removed band)
- soak bands in Buffer (water or EB) O/N at RT, store at 4 °C

Nuclease assay

Make SAN1-Flag (always C-term tag) by transfection 293T cells according to lab protocol. (For a 10 cm I would get about 20 µL eluate to assay, for 15 cm about 60 µL and I would use 4 µL/reaction)

On day of harvest (18-24 hr after transfection)

- wash cells with 1X PBS and transfer to µfuge tube
- aspirate 1X PBS (don't suck up cells)
- add HLB (250 µL for 10 cm, 750 µL for 15 cm) and incubate on ice for 5 min

- snap/freeze cells (you can store at -80°C here if you want)
- quick thaw at 37°C, repeat 2 more times and put thawed tubes on ice
- add NaCl to 300 mM, incubate on ice 5 min
- spin max speed for 20 min at 4°C
- add supernatant to µfuge tube with equal amount of HLB + 0.2% NP-40
- mix and spin 5 min at 4°C
- add supernantant to washed FLAG-M2 beads (10 µL for 10 cm, 30 µL for 15 cm)
- incubate for 1-2 hr at 4°C rocking
- wash 2X (15 min/wash) with HLB + 150 mM NaCl + 0.1% NP-40
- wash 2X (15 min/wash) with elution buffer
- add elution buffer + 150 ng/µL FLAG pepide (20 µL/10cm, 60 µL/15 cm)
- incubate at 4°C shaking at 600 rpm for 30 min
- spin and use eluate in nuclease assay

Nuclease assay:

- add 4µL eluate, 5mM labeled oligo (make 1 µL), start reaction with 5 µL start buffer (6 mM $MgCl_2$, 2 mM ß-ME, 0.05 µg/µL BSA)
- incubate @37°C for indicated time (2 hr for standard)
- stop reaction with 2.5 µL 5X loading buffer (15 mM EDTA, formamide + 0.005% BB, 0.005% XC)
- boil 3 min, ice, store at -20°C if needed

Run gel to visualize products:

- pour 7M urea, 19:1 acrylamide:bis, 1X TBE gel (run percentage based on size of products (usually run 15% until XC about 2/3 way down (XC is about 35-40 nucleotides)))
- polymerize for at least 30 min
- pre-run gel @ 20 mAmps/gel for about 15 min (blow out urea in wells)
- load gel (blow out urea in gels)
- run @ 20 mAmps/gel until desired marking (be sure glass doesn't get too hot and crack) (might need to make voltage max out at 250)
- expose gel to film at 4°C (if you can, dry gel to get better signal)

Chemically digested ladder

- combine ^{32}P-labeled oligo (usually 18 µL), with 1 µL carrier DNA (1 µg/µL), and 2 µL 4% formic acid.
- Incubate @ 37°C for 30 – 90 min, put on ice
- Add 300 µL piperidine (1/10 diluted stock)
- Incubate @ 90°C for 30 – 60 min, put on ice for 5 min
- Add 1 mL n-butanol; vortex
- Centrifuge for 5 min @ max speed to pellet DNA
- Remove supernatant, add 300 µL 1% SDS
- Add 1 mL n-butanol, vortex
- Centrifuge for 5 min @ max speed
- Remove supernatant

- Centrifuge for 5 min @ max speed
- Remove excess supernatant
- Dry in speedvac for 10 min
- Add formamide loading buffer

Immunofluorescence

Plate cells in LabTekII slides and treat as needed:

- wash 2X with 1X PBS
- fix with 3.7% PFA/1X PBS for 10 min
- wash with 50 mM NH4Cl/1X PBS for 10 min
- wash 2X with 1X PBS (if staining endogenous quench with 2% H_2O_2/PBS for 15 min and wash with 1X PBS for 5 min)
- permabilize/block with 0.3% saponin/1X PBS/1X Roche WBR O/N at 4 C (or 1 hr at RT)
- incubate with primary antibodies in 0.3% saponin/1X PBS/1X Roche WBR (1:100 for endogenous) for 1 hr at RT
- wash 3X with 0.3% saponin/1X PBS/1X Roche WBR at RT (5 min/wash)
- incubate with secondary antibodies in 0.3% saponin/1X PBS/1X Roche WBR for 1hr at RT
- wash 3X with 0.3% saponin/1X PBS/1X Roche WBR (5 min/wash)
- if staining endogenous incubate with TSA Plus Flurophore (typically used Cy3) amp solution for 10 min (1:50 following protocol)

- stain nuclei, wash, mount/seal
- image

BRCT binding assay

Make GST-vector and GST-BRCT domains following lab protocol and store at -80

Split, transfect and treat cells following lab protocol:

- pretreat plates with 10 nM calyculin A for 10 min @ 37°C
- harvest in 800 µL TGN (with C.A. inhibitor), ice for 15 min
- sonicate 3x5 sec (can store at -80 here)
- thaw/spin GST-vector and GST-BRCT proteins
- incubate Gluthione beads with GST proteins for 30 min @ 4°C rocking
- wash 2X with 1XPBS + 1% TX-100
- wash 1X with TGN buffer and divide into tubes for each condition
- spin cell lysate at max speed @ 4°C for 15 min
- divide equally into GST protein bound bead tubes (save input)
- incubate @ 4°C, rocking for 1 hr
- wash 3X with TGN buffer + 0.5% TX-100 + 0.5% NP-40, 5-10 min each
- add 2X SDS buffer, boil 5'

Strep-Flag immunoprecipitation

Using cells expressing SAN1-SSF (or SSF vector) with or without a treatment

- scrape cells with PBS into µfuge tube, spin down, aspirate

- add TGN buffer (2 mL/15cm), ice 15 min, sonicate 3x5 sec
- add DNaseI @ 30µg/mL
- incubate on ice for 30 min (can store at -80 after this)
- spin lysate at max speed @ 4°C for 20 min, save input
- add lysate to strep-tactin superflow (IBA) (150 µL/15 cm)
- incubate @ 4°C for 1 hr, rocking
- wash 3X with TGN (-DTT, -NP-40, only 5% glycerol), 5 min each
- add TGN (-DTT, -NP-40, only 5% glycerol) + 2 mM desthiobiotin (750 µL/15 cm)
- incubate @ 4°C for 30 min, rocking
- add elution to FLAG-M2 beads (50 µL/15 cm)
- incubate @ 4°C for 1 hr, rocking
- wash 3X with TGN (-DTT, -NP-40, only 5% glycerol), 5 min each
- add 2X SDS buffer, boil 5 min

References

1. Nishihama, R., Onishi, M., and Pringle, J.R. (2011). New insights into the phylogenetic distribution and evolutionary origins of the septins. Biol Chem *392*, 681-687.
2. Saarikangas, J., and Barral, Y. (2011). The emerging functions of septins in metazoans. EMBO Rep *12*, 1118-1126.
3. Hartwell, L.H. (1971). Genetic control of the cell division cycle in yeast. IV. Genes controlling bud emergence and cytokinesis. Exp Cell Res *69*, 265-276.
4. Byers, B., and Goetsch, L. (1976). A highly ordered ring of membrane-associated filaments in budding yeast. J Cell Biol *69*, 717-721.
5. Haarer, B.K., and Pringle, J.R. (1987). Immunofluorescence localization of the Saccharomyces cerevisiae CDC12 gene product to the vicinity of the 10-nm filaments in the mother-bud neck. Mol Cell Biol *7*, 3678-3687.
6. Kim, H.B., Haarer, B.K., and Pringle, J.R. (1991). Cellular morphogenesis in the Saccharomyces cerevisiae cell cycle: localization of the CDC3 gene product and the timing of events at the budding site. J Cell Biol *112*, 535-544.
7. Russell, S.E., and Hall, P.A. (2011). Septin genomics: a road less travelled. Biol Chem *392*, 763-767.
8. Mostowy, S., and Cossart, P. (2012). Septins: the fourth component of the cytoskeleton. Nat Rev Mol Cell Biol *13*, 183-194.

9. Zhang, J., Kong, C., Xie, H., McPherson, P.S., Grinstein, S., and Trimble, W.S. (1999). Phosphatidylinositol polyphosphate binding to the mammalian septin H5 is modulated by GTP. Curr Biol *9*, 1458-1467.

10. Casamayor, A., and Snyder, M. (2003). Molecular dissection of a yeast septin: distinct domains are required for septin interaction, localization, and function. Mol Cell Biol *23*, 2762-2777.

11. Sirajuddin, M., Farkasovsky, M., Hauer, F., Kuhlmann, D., Macara, I.G., Weyand, M., Stark, H., and Wittinghofer, A. (2007). Structural insight into filament formation by mammalian septins. Nature *449*, 311-315.

12. Sirajuddin, M., Farkasovsky, M., Zent, E., and Wittinghofer, A. (2009). GTP-induced conformational changes in septins and implications for function. Proc Natl Acad Sci U S A *106*, 16592-16597.

13. Huang, Y.W., Surka, M.C., Reynaud, D., Pace-Asciak, C., and Trimble, W.S. (2006). GTP binding and hydrolysis kinetics of human septin 2. Febs J *273*, 3248-3260.

14. Kinoshita, M., Kumar, S., Mizoguchi, A., Ide, C., Kinoshita, A., Haraguchi, T., Hiraoka, Y., and Noda, M. (1997). Nedd5, a mammalian septin, is a novel cytoskeletal component interacting with actin-based structures. Genes Dev *11*, 1535-1547.

15. Nagata, K., Kawajiri, A., Matsui, S., Takagishi, M., Shiromizu, T., Saitoh, N., Izawa, I., Kiyono, T., Itoh, T.J., Hotani, H., and Inagaki, M. (2003). Filament

formation of MSF-A, a mammalian septin, in human mammary epithelial cells depends on interactions with microtubules. J Biol Chem *278*, 18538-18543.

16. Sheffield, P.J., Oliver, C.J., Kremer, B.E., Sheng, S., Shao, Z., and Macara, I.G. (2003). Borg/septin interactions and the assembly of mammalian septin heterodimers, trimers, and filaments. J Biol Chem *278*, 3483-3488.
17. Versele, M., Gullbrand, B., Shulewitz, M.J., Cid, V.J., Bahmanyar, S., Chen, R.E., Barth, P., Alber, T., and Thorner, J. (2004). Protein-protein interactions governing septin heteropentamer assembly and septin filament organization in Saccharomyces cerevisiae. Mol Biol Cell *15*, 4568-4583.
18. Cao, L., Yu, W., Wu, Y., and Yu, L. (2009). The evolution, complex structures and function of septin proteins. Cell Mol Life Sci *66*, 3309-3323.
19. Low, C., and Macara, I.G. (2006). Structural analysis of septin 2, 6, and 7 complexes. J Biol Chem *281*, 30697-30706.
20. Zent, E., Vetter, I., and Wittinghofer, A. (2011). Structural and biochemical properties of Sept7, a unique septin required for filament formation. Biol Chem *392*, 791-797.
21. Sandrock, K., Bartsch, I., Blaser, S., Busse, A., Busse, E., and Zieger, B. (2011). Characterization of human septin interactions. Biol Chem *392*, 751-761.
22. Kim, M.S., Froese, C.D., Estey, M.P., and Trimble, W.S. (2011). SEPT9 occupies the terminal positions in septin octamers and mediates polymerization-dependent functions in abscission. J Cell Biol *195*, 815-826.

23. Lukoyanova, N., Baldwin, S.A., and Trinick, J. (2008). 3D reconstruction of mammalian septin filaments. J Mol Biol *376*, 1-7.

24. Sellin, M.E., Sandblad, L., Stenmark, S., and Gullberg, M. (2011). Deciphering the rules governing assembly order of mammalian septin complexes. Mol Biol Cell *22*, 3152-3164.

25. Macedo, J.N., Valadares, N.F., Marques, I.A., Ferreira, F.M., Damalio, J.C., Pereira, H.M., Garratt, R.C., and Araujo, A.P. (2013). The structure and properties of septin 3: a possible missing link in septin filament formation. Biochem J *450*, 95-105.

26. Ihara, M., Kinoshita, A., Yamada, S., Tanaka, H., Tanigaki, A., Kitano, A., Goto, M., Okubo, K., Nishiyama, H., Ogawa, O., Takahashi, C., Itohara, S., Nishimune, Y., Noda, M., and Kinoshita, M. (2005). Cortical organization by the septin cytoskeleton is essential for structural and mechanical integrity of mammalian spermatozoa. Dev Cell *8*, 343-352.

27. Kissel, H., Georgescu, M.M., Larisch, S., Manova, K., Hunnicutt, G.R., and Steller, H. (2005). The Sept4 septin locus is required for sperm terminal differentiation in mice. Dev Cell *8*, 353-364.

28. Steels, J.D., Estey, M.P., Froese, C.D., Reynaud, D., Pace-Asciak, C., and Trimble, W.S. (2007). Sept12 is a component of the mammalian sperm tail annulus. Cell Motil Cytoskeleton *64*, 794-807.

29. Hu, Q., Milenkovic, L., Jin, H., Scott, M.P., Nachury, M.V., Spiliotis, E.T., and Nelson, W.J. (2010). A septin diffusion barrier at the base of the primary cilium maintains ciliary membrane protein distribution. Science *329*, 436-439.

30. Chih, B., Liu, P., Chinn, Y., Chalouni, C., Komuves, L.G., Hass, P.E., Sandoval, W., and Peterson, A.S. (2011). A ciliopathy complex at the transition zone protects the cilia as a privileged membrane domain. Nat Cell Biol *14*, 61-72.

31. Cho, S.J., Lee, H., Dutta, S., Song, J., Walikonis, R., and Moon, I.S. (2011). Septin 6 regulates the cytoarchitecture of neurons through localization at dendritic branch points and bases of protrusions. Mol Cells *32*, 89-98.

32. Tada, T., Simonetta, A., Batterton, M., Kinoshita, M., Edbauer, D., and Sheng, M. (2007). Role of Septin cytoskeleton in spine morphogenesis and dendrite development in neurons. Curr Biol *17*, 1752-1758.

33. Xie, Y., Vessey, J.P., Konecna, A., Dahm, R., Macchi, P., and Kiebler, M.A. (2007). The GTP-binding protein Septin 7 is critical for dendrite branching and dendritic-spine morphology. Curr Biol *17*, 1746-1751.

34. Mostowy, S., Nam Tham, T., Danckaert, A., Guadagnini, S., Boisson-Dupuis, S., Pizarro-Cerda, J., and Cossart, P. (2009). Septins regulate bacterial entry into host cells. PLoS One *4*, e4196.

35. Mostowy, S., Bonazzi, M., Hamon, M.A., Tham, T.N., Mallet, A., Lelek, M., Gouin, E., Demangel, C., Brosch, R., Zimmer, C., Sartori, A., Kinoshita, M., Lecuit, M., and Cossart, P. (2010). Entrapment of intracytosolic bacteria by septin cage-like structures. Cell Host Microbe *8*, 433-444.

36. Li, X., Serwanski, D.R., Miralles, C.P., Nagata, K., and De Blas, A.L. (2009). Septin 11 is present in GABAergic synapses and plays a functional role in the cytoarchitecture of neurons and GABAergic synaptic connectivity. J Biol Chem *284*, 17253-17265.

37. Caudron, F., and Barral, Y. (2009). Septins and the lateral compartmentalization of eukaryotic membranes. Dev Cell *16*, 493-506.

38. Kremer, B.E., Haystead, T., and Macara, I.G. (2005). Mammalian septins regulate microtubule stability through interaction with the microtubule-binding protein MAP4. Mol Biol Cell *16*, 4648-4659.

39. Surka, M.C., Tsang, C.W., and Trimble, W.S. (2002). The mammalian septin MSF localizes with microtubules and is required for completion of cytokinesis. Mol Biol Cell *13*, 3532-3545.

40. Xie, H., Surka, M., Howard, J., and Trimble, W.S. (1999). Characterization of the mammalian septin H5: distinct patterns of cytoskeletal and membrane association from other septin proteins. Cell Motil Cytoskeleton *43*, 52-62.

41. Spiliotis, E.T., Kinoshita, M., and Nelson, W.J. (2005). A mitotic septin scaffold required for Mammalian chromosome congression and segregation. Science *307*, 1781-1785.

42. Estey, M.P., Di Ciano-Oliveira, C., Froese, C.D., Bejide, M.T., and Trimble, W.S. (2010). Distinct roles of septins in cytokinesis: SEPT9 mediates midbody abscission. J Cell Biol *191*, 741-749.

43. Qi, M., Yu, W., Liu, S., Jia, H., Tang, L., Shen, M., Yan, X., Saiyin, H., Lang, Q., Wan, B., Zhao, S., and Yu, L. (2005). Septin1, a new interaction partner for human serine/threonine kinase aurora-B. Biochem Biophys Res Commun *336*, 994-1000.

44. Zhu, M., Wang, F., Yan, F., Yao, P.Y., Du, J., Gao, X., Wang, X., Wu, Q., Ward, T., Li, J., Kioko, S., Hu, R., Xie, W., Ding, X., and Yao, X. (2008). Septin 7 interacts with centromere-associated protein E and is required for its kinetochore localization. J Biol Chem *283*, 18916-18925.

45. Joberty, G., Perlungher, R.R., Sheffield, P.J., Kinoshita, M., Noda, M., Haystead, T., and Macara, I.G. (2001). Borg proteins control septin organization and are negatively regulated by Cdc42. Nat Cell Biol *3*, 861-866.

46. Kinoshita, M., Field, C.M., Coughlin, M.L., Straight, A.F., and Mitchison, T.J. (2002). Self- and actin-templated assembly of Mammalian septins. Dev Cell *3*, 791-802.

47. Nagata, K., Asano, T., Nozawa, Y., and Inagaki, M. (2004). Biochemical and cell biological analyses of a mammalian septin complex, Sept7/9b/11. J Biol Chem *279*, 55895-55904.

48. Hanai, N., Nagata, K., Kawajiri, A., Shiromizu, T., Saitoh, N., Hasegawa, Y., Murakami, S., and Inagaki, M. (2004). Biochemical and cell biological characterization of a mammalian septin, Sept11. FEBS Lett *568*, 83-88.

49. Vega, I.E., and Hsu, S.C. (2003). The septin protein Nedd5 associates with both the exocyst complex and microtubules and disruption of its GTPase activity promotes aberrant neurite sprouting in PC12 cells. Neuroreport *14*, 31-37.

50. Martinez, C., Corral, J., Dent, J.A., Sesma, L., Vicente, V., and Ware, J. (2006). Platelet septin complexes form rings and associate with the microtubular network. J Thromb Haemost *4*, 1388-1395.

51. Joo, E., Surka, M.C., and Trimble, W.S. (2007). Mammalian SEPT2 is required for scaffolding nonmuscle myosin II and its kinases. Dev Cell *13*, 677-690.

52. Nagata, K., and Inagaki, M. (2005). Cytoskeletal modification of Rho guanine nucleotide exchange factor activity: identification of a Rho guanine nucleotide exchange factor as a binding partner for Sept9b, a mammalian septin. Oncogene *24*, 65-76.

53. Ito, H., Iwamoto, I., Morishita, R., Nozawa, Y., Narumiya, S., Asano, T., and Nagata, K. (2005). Possible role of Rho/Rhotekin signaling in mammalian septin organization. Oncogene *24*, 7064-7072.

54. Ghossoub, R., Hu, Q., Failler, M., Rouyez, M.C., Spitzbarth, B., Mostowy, S., Wolfrum, U., Saunier, S., Cossart, P., Nelson, W.J., and Benmerah, A. (2013). Septins 2, 7, and 9 and MAP4 co-localize along the axoneme in the primary cilium and control ciliary length. J Cell Sci.

55. Mostowy, S., Janel, S., Forestier, C., Roduit, C., Kasas, S., Pizarro-Cerda, J., Cossart, P., and Lafont, F. (2011). A role for septins in the interaction between the

Listeria monocytogenes INVASION PROTEIN InlB and the Met receptor. Biophys J *100*, 1949-1959.

56. Beites, C.L., Xie, H., Bowser, R., and Trimble, W.S. (1999). The septin CDCrel-1 binds syntaxin and inhibits exocytosis. Nat Neurosci *2*, 434-439.

57. Beites, C.L., Campbell, K.A., and Trimble, W.S. (2005). The septin Sept5/CDCrel-1 competes with alpha-SNAP for binding to the SNARE complex. Biochem J *385*, 347-353.

58. Amin, N.D., Zheng, Y.L., Kesavapany, S., Kanungo, J., Guszczynski, T., Sihag, R.K., Rudrabhatla, P., Albers, W., Grant, P., and Pant, H.C. (2008). Cyclin-dependent kinase 5 phosphorylation of human septin SEPT5 (hCDCrel-1) modulates exocytosis. J Neurosci *28*, 3631-3643.

59. Hsu, S.C., Hazuka, C.D., Roth, R., Foletti, D.L., Heuser, J., and Scheller, R.H. (1998). Subunit composition, protein interactions, and structures of the mammalian brain sec6/8 complex and septin filaments. Neuron *20*, 1111-1122.

60. Ito, H., Atsuzawa, K., Morishita, R., Usuda, N., Sudo, K., Iwamoto, I., Mizutani, K., Katoh-Semba, R., Nozawa, Y., Asano, T., and Nagata, K. (2009). Sept8 controls the binding of vesicle-associated membrane protein 2 to synaptophysin. J Neurochem *108*, 867-880.

61. Spiliotis, E.T., Hunt, S.J., Hu, Q., Kinoshita, M., and Nelson, W.J. (2008). Epithelial polarity requires septin coupling of vesicle transport to polyglutamylated microtubules. J Cell Biol *180*, 295-303.

62. Maimaitiyiming, M., Kobayashi, Y., Kumanogoh, H., Nakamura, S., Morita, M., and Maekawa, S. (2013). Identification of dynamin as a septin-binding protein. Neurosci Lett *534*, 322-326.

63. Kinoshita, N., Kimura, K., Matsumoto, N., Watanabe, M., Fukaya, M., and Ide, C. (2004). Mammalian septin Sept2 modulates the activity of GLAST, a glutamate transporter in astrocytes. Genes Cells *9*, 1-14.

64. Tanaka-Takiguchi, Y., Kinoshita, M., and Takiguchi, K. (2009). Septin-mediated uniform bracing of phospholipid membranes. Curr Biol *19*, 140-145.

65. Tooley, A.J., Gilden, J., Jacobelli, J., Beemiller, P., Trimble, W.S., Kinoshita, M., and Krummel, M.F. (2009). Amoeboid T lymphocytes require the septin cytoskeleton for cortical integrity and persistent motility. Nat Cell Biol *11*, 17-26.

66. Gilden, J.K., Peck, S., Chen, Y.C., and Krummel, M.F. (2012). The septin cytoskeleton facilitates membrane retraction during motility and blebbing. J Cell Biol *196*, 103-114.

67. Blaser, S., Horn, J., Wurmell, P., Bauer, H., Strumpell, S., Nurden, P., Pagenstecher, A., Busse, A., Wunderle, D., Hainmann, I., and Zieger, B. (2004). The novel human platelet septin SEPT8 is an interaction partner of SEPT4. Thromb Haemost *91*, 959-966.

68. Dent, J., Kato, K., Peng, X.R., Martinez, C., Cattaneo, M., Poujol, C., Nurden, P., Nurden, A., Trimble, W.S., and Ware, J. (2002). A prototypic platelet septin and its participation in secretion. Proc Natl Acad Sci U S A *99*, 3064-3069.

69. Ahuja, P., Perriard, E., Trimble, W., Perriard, J.C., and Ehler, E. (2006). Probing the role of septins in cardiomyocytes. Exp Cell Res *312*, 1598-1609.

70. Choi, P., Snyder, H., Petrucelli, L., Theisler, C., Chong, M., Zhang, Y., Lim, K., Chung, K.K., Kehoe, K., D'Adamio, L., Lee, J.M., Cochran, E., Bowser, R., Dawson, T.M., and Wolozin, B. (2003). SEPT5_v2 is a parkin-binding protein. Brain Res Mol Brain Res *117*, 179-189.

71. Amir, S., Wang, R., Matzkin, H., Simons, J.W., and Mabjeesh, N.J. (2006). MSF-A interacts with hypoxia-inducible factor-1alpha and augments hypoxia-inducible factor transcriptional activation to affect tumorigenicity and angiogenesis. Cancer Res *66*, 856-866.

72. Amir, S., Wang, R., Simons, J.W., and Mabjeesh, N.J. (2009). SEPT9_v1 up-regulates hypoxia-inducible factor 1 by preventing its RACK1-mediated degradation. J Biol Chem *284*, 11142-11151.

73. Gonzalez, M.E., Makarova, O., Peterson, E.A., Privette, L.M., and Petty, E.M. (2009). Up-regulation of SEPT9_v1 stabilizes c-Jun-N-terminal kinase and contributes to its pro-proliferative activity in mammary epithelial cells. Cell Signal *21*, 477-487.

74. Shehadeh, L., Mitsi, G., Adi, N., Bishopric, N., and Papapetropoulos, S. (2009). Expression of Lewy body protein septin 4 in postmortem brain of Parkinson's disease and control subjects. Mov Disord *24*, 204-210.

75. Connolly, D., Abdesselam, I., Verdier-Pinard, P., and Montagna, C. (2011). Septin roles in tumorigenesis. Biol Chem *392*, 725-738.

76. Kremer, B.E., Adang, L.A., and Macara, I.G. (2007). Septins regulate actin organization and cell-cycle arrest through nuclear accumulation of NCK mediated by SOCS7. Cell *130*, 837-850.

77. Enserink, J.M., Smolka, M.B., Zhou, H., and Kolodner, R.D. (2006). Checkpoint proteins control morphogenetic events during DNA replication stress in Saccharomyces cerevisiae. J Cell Biol *175*, 729-741.

78. Smolka, M.B., Chen, S.H., Maddox, P.S., Enserink, J.M., Albuquerque, C.P., Wei, X.X., Desai, A., Kolodner, R.D., and Zhou, H. (2006). An FHA domain-mediated protein interaction network of Rad53 reveals its role in polarized cell growth. J Cell Biol *175*, 743-753.

79. De Bont, R., and van Larebeke, N. (2004). Endogenous DNA damage in humans: a review of quantitative data. Mutagenesis *19*, 169-185.

80. Latonen, L., and Laiho, M. (2005). Cellular UV damage responses--functions of tumor suppressor p53. Biochim Biophys Acta *1755*, 71-89.

81. Sancar, A., Lindsey-Boltz, L.A., Unsal-Kacmaz, K., and Linn, S. (2004). Molecular mechanisms of mammalian DNA repair and the DNA damage checkpoints. Annu Rev Biochem *73*, 39-85.

82. Harper, J.W., and Elledge, S.J. (2007). The DNA damage response: ten years after. Mol Cell *28*, 739-745.

83. Hartwell, L.H., and Weinert, T.A. (1989). Checkpoints: controls that ensure the order of cell cycle events. Science *246*, 629-634.

84. Lukas, J., Lukas, C., and Bartek, J. (2004). Mammalian cell cycle checkpoints: signalling pathways and their organization in space and time. DNA Repair (Amst) *3*, 997-1007.

85. Li, L., and Zou, L. (2005). Sensing, signaling, and responding to DNA damage: organization of the checkpoint pathways in mammalian cells. J Cell Biochem *94*, 298-306.

86. McGowan, C.H., and Russell, P. (2004). The DNA damage response: sensing and signaling. Curr Opin Cell Biol *16*, 629-633.

87. Bakkenist, C.J., and Kastan, M.B. (2003). DNA damage activates ATM through intermolecular autophosphorylation and dimer dissociation. Nature *421*, 499-506.

88. Lee, J.H., and Paull, T.T. (2004). Direct activation of the ATM protein kinase by the Mre11/Rad50/Nbs1 complex. Science *304*, 93-96.

89. Soutoglou, E., and Misteli, T. (2008). Activation of the cellular DNA damage response in the absence of DNA lesions. Science *320*, 1507-1510.

90. Kanu, N., and Behrens, A. (2007). ATMIN defines an NBS1-independent pathway of ATM signalling. Embo J *26*, 2933-2941.

91. Zhou, W., Otto, E.A., Cluckey, A., Airik, R., Hurd, T.W., Chaki, M., Diaz, K., Lach, F.P., Bennett, G.R., Gee, H.Y., Ghosh, A.K., Natarajan, S., Thongthip, S., Veturi, U., Allen, S.J., Janssen, S., Ramaswami, G., Dixon, J., Burkhalter, F., Spoendlin, M., Moch, H., Mihatsch, M.J., Verine, J., Reade, R., Soliman, H., Godin, M., Kiss, D., Monga, G., Mazzucco, G., Amann, K., Artunc, F., Newland, R.C., Wiech, T., Zschiedrich, S., Huber, T.B., Friedl, A., Slaats, G.G., Joles, J.A.,

Goldschmeding, R., Washburn, J., Giles, R.H., Levy, S., Smogorzewska, A., and Hildebrandt, F. (2012). FAN1 mutations cause karyomegalic interstitial nephritis, linking chronic kidney failure to defective DNA damage repair. Nat Genet *44*, 910-915.

92. Gottlieb, T.M., and Jackson, S.P. (1993). The DNA-dependent protein kinase: requirement for DNA ends and association with Ku antigen. Cell *72*, 131-142.

93. Zou, L., and Elledge, S.J. (2003). Sensing DNA damage through ATRIP recognition of RPA-ssDNA complexes. Science *300*, 1542-1548.

94. Shiotani, B., and Zou, L. (2009). Single-stranded DNA orchestrates an ATM-to-ATR switch at DNA breaks. Mol Cell *33*, 547-558.

95. Stiff, T., Walker, S.A., Cerosaletti, K., Goodarzi, A.A., Petermann, E., Concannon, P., O'Driscoll, M., and Jeggo, P.A. (2006). ATR-dependent phosphorylation and activation of ATM in response to UV treatment or replication fork stalling. Embo J *25*, 5775-5782.

96. Liu, S., Opiyo, S.O., Manthey, K., Glanzer, J.G., Ashley, A.K., Amerin, C., Troksa, K., Shrivastav, M., Nickoloff, J.A., and Oakley, G.G. (2012). Distinct roles for DNA-PK, ATM and ATR in RPA phosphorylation and checkpoint activation in response to replication stress. Nucleic Acids Res *40*, 10780-10794.

97. Yajima, H., Lee, K.J., and Chen, B.P. (2006). ATR-dependent phosphorylation of DNA-dependent protein kinase catalytic subunit in response to UV-induced replication stress. Mol Cell Biol *26*, 7520-7528.

98. Rogakou, E.P., Pilch, D.R., Orr, A.H., Ivanova, V.S., and Bonner, W.M. (1998). DNA double-stranded breaks induce histone H2AX phosphorylation on serine 139. J Biol Chem *273*, 5858-5868.

99. Polo, S.E., and Jackson, S.P. (2011). Dynamics of DNA damage response proteins at DNA breaks: a focus on protein modifications. Genes Dev *25*, 409-433.

100. Manke, I.A., Lowery, D.M., Nguyen, A., and Yaffe, M.B. (2003). BRCT repeats as phosphopeptide-binding modules involved in protein targeting. Science *302*, 636-639.

101. Rodriguez, M., Yu, X., Chen, J., and Songyang, Z. (2003). Phosphopeptide binding specificities of BRCA1 COOH-terminal (BRCT) domains. J Biol Chem *278*, 52914-52918.

102. Mohammad, D.H., and Yaffe, M.B. (2009). 14-3-3 proteins, FHA domains and BRCT domains in the DNA damage response. DNA Repair (Amst) *8*, 1009-1017.

103. Lisby, M., and Rothstein, R. (2004). DNA damage checkpoint and repair centers. Curr Opin Cell Biol *16*, 328-334.

104. Reinhardt, H.C., and Yaffe, M.B. (2009). Kinases that control the cell cycle in response to DNA damage: Chk1, Chk2, and MK2. Curr Opin Cell Biol *21*, 245-255.

105. Zhao, H., Watkins, J.L., and Piwnica-Worms, H. (2002). Disruption of the checkpoint kinase 1/cell division cycle 25A pathway abrogates ionizing radiation-induced S and G2 checkpoints. Proc Natl Acad Sci U S A *99*, 14795-14800.

106. Bartek, J., and Lukas, J. (2003). Chk1 and Chk2 kinases in checkpoint control and cancer. Cancer Cell *3*, 421-429.

107. Stracker, T.H., Usui, T., and Petrini, J.H. (2009). Taking the time to make important decisions: the checkpoint effector kinases Chk1 and Chk2 and the DNA damage response. DNA Repair (Amst) *8*, 1047-1054.

108. Takai, H., Tominaga, K., Motoyama, N., Minamishima, Y.A., Nagahama, H., Tsukiyama, T., Ikeda, K., Nakayama, K., and Nakanishi, M. (2000). Aberrant cell cycle checkpoint function and early embryonic death in Chk1(-/-) mice. Genes Dev *14*, 1439-1447.

109. Liu, Q., Guntuku, S., Cui, X.S., Matsuoka, S., Cortez, D., Tamai, K., Luo, G., Carattini-Rivera, S., DeMayo, F., Bradley, A., Donehower, L.A., and Elledge, S.J. (2000). Chk1 is an essential kinase that is regulated by Atr and required for the G(2)/M DNA damage checkpoint. Genes Dev *14*, 1448-1459.

110. Jack, M.T., Woo, R.A., Hirao, A., Cheung, A., Mak, T.W., and Lee, P.W. (2002). Chk2 is dispensable for p53-mediated G1 arrest but is required for a latent p53-mediated apoptotic response. Proc Natl Acad Sci U S A *99*, 9825-9829.

111. Takai, H., Naka, K., Okada, Y., Watanabe, M., Harada, N., Saito, S., Anderson, C.W., Appella, E., Nakanishi, M., Suzuki, H., Nagashima, K., Sawa, H., Ikeda, K., and Motoyama, N. (2002). Chk2-deficient mice exhibit radioresistance and defective p53-mediated transcription. Embo J *21*, 5195-5205.

112. Ahn, J., Urist, M., and Prives, C. (2004). The Chk2 protein kinase. DNA Repair (Amst) *3*, 1039-1047.

113. Ward, I.M., Wu, X., and Chen, J. (2001). Threonine 68 of Chk2 is phosphorylated at sites of DNA strand breaks. J Biol Chem *276*, 47755-47758.

114. Xu, X., Tsvetkov, L.M., and Stern, D.F. (2002). Chk2 activation and phosphorylation-dependent oligomerization. Mol Cell Biol *22*, 4419-4432.

115. Wang, X.Q., Redpath, J.L., Fan, S.T., and Stanbridge, E.J. (2006). ATR dependent activation of Chk2. J Cell Physiol *208*, 613-619.

116. Gatei, M., Sloper, K., Sorensen, C., Syljuasen, R., Falck, J., Hobson, K., Savage, K., Lukas, J., Zhou, B.B., Bartek, J., and Khanna, K.K. (2003). Ataxia-telangiectasia-mutated (ATM) and NBS1-dependent phosphorylation of Chk1 on Ser-317 in response to ionizing radiation. J Biol Chem *278*, 14806-14811.

117. Li, J., and Stern, D.F. (2005). Regulation of CHK2 by DNA-dependent protein kinase. J Biol Chem *280*, 12041-12050.

118. Tomimatsu, N., Mukherjee, B., and Burma, S. (2009). Distinct roles of ATR and DNA-PKcs in triggering DNA damage responses in ATM-deficient cells. EMBO Rep *10*, 629-635.

119. Lee, J.S., Collins, K.M., Brown, A.L., Lee, C.H., and Chung, J.H. (2000). hCds1-mediated phosphorylation of BRCA1 regulates the DNA damage response. Nature *404*, 201-204.

120. Shieh, S.Y., Ahn, J., Tamai, K., Taya, Y., and Prives, C. (2000). The human homologs of checkpoint kinases Chk1 and Cds1 (Chk2) phosphorylate p53 at multiple DNA damage-inducible sites. Genes Dev *14*, 289-300.

121. Stevens, C., Smith, L., and La Thangue, N.B. (2003). Chk2 activates E2F-1 in response to DNA damage. Nat Cell Biol *5*, 401-409.

122. Blasina, A., de Weyer, I.V., Laus, M.C., Luyten, W.H., Parker, A.E., and McGowan, C.H. (1999). A human homologue of the checkpoint kinase Cds1 directly inhibits Cdc25 phosphatase. Curr Biol *9*, 1-10.

123. Weber, J.D., and Zambetti, G.P. (2003). Renewing the debate over the p53 apoptotic response. Cell Death Differ *10*, 409-412.

124. Vousden, K.H. (2002). Activation of the p53 tumor suppressor protein. Biochim Biophys Acta *1602*, 47-59.

125. Lavin, M.F., and Gueven, N. (2006). The complexity of p53 stabilization and activation. Cell Death Differ *13*, 941-950.

126. Hussain, S.P., and Harris, C.C. (2006). p53 biological network: at the crossroads of the cellular-stress response pathway and molecular carcinogenesis. J Nippon Med Sch *73*, 54-64.

127. Kruse, J.P., and Gu, W. (2008). SnapShot: p53 posttranslational modifications. Cell *133*, 930-930 e931.

128. Banin, S., Moyal, L., Shieh, S., Taya, Y., Anderson, C.W., Chessa, L., Smorodinsky, N.I., Prives, C., Reiss, Y., Shiloh, Y., and Ziv, Y. (1998). Enhanced phosphorylation of p53 by ATM in response to DNA damage. Science *281*, 1674-1677.

129. Khanna, K.K., Keating, K.E., Kozlov, S., Scott, S., Gatei, M., Hobson, K., Taya, Y., Gabrielli, B., Chan, D., Lees-Miller, S.P., and Lavin, M.F. (1998). ATM

associates with and phosphorylates p53: mapping the region of interaction. Nat Genet *20*, 398-400.

130. Hirao, A., Kong, Y.Y., Matsuoka, S., Wakeham, A., Ruland, J., Yoshida, H., Liu, D., Elledge, S.J., and Mak, T.W. (2000). DNA damage-induced activation of p53 by the checkpoint kinase Chk2. Science *287*, 1824-1827.

131. Turenne, G.A., Paul, P., Laflair, L., and Price, B.D. (2001). Activation of p53 transcriptional activity requires ATM's kinase domain and multiple N-terminal serine residues of p53. Oncogene *20*, 5100-5110.

132. Wang, S., Guo, M., Ouyang, H., Li, X., Cordon-Cardo, C., Kurimasa, A., Chen, D.J., Fuks, Z., Ling, C.C., and Li, G.C. (2000). The catalytic subunit of DNA-dependent protein kinase selectively regulates p53-dependent apoptosis but not cell-cycle arrest. Proc Natl Acad Sci U S A *97*, 1584-1588.

133. Norbury, C.J., and Zhivotovsky, B. (2004). DNA damage-induced apoptosis. Oncogene *23*, 2797-2808.

134. Roos, W.P., and Kaina, B. (2006). DNA damage-induced cell death by apoptosis. Trends Mol Med *12*, 440-450.

135. Zhao, R., Gish, K., Murphy, M., Yin, Y., Notterman, D., Hoffman, W.H., Tom, E., Mack, D.H., and Levine, A.J. (2000). Analysis of p53-regulated gene expression patterns using oligonucleotide arrays. Genes Dev *14*, 981-993.

136. Degterev, A., and Yuan, J. (2008). Expansion and evolution of cell death programmes. Nat Rev Mol Cell Biol *9*, 378-390.

137. Wang, J.Y. (2005). Nucleo-cytoplasmic communication in apoptotic response to genotoxic and inflammatory stress. Cell Res *15*, 43-48.

138. Youle, R.J., and Strasser, A. (2008). The BCL-2 protein family: opposing activities that mediate cell death. Nat Rev Mol Cell Biol *9*, 47-59.

139. Degterev, A., Boyce, M., and Yuan, J. (2003). A decade of caspases. Oncogene *22*, 8543-8567.

140. d'Adda di Fagagna, F. (2008). Living on a break: cellular senescence as a DNA-damage response. Nat Rev Cancer *8*, 512-522.

141. d'Adda di Fagagna, F., Reaper, P.M., Clay-Farrace, L., Fiegler, H., Carr, P., Von Zglinicki, T., Saretzki, G., Carter, N.P., and Jackson, S.P. (2003). A DNA damage checkpoint response in telomere-initiated senescence. Nature *426*, 194-198.

142. Takai, H., Smogorzewska, A., and de Lange, T. (2003). DNA damage foci at dysfunctional telomeres. Curr Biol *13*, 1549-1556.

143. Marti, T.M., and Fleck, O. (2004). DNA repair nucleases. Cell Mol Life Sci *61*, 336-354.

144. Hegde, M.L., Hazra, T.K., and Mitra, S. (2008). Early steps in the DNA base excision/single-strand interruption repair pathway in mammalian cells. Cell Res *18*, 27-47.

145. Caldecott, K.W. (2008). Single-strand break repair and genetic disease. Nat Rev Genet *9*, 619-631.

146. Dianov, G.L., and Parsons, J.L. (2007). Co-ordination of DNA single strand break repair. DNA Repair (Amst) *6*, 454-460.

147. Pena-Diaz, J., and Jiricny, J. (2012). Mammalian mismatch repair: error-free or error-prone? Trends Biochem Sci *37*, 206-214.

148. Zhang, Y., Yuan, F., Presnell, S.R., Tian, K., Gao, Y., Tomkinson, A.E., Gu, L., and Li, G.M. (2005). Reconstitution of 5'-directed human mismatch repair in a purified system. Cell *122*, 693-705.

149. Nishino, T., and Morikawa, K. (2002). Structure and function of nucleases in DNA repair: shape, grip and blade of the DNA scissors. Oncogene *21*, 9022-9032.

150. Pluciennik, A., Dzantiev, L., Iyer, R.R., Constantin, N., Kadyrov, F.A., and Modrich, P. (2010). PCNA function in the activation and strand direction of MutLalpha endonuclease in mismatch repair. Proc Natl Acad Sci U S A *107*, 16066-16071.

151. Jalal, S., Earley, J.N., and Turchi, J.J. (2011). DNA repair: from genome maintenance to biomarker and therapeutic target. Clin Cancer Res *17*, 6973-6984.

152. Lagerwerf, S., Vrouwe, M.G., Overmeer, R.M., Fousteri, M.I., and Mullenders, L.H. (2011). DNA damage response and transcription. DNA Repair (Amst) *10*, 743-750.

153. Bardwell, A.J., Bardwell, L., Tomkinson, A.E., and Friedberg, E.C. (1994). Specific cleavage of model recombination and repair intermediates by the yeast Rad1-Rad10 DNA endonuclease. Science *265*, 2082-2085.

154. O'Donovan, A., Davies, A.A., Moggs, J.G., West, S.C., and Wood, R.D. (1994). XPG endonuclease makes the 3' incision in human DNA nucleotide excision repair. Nature *371*, 432-435.

155. Ogi, T., Limsirichaikul, S., Overmeer, R.M., Volker, M., Takenaka, K., Cloney, R., Nakazawa, Y., Niimi, A., Miki, Y., Jaspers, N.G., Mullenders, L.H., Yamashita, S., Fousteri, M.I., and Lehmann, A.R. (2010). Three DNA polymerases, recruited by different mechanisms, carry out NER repair synthesis in human cells. Mol Cell *37*, 714-727.

156. Staresincic, L., Fagbemi, A.F., Enzlin, J.H., Gourdin, A.M., Wijgers, N., Dunand-Sauthier, I., Giglia-Mari, G., Clarkson, S.G., Vermeulen, W., and Scharer, O.D. (2009). Coordination of dual incision and repair synthesis in human nucleotide excision repair. Embo J *28*, 1111-1120.

157. Nouspikel, T. (2009). DNA repair in mammalian cells: So DNA repair really is that important? Cell Mol Life Sci *66*, 965-967.

158. Sonoda, E., Hochegger, H., Saberi, A., Taniguchi, Y., and Takeda, S. (2006). Differential usage of non-homologous end-joining and homologous recombination in double strand break repair. DNA Repair (Amst) *5*, 1021-1029.

159. Aziz, K., Nowsheen, S., Pantelias, G., Iliakis, G., Gorgoulis, V.G., and Georgakilas, A.G. (2012). Targeting DNA damage and repair: embracing the pharmacological era for successful cancer therapy. Pharmacol Ther *133*, 334-350.

160. Langerak, P., and Russell, P. (2011). Regulatory networks integrating cell cycle control with DNA damage checkpoints and double-strand break repair. Philos Trans R Soc Lond B Biol Sci *366*, 3562-3571.

161. Takata, M., Sasaki, M.S., Sonoda, E., Morrison, C., Hashimoto, M., Utsumi, H., Yamaguchi-Iwai, Y., Shinohara, A., and Takeda, S. (1998). Homologous

recombination and non-homologous end-joining pathways of DNA double-strand break repair have overlapping roles in the maintenance of chromosomal integrity in vertebrate cells. Embo J *17*, 5497-5508.

162. Grawunder, U., Zimmer, D., and Leiber, M.R. (1998). DNA ligase IV binds to XRCC4 via a motif located between rather than within its BRCT domains. Curr Biol *8*, 873-876.

163. Buck, D., Malivert, L., de Chasseval, R., Barraud, A., Fondaneche, M.C., Sanal, O., Plebani, A., Stephan, J.L., Hufnagel, M., le Deist, F., Fischer, A., Durandy, A., de Villartay, J.P., and Revy, P. (2006). Cernunnos, a novel nonhomologous end-joining factor, is mutated in human immunodeficiency with microcephaly. Cell *124*, 287-299.

164. Weterings, E., and Chen, D.J. (2008). The endless tale of non-homologous end-joining. Cell Res *18*, 114-124.

165. Ahnesorg, P., Smith, P., and Jackson, S.P. (2006). XLF interacts with the XRCC4-DNA ligase IV complex to promote DNA nonhomologous end-joining. Cell *124*, 301-313.

166. McVey, M., and Lee, S.E. (2008). MMEJ repair of double-strand breaks (director's cut): deleted sequences and alternative endings. Trends Genet *24*, 529-538.

167. Bennardo, N., Cheng, A., Huang, N., and Stark, J.M. (2008). Alternative-NHEJ is a mechanistically distinct pathway of mammalian chromosome break repair. PLoS Genet *4*, e1000110.

168. Decottignies, A. (2013). Alternative end-joining mechanisms: a historical perspective. Front Genet *4*, 1-7.

169. Pardo, B., Gomez-Gonzalez, B., and Aguilera, A. (2009). DNA repair in mammalian cells: DNA double-strand break repair: how to fix a broken relationship. Cell Mol Life Sci *66*, 1039-1056.

170. van den Bosch, M., Bree, R.T., and Lowndes, N.F. (2003). The MRN complex: coordinating and mediating the response to broken chromosomes. EMBO Rep *4*, 844-849.

171. Baumann, P., and West, S.C. (1998). Role of the human RAD51 protein in homologous recombination and double-stranded-break repair. Trends Biochem Sci *23*, 247-251.

172. Ira, G., Pellicioli, A., Balijja, A., Wang, X., Fiorani, S., Carotenuto, W., Liberi, G., Bressan, D., Wan, L., Hollingsworth, N.M., Haber, J.E., and Foiani, M. (2004). DNA end resection, homologous recombination and DNA damage checkpoint activation require CDK1. Nature *431*, 1011-1017.

173. Symington, L.S., and Gautier, J. (2011). Double-strand break end resection and repair pathway choice. Annu Rev Genet *45*, 247-271.

174. Huertas, P. (2010). DNA resection in eukaryotes: deciding how to fix the break. Nat Struct Mol Biol *17*, 11-16.

175. Falck, J., Forment, J.V., Coates, J., Mistrik, M., Lukas, J., Bartek, J., and Jackson, S.P. (2012). CDK targeting of NBS1 promotes DNA-end resection, replication restart and homologous recombination. EMBO Rep *13*, 561-568.

176. Wang, H., Shi, L.Z., Wong, C.C., Han, X., Hwang, P.Y., Truong, L.N., Zhu, Q., Shao, Z., Chen, D.J., Berns, M.W., Yates, J.R., 3rd, Chen, L., and Wu, X. (2013). The interaction of CtIP and Nbs1 connects CDK and ATM to regulate HR-mediated double-strand break repair. PLoS Genet *9*, e1003277.

177. Yu, X., and Chen, J. (2004). DNA damage-induced cell cycle checkpoint control requires CtIP, a phosphorylation-dependent binding partner of BRCA1 C-terminal domains. Mol Cell Biol *24*, 9478-9486.

178. Sartori, A.A., Lukas, C., Coates, J., Mistrik, M., Fu, S., Bartek, J., Baer, R., Lukas, J., and Jackson, S.P. (2007). Human CtIP promotes DNA end resection. Nature *450*, 509-514.

179. Chen, L., Nievera, C.J., Lee, A.Y., and Wu, X. (2008). Cell cycle-dependent complex formation of BRCA1.CtIP.MRN is important for DNA double-strand break repair. J Biol Chem *283*, 7713-7720.

180. Yun, M.H., and Hiom, K. (2009). CtIP-BRCA1 modulates the choice of DNA double-strand-break repair pathway throughout the cell cycle. Nature *459*, 460-463.

181. Chapman, J.R., Sossick, A.J., Boulton, S.J., and Jackson, S.P. (2012). BRCA1-associated exclusion of 53BP1 from DNA damage sites underlies temporal control of DNA repair. J Cell Sci *125*, 3529-3534.

182. Bunting, S.F., Callen, E., Wong, N., Chen, H.T., Polato, F., Gunn, A., Bothmer, A., Feldhahn, N., Fernandez-Capetillo, O., Cao, L., Xu, X., Deng, C.X., Finkel, T., Nussenzweig, M., Stark, J.M., and Nussenzweig, A. (2010). 53BP1 inhibits

homologous recombination in Brca1-deficient cells by blocking resection of DNA breaks. Cell *141*, 243-254.

183. Noon, A.T., and Goodarzi, A.A. (2011). 53BP1-mediated DNA double strand break repair: insert bad pun here. DNA Repair (Amst) *10*, 1071-1076.

184. Feng, L., Fong, K.W., Wang, J., Wang, W., and Chen, J. (2013). RIF1 counteracts BRCA1-mediated end resection during DNA repair. J Biol Chem.

185. Zimmermann, M., Lottersberger, F., Buonomo, S.B., Sfeir, A., and de Lange, T. (2013). 53BP1 regulates DSB repair using Rif1 to control 5' end resection. Science *339*, 700-704.

186. Chapman, J.R., Barral, P., Vannier, J.B., Borel, V., Steger, M., Tomas-Loba, A., Sartori, A.A., Adams, I.R., Batista, F.D., and Boulton, S.J. (2013). RIF1 Is Essential for 53BP1-Dependent Nonhomologous End Joining and Suppression of DNA Double-Strand Break Resection. Mol Cell *49*, 858-871.

187. Di Virgilio, M., Callen, E., Yamane, A., Zhang, W., Jankovic, M., Gitlin, A.D., Feldhahn, N., Resch, W., Oliveira, T.Y., Chait, B.T., Nussenzweig, A., Casellas, R., Robbiani, D.F., and Nussenzweig, M.C. (2013). Rif1 prevents resection of DNA breaks and promotes immunoglobulin class switching. Science *339*, 711-715.

188. Bouwman, P., Aly, A., Escandell, J.M., Pieterse, M., Bartkova, J., van der Gulden, H., Hiddingh, S., Thanasoula, M., Kulkarni, A., Yang, Q., Haffty, B.G., Tommiska, J., Blomqvist, C., Drapkin, R., Adams, D.J., Nevanlinna, H., Bartek, J., Tarsounas, M., Ganesan, S., and Jonkers, J. (2010). 53BP1 loss rescues

BRCA1 deficiency and is associated with triple-negative and BRCA-mutated breast cancers. Nat Struct Mol Biol *17*, 688-695.

189. Cao, L., Xu, X., Bunting, S.F., Liu, J., Wang, R.H., Cao, L.L., Wu, J.J., Peng, T.N., Chen, J., Nussenzweig, A., Deng, C.X., and Finkel, T. (2009). A selective requirement for 53BP1 in the biological response to genomic instability induced by Brca1 deficiency. Mol Cell *35*, 534-541.

190. Mimitou, E.P., and Symington, L.S. (2009). Nucleases and helicases take center stage in homologous recombination. Trends Biochem Sci *34*, 264-272.

191. Amundsen, S.K., and Smith, G.R. (2003). Interchangeable parts of the Escherichia coli recombination machinery. Cell *112*, 741-744.

192. Gravel, S., Chapman, J.R., Magill, C., and Jackson, S.P. (2008). DNA helicases Sgs1 and BLM promote DNA double-strand break resection. Genes Dev *22*, 2767-2772.

193. Zhu, Z., Chung, W.H., Shim, E.Y., Lee, S.E., and Ira, G. (2008). Sgs1 helicase and two nucleases Dna2 and Exo1 resect DNA double-strand break ends. Cell *134*, 981-994.

194. Mimitou, E.P., and Symington, L.S. (2008). Sae2, Exo1 and Sgs1 collaborate in DNA double-strand break processing. Nature *455*, 770-774.

195. Nimonkar, A.V., Genschel, J., Kinoshita, E., Polaczek, P., Campbell, J.L., Wyman, C., Modrich, P., and Kowalczykowski, S.C. (2011). BLM-DNA2-RPA-MRN and EXO1-BLM-RPA-MRN constitute two DNA end resection machineries for human DNA break repair. Genes Dev *25*, 350-362.

196. Bothmer, A., Rommel, P.C., Gazumyan, A., Polato, F., Reczek, C.R., Muellenbeck, M.F., Schaetzlein, S., Edelmann, W., Chen, P.L., Brosh, R.M., Jr., Casellas, R., Ludwig, T., Baer, R., Nussenzweig, A., Nussenzweig, M.C., and Robbiani, D.F. (2013). Mechanism of DNA resection during intrachromosomal recombination and immunoglobulin class switching. J Exp Med *210*, 115-123.

197. Tomimatsu, N., Mukherjee, B., Deland, K., Kurimasa, A., Bolderson, E., Khanna, K.K., and Burma, S. (2012). Exo1 plays a major role in DNA end resection in humans and influences double-strand break repair and damage signaling decisions. DNA Repair (Amst) *11*, 441-448.

198. Larsen, N.B., and Hickson, I.D. (2013). RecQ Helicases: Conserved Guardians of Genomic Integrity. Adv Exp Med Biol *767*, 161-184.

199. Zheng, L., Kanagaraj, R., Mihaljevic, B., Schwendener, S., Sartori, A.A., Gerrits, B., Shevelev, I., and Janscak, P. (2009). MRE11 complex links RECQ5 helicase to sites of DNA damage. Nucleic Acids Res *37*, 2645-2657.

200. Yan, H., Toczylowski, T., McCane, J., Chen, C., and Liao, S. (2011). Replication protein A promotes 5'-->3' end processing during homology-dependent DNA double-strand break repair. J Cell Biol *192*, 251-261.

201. Binz, S.K., Sheehan, A.M., and Wold, M.S. (2004). Replication protein A phosphorylation and the cellular response to DNA damage. DNA Repair (Amst) *3*, 1015-1024.

202. San Filippo, J., Sung, P., and Klein, H. (2008). Mechanism of eukaryotic homologous recombination. Annu Rev Biochem *77*, 229-257.

203. Jensen, R.B., Carreira, A., and Kowalczykowski, S.C. (2010). Purified human BRCA2 stimulates RAD51-mediated recombination. Nature *467*, 678-683.

204. Liu, J., Doty, T., Gibson, B., and Heyer, W.D. (2010). Human BRCA2 protein promotes RAD51 filament formation on RPA-covered single-stranded DNA. Nat Struct Mol Biol *17*, 1260-1262.

205. Thorslund, T., McIlwraith, M.J., Compton, S.A., Lekomtsev, S., Petronczki, M., Griffith, J.D., and West, S.C. (2010). The breast cancer tumor suppressor BRCA2 promotes the specific targeting of RAD51 to single-stranded DNA. Nat Struct Mol Biol *17*, 1263-1265.

206. Xia, B., Sheng, Q., Nakanishi, K., Ohashi, A., Wu, J., Christ, N., Liu, X., Jasin, M., Couch, F.J., and Livingston, D.M. (2006). Control of BRCA2 cellular and clinical functions by a nuclear partner, PALB2. Mol Cell *22*, 719-729.

207. Sy, S.M., Huen, M.S., and Chen, J. (2009). PALB2 is an integral component of the BRCA complex required for homologous recombination repair. Proc Natl Acad Sci U S A *106*, 7155-7160.

208. Zhang, F., Fan, Q., Ren, K., and Andreassen, P.R. (2009). PALB2 functionally connects the breast cancer susceptibility proteins BRCA1 and BRCA2. Mol Cancer Res *7*, 1110-1118.

209. Zhang, F., Ma, J., Wu, J., Ye, L., Cai, H., Xia, B., and Yu, X. (2009). PALB2 links BRCA1 and BRCA2 in the DNA-damage response. Curr Biol *19*, 524-529.

210. Mazon, G., Mimitou, E.P., and Symington, L.S. (2010). SnapShot: Homologous recombination in DNA double-strand break repair. Cell *142*, 646, 646 e641.

211. Modesti, M., Budzowska, M., Baldeyron, C., Demmers, J.A., Ghirlando, R., and Kanaar, R. (2007). RAD51AP1 is a structure-specific DNA binding protein that stimulates joint molecule formation during RAD51-mediated homologous recombination. Mol Cell *28*, 468-481.

212. Wiese, C., Dray, E., Groesser, T., San Filippo, J., Shi, I., Collins, D.W., Tsai, M.S., Williams, G.J., Rydberg, B., Sung, P., and Schild, D. (2007). Promotion of homologous recombination and genomic stability by RAD51AP1 via RAD51 recombinase enhancement. Mol Cell *28*, 482-490.

213. Lok, B.H., Carley, A.C., Tchang, B., and Powell, S.N. (2012). RAD52 inactivation is synthetically lethal with deficiencies in BRCA1 and PALB2 in addition to BRCA2 through RAD51-mediated homologous recombination. Oncogene.

214. Stark, J.M., Pierce, A.J., Oh, J., Pastink, A., and Jasin, M. (2004). Genetic steps of mammalian homologous repair with distinct mutagenic consequences. Mol Cell Biol *24*, 9305-9316.

215. Liu, Y., and West, S.C. (2004). Happy Hollidays: 40th anniversary of the Holliday junction. Nat Rev Mol Cell Biol *5*, 937-944.

216. Deans, A.J., and West, S.C. (2011). DNA interstrand crosslink repair and cancer. Nat Rev Cancer *11*, 467-480.

217. Dronkert, M.L., and Kanaar, R. (2001). Repair of DNA interstrand cross-links. Mutat Res *486*, 217-247.

218. Muniandy, P.A., Liu, J., Majumdar, A., Liu, S.T., and Seidman, M.M. (2010). DNA interstrand crosslink repair in mammalian cells: step by step. Crit Rev Biochem Mol Biol *45*, 23-49.

219. Hlavin, E.M., Smeaton, M.B., and Miller, P.S. (2010). Initiation of DNA interstrand cross-link repair in mammalian cells. Environ Mol Mutagen *51*, 604-624.

220. Nakanishi, K., Cavallo, F., Perrouault, L., Giovannangeli, C., Moynahan, M.E., Barchi, M., Brunet, E., and Jasin, M. (2011). Homology-directed Fanconi anemia pathway cross-link repair is dependent on DNA replication. Nat Struct Mol Biol *18*, 500-503.

221. Hinz, J.M. (2010). Role of homologous recombination in DNA interstrand crosslink repair. Environ Mol Mutagen *51*, 582-603.

222. Akkari, Y.M., Bateman, R.L., Reifsteck, C.A., Olson, S.B., and Grompe, M. (2000). DNA replication is required To elicit cellular responses to psoralen-induced DNA interstrand cross-links. Mol Cell Biol *20*, 8283-8289.

223. Long, D.T., Raschle, M., Joukov, V., and Walter, J.C. (2011). Mechanism of RAD51-dependent DNA interstrand cross-link repair. Science *333*, 84-87.

224. Kottemann, M.C., and Smogorzewska, A. (2013). Fanconi anaemia and the repair of Watson and Crick DNA crosslinks. Nature *493*, 356-363.

225. Ciccia, A., McDonald, N., and West, S.C. (2008). Structural and functional relationships of the XPF/MUS81 family of proteins. Annu Rev Biochem *77*, 259-287.

226. Singh, T.R., Saro, D., Ali, A.M., Zheng, X.F., Du, C.H., Killen, M.W., Sachpatzidis, A., Wahengbam, K., Pierce, A.J., Xiong, Y., Sung, P., and Meetei, A.R. (2010). MHF1-MHF2, a histone-fold-containing protein complex, participates in the Fanconi anemia pathway via FANCM. Mol Cell *37*, 879-886.

227. Kim, J.M., Kee, Y., Gurtan, A., and D'Andrea, A.D. (2008). Cell cycle-dependent chromatin loading of the Fanconi anemia core complex by FANCM/FAAP24. Blood *111*, 5215-5222.

228. Yan, Z., Delannoy, M., Ling, C., Daee, D., Osman, F., Muniandy, P.A., Shen, X., Oostra, A.B., Du, H., Steltenpool, J., Lin, T., Schuster, B., Decaillet, C., Stasiak, A., Stasiak, A.Z., Stone, S., Hoatlin, M.E., Schindler, D., Woodcock, C.L., Joenje, H., Sen, R., de Winter, J.P., Li, L., Seidman, M.M., Whitby, M.C., Myung, K., Constantinou, A., and Wang, W. (2010). A histone-fold complex and FANCM form a conserved DNA-remodeling complex to maintain genome stability. Mol Cell *37*, 865-878.

229. Gari, K., Decaillet, C., Delannoy, M., Wu, L., and Constantinou, A. (2008). Remodeling of DNA replication structures by the branch point translocase FANCM. Proc Natl Acad Sci U S A *105*, 16107-16112.

230. Deans, A.J., and West, S.C. (2009). FANCM connects the genome instability disorders Bloom's Syndrome and Fanconi Anemia. Mol Cell *36*, 943-953.

231. Gari, K., Decaillet, C., Stasiak, A.Z., Stasiak, A., and Constantinou, A. (2008). The Fanconi anemia protein FANCM can promote branch migration of Holliday junctions and replication forks. Mol Cell *29*, 141-148.

232. Leung, J.W., Wang, Y., Fong, K.W., Huen, M.S., Li, L., and Chen, J. (2012). Fanconi anemia (FA) binding protein FAAP20 stabilizes FA complementation group A (FANCA) and participates in interstrand cross-link repair. Proc Natl Acad Sci U S A *109*, 4491-4496.

233. Ling, C., Ishiai, M., Ali, A.M., Medhurst, A.L., Neveling, K., Kalb, R., Yan, Z., Xue, Y., Oostra, A.B., Auerbach, A.D., Hoatlin, M.E., Schindler, D., Joenje, H., de Winter, J.P., Takata, M., Meetei, A.R., and Wang, W. (2007). FAAP100 is essential for activation of the Fanconi anemia-associated DNA damage response pathway. Embo J *26*, 2104-2114.

234. Smogorzewska, A., Matsuoka, S., Vinciguerra, P., McDonald, E.R., 3rd, Hurov, K.E., Luo, J., Ballif, B.A., Gygi, S.P., Hofmann, K., D'Andrea, A.D., and Elledge, S.J. (2007). Identification of the FANCI protein, a monoubiquitinated FANCD2 paralog required for DNA repair. Cell *129*, 289-301.

235. Matsushita, N., Kitao, H., Ishiai, M., Nagashima, N., Hirano, S., Okawa, K., Ohta, T., Yu, D.S., McHugh, P.J., Hickson, I.D., Venkitaraman, A.R., Kurumizaka, H., and Takata, M. (2005). A FancD2-monoubiquitin fusion reveals hidden functions of Fanconi anemia core complex in DNA repair. Mol Cell *19*, 841-847.

236. Alpi, A.F., Pace, P.E., Babu, M.M., and Patel, K.J. (2008). Mechanistic insight into site-restricted monoubiquitination of FANCD2 by Ube2t, FANCL, and FANCI. Mol Cell *32*, 767-777.

237. Meetei, A.R., de Winter, J.P., Medhurst, A.L., Wallisch, M., Waisfisz, Q., van de Vrugt, H.J., Oostra, A.B., Yan, Z., Ling, C., Bishop, C.E., Hoatlin, M.E., Joenje,

H., and Wang, W. (2003). A novel ubiquitin ligase is deficient in Fanconi anemia. Nat Genet *35*, 165-170.

238. Machida, Y.J., Machida, Y., Chen, Y., Gurtan, A.M., Kupfer, G.M., D'Andrea, A.D., and Dutta, A. (2006). UBE2T is the E2 in the Fanconi anemia pathway and undergoes negative autoregulation. Mol Cell *23*, 589-596.

239. Ciccia, A., Ling, C., Coulthard, R., Yan, Z., Xue, Y., Meetei, A.R., Laghmani el, H., Joenje, H., McDonald, N., de Winter, J.P., Wang, W., and West, S.C. (2007). Identification of FAAP24, a Fanconi anemia core complex protein that interacts with FANCM. Mol Cell *25*, 331-343.

240. Sato, K., Toda, K., Ishiai, M., Takata, M., and Kurumizaka, H. (2012). DNA robustly stimulates FANCD2 monoubiquitylation in the complex with FANCI. Nucleic Acids Res *40*, 4553-4561.

241. Stoepker, C., Hain, K., Schuster, B., Hilhorst-Hofstee, Y., Rooimans, M.A., Steltenpool, J., Oostra, A.B., Eirich, K., Korthof, E.T., Nieuwint, A.W., Jaspers, N.G., Bettecken, T., Joenje, H., Schindler, D., Rouse, J., and de Winter, J.P. (2011). SLX4, a coordinator of structure-specific endonucleases, is mutated in a new Fanconi anemia subtype. Nat Genet *43*, 138-141.

242. Munoz, I.M., Hain, K., Declais, A.C., Gardiner, M., Toh, G.W., Sanchez-Pulido, L., Heuckmann, J.M., Toth, R., Macartney, T., Eppink, B., Kanaar, R., Ponting, C.P., Lilley, D.M., and Rouse, J. (2009). Coordination of structure-specific nucleases by human SLX4/BTBD12 is required for DNA repair. Mol Cell *35*, 116-127.

243. Andersen, S.L., Bergstralh, D.T., Kohl, K.P., LaRocque, J.R., Moore, C.B., and Sekelsky, J. (2009). Drosophila MUS312 and the vertebrate ortholog BTBD12 interact with DNA structure-specific endonucleases in DNA repair and recombination. Mol Cell *35*, 128-135.

244. Svendsen, J.M., Smogorzewska, A., Sowa, M.E., O'Connell, B.C., Gygi, S.P., Elledge, S.J., and Harper, J.W. (2009). Mammalian BTBD12/SLX4 assembles a Holliday junction resolvase and is required for DNA repair. Cell *138*, 63-77.

245. Kim, Y., Spitz, G.S., Veturi, U., Lach, F.P., Auerbach, A.D., and Smogorzewska, A. (2012). Regulation of multiple DNA repair pathways by the Fanconi anemia protein SLX4. Blood *121*, 54-63.

246. Al-Minawi, A.Z., Lee, Y.F., Hakansson, D., Johansson, F., Lundin, C., Saleh-Gohari, N., Schultz, N., Jenssen, D., Bryant, H.E., Meuth, M., Hinz, J.M., and Helleday, T. (2009). The ERCC1/XPF endonuclease is required for completion of homologous recombination at DNA replication forks stalled by inter-strand cross-links. Nucleic Acids Res *37*, 6400-6413.

247. Fekairi, S., Scaglione, S., Chahwan, C., Taylor, E.R., Tissier, A., Coulon, S., Dong, M.Q., Ruse, C., Yates, J.R., 3rd, Russell, P., Fuchs, R.P., McGowan, C.H., and Gaillard, P.H. (2009). Human SLX4 is a Holliday junction resolvase subunit that binds multiple DNA repair/recombination endonucleases. Cell *138*, 78-89.

248. Smogorzewska, A., Desetty, R., Saito, T.T., Schlabach, M., Lach, F.P., Sowa, M.E., Clark, A.B., Kunkel, T.A., Harper, J.W., Colaiacovo, M.P., and Elledge,

S.J. (2010). A genetic screen identifies FAN1, a Fanconi anemia-associated nuclease necessary for DNA interstrand crosslink repair. Mol Cell *39*, 36-47.

249. Kratz, K., Schopf, B., Kaden, S., Sendoel, A., Eberhard, R., Lademann, C., Cannavo, E., Sartori, A.A., Hengartner, M.O., and Jiricny, J. (2010). Deficiency of FANCD2-associated nuclease KIAA1018/FAN1 sensitizes cells to interstrand crosslinking agents. Cell *142*, 77-88.

250. MacKay, C., Declais, A.C., Lundin, C., Agostinho, A., Deans, A.J., MacArtney, T.J., Hofmann, K., Gartner, A., West, S.C., Helleday, T., Lilley, D.M., and Rouse, J. (2010). Identification of KIAA1018/FAN1, a DNA repair nuclease recruited to DNA damage by monoubiquitinated FANCD2. Cell *142*, 65-76.

251. Moldovan, G.L., Madhavan, M.V., Mirchandani, K.D., McCaffrey, R.M., Vinciguerra, P., and D'Andrea, A.D. (2010). DNA polymerase POLN participates in cross-link repair and homologous recombination. Mol Cell Biol *30*, 1088-1096.

252. Liu, T., Ghosal, G., Yuan, J., Chen, J., and Huang, J. (2010). FAN1 acts with FANCI-FANCD2 to promote DNA interstrand cross-link repair. Science *329*, 693-696.

253. Wang, A.T., Sengerova, B., Cattell, E., Inagawa, T., Hartley, J.M., Kiakos, K., Burgess-Brown, N.A., Swift, L.P., Enzlin, J.H., Schofield, C.J., Gileadi, O., Hartley, J.A., and McHugh, P.J. (2011). Human SNM1A and XPF-ERCC1 collaborate to initiate DNA interstrand cross-link repair. Genes Dev *25*, 1859-1870.

254. Lio, Y.C., Schild, D., Brenneman, M.A., Redpath, J.L., and Chen, D.J. (2004). Human Rad51C deficiency destabilizes XRCC3, impairs recombination, and radiosensitizes S/G2-phase cells. J Biol Chem *279*, 42313-42320.

255. Lio, Y.C., Mazin, A.V., Kowalczykowski, S.C., and Chen, D.J. (2003). Complex formation by the human Rad51B and Rad51C DNA repair proteins and their activities in vitro. J Biol Chem *278*, 2469-2478.

256. Meetei, A.R., Sechi, S., Wallisch, M., Yang, D., Young, M.K., Joenje, H., Hoatlin, M.E., and Wang, W. (2003). A multiprotein nuclear complex connects Fanconi anemia and Bloom syndrome. Mol Cell Biol *23*, 3417-3426.

257. Wechsler, T., Newman, S., and West, S.C. (2011). Aberrant chromosome morphology in human cells defective for Holliday junction resolution. Nature *471*, 642-646.

258. Hashimoto, Y., Ray Chaudhuri, A., Lopes, M., and Costanzo, V. (2010). Rad51 protects nascent DNA from Mre11-dependent degradation and promotes continuous DNA synthesis. Nat Struct Mol Biol *17*, 1305-1311.

259. Lutzmann, M., Grey, C., Traver, S., Ganier, O., Maya-Mendoza, A., Ranisavljevic, N., Bernex, F., Nishiyama, A., Montel, N., Gavois, E., Forichon, L., de Massy, B., and Mechali, M. (2012). MCM8- and MCM9-deficient mice reveal gametogenesis defects and genome instability due to impaired homologous recombination. Mol Cell *47*, 523-534.

260. Nishimura, K., Ishiai, M., Horikawa, K., Fukagawa, T., Takata, M., Takisawa, H., and Kanemaki, M.T. (2012). Mcm8 and Mcm9 form a complex that functions in

homologous recombination repair induced by DNA interstrand crosslinks. Mol Cell *47*, 511-522.

261. Park, J., Long, D.T., Lee, K.Y., Abbas, T., Shibata, E., Negishi, M., Luo, Y., Schimenti, J.C., Gambus, A., Walter, J.C., and Dutta, A. (2013). The MCM8-MCM9 Complex Promotes RAD51 Recruitment at DNA Damage Sites To Facilitate Homologous Recombination. Mol Cell Biol *33*, 1632-1644.

262. Jackson, S.P., and Bartek, J. (2009). The DNA-damage response in human biology and disease. Nature *461*, 1071-1078.

263. Kerzendorfer, C., and O'Driscoll, M. (2009). Human DNA damage response and repair deficiency syndromes: linking genomic instability and cell cycle checkpoint proficiency. DNA Repair (Amst) *8*, 1139-1152.

264. Rass, U., Ahel, I., and West, S.C. (2007). Defective DNA repair and neurodegenerative disease. Cell *130*, 991-1004.

265. Weissman, L., de Souza-Pinto, N.C., Stevnsner, T., and Bohr, V.A. (2007). DNA repair, mitochondria, and neurodegeneration. Neuroscience *145*, 1318-1329.

266. Kumari, D., Somma, V., Nakamura, A.J., Bonner, W.M., D'Ambrosio, E., and Usdin, K. (2009). The role of DNA damage response pathways in chromosome fragility in Fragile X syndrome. Nucleic Acids Res *37*, 4385-4392.

267. Savitsky, K., Bar-Shira, A., Gilad, S., Rotman, G., Ziv, Y., Vanagaite, L., Tagle, D.A., Smith, S., Uziel, T., Sfez, S., Ashkenazi, M., Pecker, I., Frydman, M., Harnik, R., Patanjali, S.R., Simmons, A., Clines, G.A., Sartiel, A., Gatti, R.A., Chessa, L., Sanal, O., Lavin, M.F., Jaspers, N.G., Taylor, A.M., Arlett, C.F.,

Miki, T., Weissman, S.M., Lovett, M., Collins, F.S., and Shiloh, Y. (1995). A single ataxia telangiectasia gene with a product similar to PI-3 kinase. Science *268*, 1749-1753.

268. Ogi, T., Walker, S., Stiff, T., Hobson, E., Limsirichaikul, S., Carpenter, G., Prescott, K., Suri, M., Byrd, P.J., Matsuse, M., Mitsutake, N., Nakazawa, Y., Vasudevan, P., Barrow, M., Stewart, G.S., Taylor, A.M., O'Driscoll, M., and Jeggo, P.A. (2012). Identification of the first ATRIP-deficient patient and novel mutations in ATR define a clinical spectrum for ATR-ATRIP Seckel Syndrome. PLoS Genet *8*, e1002945.

269. Martin-Lopez, J.V., and Fishel, R. (2013). The mechanism of mismatch repair and the functional analysis of mismatch repair defects in Lynch syndrome. Fam Cancer.

270. O'Driscoll, M., Cerosaletti, K.M., Girard, P.M., Dai, Y., Stumm, M., Kysela, B., Hirsch, B., Gennery, A., Palmer, S.E., Seidel, J., Gatti, R.A., Varon, R., Oettinger, M.A., Neitzel, H., Jeggo, P.A., and Concannon, P. (2001). DNA ligase IV mutations identified in patients exhibiting developmental delay and immunodeficiency. Mol Cell *8*, 1175-1185.

271. Kamileri, I., Karakasilioti, I., and Garinis, G.A. (2012). Nucleotide excision repair: new tricks with old bricks. Trends Genet *28*, 566-573.

272. Cleaver, J.E. (1969). Xeroderma pigmentosum: a human disease in which an initial stage of DNA repair is defective. Proc Natl Acad Sci U S A *63*, 428-435.

273. Nouspikel, T. (2008). Nucleotide excision repair and neurological diseases. DNA Repair (Amst) *7*, 1155-1167.

274. Niedernhofer, L.J., Lalai, A.S., and Hoeijmakers, J.H. (2005). Fanconi anemia (cross)linked to DNA repair. Cell *123*, 1191-1198.

275. Monnat, R.J., Jr. (2010). Human RECQ helicases: roles in DNA metabolism, mutagenesis and cancer biology. Semin Cancer Biol *20*, 329-339.

276. Matsuoka, S., Rotman, G., Ogawa, A., Shiloh, Y., Tamai, K., and Elledge, S.J. (2000). Ataxia telangiectasia-mutated phosphorylates Chk2 in vivo and in vitro. Proc Natl Acad Sci U S A *97*, 10389-10394.

277. Matsuoka, S., Ballif, B.A., Smogorzewska, A., McDonald, E.R., 3rd, Hurov, K.E., Luo, J., Bakalarski, C.E., Zhao, Z., Solimini, N., Lerenthal, Y., Shiloh, Y., Gygi, S.P., and Elledge, S.J. (2007). ATM and ATR substrate analysis reveals extensive protein networks responsive to DNA damage. Science *316*, 1160-1166.

278. Buday, L. (1999). Membrane-targeting of signalling molecules by SH2/SH3 domain-containing adaptor proteins. Biochim Biophys Acta *1422*, 187-204.

279. McCarty, J.H. (1998). The Nck SH2/SH3 adaptor protein: a regulator of multiple intracellular signal transduction events. Bioessays *20*, 913-921.

280. Lehmann, J.M., Riethmuller, G., and Johnson, J.P. (1990). Nck, a melanoma cDNA encoding a cytoplasmic protein consisting of the src homology units SH2 and SH3. Nucleic Acids Res *18*, 1048.

281. Braverman, L.E., and Quilliam, L.A. (1999). Identification of Grb4/Nckbeta, a src homology 2 and 3 domain-containing adapter protein having similar binding and biological properties to Nck. J Biol Chem *274*, 5542-5549.

282. Bladt, F., Aippersbach, E., Gelkop, S., Strasser, G.A., Nash, P., Tafuri, A., Gertler, F.B., and Pawson, T. (2003). The murine Nck SH2/SH3 adaptors are important for the development of mesoderm-derived embryonic structures and for regulating the cellular actin network. Mol Cell Biol *23*, 4586-4597.

283. Matuoka, K., Miki, H., Takahashi, K., and Takenawa, T. (1997). A novel ligand for an SH3 domain of the adaptor protein Nck bears an SH2 domain and nuclear signaling motifs. Biochem Biophys Res Commun *239*, 488-492.

284. Smith, J.A., Poteet-Smith, C.E., Xu, Y., Errington, T.M., Hecht, S.M., and Lannigan, D.A. (2005). Identification of the first specific inhibitor of p90 ribosomal S6 kinase (RSK) reveals an unexpected role for RSK in cancer cell proliferation. Cancer Res *65*, 1027-1034.

285. Reaper, P.M., Griffiths, M.R., Long, J.M., Charrier, J.D., Maccormick, S., Charlton, P.A., Golec, J.M., and Pollard, J.R. (2011). Selective killing of ATM- or p53-deficient cancer cells through inhibition of ATR. Nat Chem Biol *7*, 428-430.

286. Joberty, G., Petersen, C., Gao, L., and Macara, I.G. (2000). The cell-polarity protein Par6 links Par3 and atypical protein kinase C to Cdc42. Nat Cell Biol *2*, 531-539.

287. Richards, S.A., Lounsbury, K.M., and Macara, I.G. (1995). The C terminus of the nuclear RAN/TC4 GTPase stabilizes the GDP-bound state and mediates

interactions with RCC1, RAN-GAP, and HTF9A/RANBP1. J Biol Chem *270*, 14405-14411.

288. Kirch, H.C., Flaswinkel, S., Rumpf, H., Brockmann, D., and Esche, H. (1999). Expression of human p53 requires synergistic activation of transcription from the p53 promoter by AP-1, NF-kappaB and Myc/Max. Oncogene *18*, 2728-2738.

289. Labelle-Cote, M., Dusseault, J., Ismail, S., Picard-Cloutier, A., Siegel, P.M., and Larose, L. (2011). Nck2 promotes human melanoma cell proliferation, migration and invasion in vitro and primary melanoma-derived tumor growth in vivo. BMC Cancer *11*, 443.

290. Dogusan, Z., Hooghe-Peters, E.L., Berus, D., Velkeniers, B., and Hooghe, R. (2000). Expression of SOCS genes in normal and leukemic human leukocytes stimulated by prolactin, growth hormone and cytokines. J Neuroimmunol *109*, 34-39.

291. Lal, A., Haynes, S.R., and Gorospe, M. (2005). Clean Western blot signals from immunoprecipitated samples. Mol Cell Probes *19*, 385-388.

292. Sarkaria, J.N., Tibbetts, R.S., Busby, E.C., Kennedy, A.P., Hill, D.E., and Abraham, R.T. (1998). Inhibition of phosphoinositide 3-kinase related kinases by the radiosensitizing agent wortmannin. Cancer Res *58*, 4375-4382.

293. Scheffner, M., Werness, B.A., Huibregtse, J.M., Levine, A.J., and Howley, P.M. (1990). The E6 oncoprotein encoded by human papillomavirus types 16 and 18 promotes the degradation of p53. Cell *63*, 1129-1136.

294. Chen, M., She, H., Davis, E.M., Spicer, C.M., Kim, L., Ren, R., Le Beau, M.M., and Li, W. (1998). Identification of Nck family genes, chromosomal localization, expression, and signaling specificity. J Biol Chem *273*, 25171-25178.

295. Chen, L.Y., and Chen, J.D. (2003). Daxx silencing sensitizes cells to multiple apoptotic pathways. Mol Cell Biol *23*, 7108-7121.

296. Liu, W., Li, W., Fujita, T., Yang, Q., and Wan, Y. (2008). Proteolysis of CDH1 enhances susceptibility to UV radiation-induced apoptosis. Carcinogenesis *29*, 263-272.

297. Lettau, M., Pieper, J., and Janssen, O. (2009). Nck adapter proteins: functional versatility in T cells. Cell Commun Signal *7*, 1.

298. Weirich, C.S., Erzberger, J.P., and Barral, Y. (2008). The septin family of GTPases: architecture and dynamics. Nat Rev Mol Cell Biol *9*, 478-489.

299. Raschle, M., Knipscheer, P., Enoiu, M., Angelov, T., Sun, J., Griffith, J.D., Ellenberger, T.E., Scharer, O.D., and Walter, J.C. (2008). Mechanism of replication-coupled DNA interstrand crosslink repair. Cell *134*, 969-980.

300. Moldovan, G.L., and D'Andrea, A.D. (2009). How the fanconi anemia pathway guards the genome. Annu Rev Genet *43*, 223-249.

301. Li, D., Kang, Q., and Wang, D.M. (2007). Constitutive coactivator of peroxisome proliferator-activated receptor (PPARgamma), a novel coactivator of PPARgamma that promotes adipogenesis. Mol Endocrinol *21*, 2320-2333.

302. Grasby, J.A., Finger, L.D., Tsutakawa, S.E., Atack, J.M., and Tainer, J.A. (2012). Unpairing and gating: sequence-independent substrate recognition by FEN superfamily nucleases. Trends Biochem Sci *37*, 74-84.

303. McCaffrey, L.M., and Macara, I.G. (2009). The Par3/aPKC interaction is essential for end bud remodeling and progenitor differentiation during mammary gland morphogenesis. Genes Dev *23*, 1450-1460.

304. Parvin, J., Chiba, N., and Ransburgh, D. (2011). Identifying the effects of BRCA1 mutations on homologous recombination using cells that express endogenous wild-type BRCA1. J Vis Exp.

305. Swann, P.F., Waters, T.R., Moulton, D.C., Xu, Y.Z., Zheng, Q., Edwards, M., and Mace, R. (1996). Role of postreplicative DNA mismatch repair in the cytotoxic action of thioguanine. Science *273*, 1109-1111.

306. Pierce, A.J., Johnson, R.D., Thompson, L.H., and Jasin, M. (1999). XRCC3 promotes homology-directed repair of DNA damage in mammalian cells. Genes Dev *13*, 2633-2638.

307. Pierce, A.J., Hu, P., Han, M., Ellis, N., and Jasin, M. (2001). Ku DNA end-binding protein modulates homologous repair of double-strand breaks in mammalian cells. Genes Dev *15*, 3237-3242.

308. Cotta-Ramusino, C., McDonald, E.R., 3rd, Hurov, K., Sowa, M.E., Harper, J.W., and Elledge, S.J. (2011). A DNA damage response screen identifies RHINO, a 9-1-1 and TopBP1 interacting protein required for ATR signaling. Science *332*, 1313-1317.

309. Hurov, K.E., Cotta-Ramusino, C., and Elledge, S.J. (2010). A genetic screen identifies the Triple T complex required for DNA damage signaling and ATM and ATR stability. Genes Dev *24*, 1939-1950.

310. Kim, S.T., Lim, D.S., Canman, C.E., and Kastan, M.B. (1999). Substrate specificities and identification of putative substrates of ATM kinase family members. J Biol Chem *274*, 37538-37543.

311. O'Neill, T., Dwyer, A.J., Ziv, Y., Chan, D.W., Lees-Miller, S.P., Abraham, R.H., Lai, J.H., Hill, D., Shiloh, Y., Cantley, L.C., and Rathbun, G.A. (2000). Utilization of oriented peptide libraries to identify substrate motifs selected by ATM. J Biol Chem *275*, 22719-22727.

312. Smolka, M.B., Albuquerque, C.P., Chen, S.H., and Zhou, H. (2007). Proteome-wide identification of in vivo targets of DNA damage checkpoint kinases. Proc Natl Acad Sci U S A *104*, 10364-10369.

313. Tibbetts, R.S., Brumbaugh, K.M., Williams, J.M., Sarkaria, J.N., Cliby, W.A., Shieh, S.Y., Taya, Y., Prives, C., and Abraham, R.T. (1999). A role for ATR in the DNA damage-induced phosphorylation of p53. Genes Dev *13*, 152-157.

314. Shafman, T., Khanna, K.K., Kedar, P., Spring, K., Kozlov, S., Yen, T., Hobson, K., Gatei, M., Zhang, N., Watters, D., Egerton, M., Shiloh, Y., Kharbanda, S., Kufe, D., and Lavin, M.F. (1997). Interaction between ATM protein and c-Abl in response to DNA damage. Nature *387*, 520-523.

315. Kharbanda, S., Ren, R., Pandey, P., Shafman, T.D., Feller, S.M., Weichselbaum, R.R., and Kufe, D.W. (1995). Activation of the c-Abl tyrosine kinase in the stress response to DNA-damaging agents. Nature *376*, 785-788.

316. Kharbanda, S., Pandey, P., Jin, S., Inoue, S., Bharti, A., Yuan, Z.M., Weichselbaum, R., Weaver, D., and Kufe, D. (1997). Functional interaction between DNA-PK and c-Abl in response to DNA damage. Nature *386*, 732-735.

317. Dittmann, K., Mayer, C., Fehrenbacher, B., Schaller, M., Raju, U., Milas, L., Chen, D.J., Kehlbach, R., and Rodemann, H.P. (2005). Radiation-induced epidermal growth factor receptor nuclear import is linked to activation of DNA-dependent protein kinase. J Biol Chem *280*, 31182-31189.

318. Ren, R., Ye, Z.S., and Baltimore, D. (1994). Abl protein-tyrosine kinase selects the Crk adapter as a substrate using SH3-binding sites. Genes Dev *8*, 783-795.

319. Li, W., Hu, P., Skolnik, E.Y., Ullrich, A., and Schlessinger, J. (1992). The SH2 and SH3 domain-containing Nck protein is oncogenic and a common target for phosphorylation by different surface receptors. Mol Cell Biol *12*, 5824-5833.

320. Purvis, J.E., Karhohs, K.W., Mock, C., Batchelor, E., Loewer, A., and Lahav, G. (2012). p53 dynamics control cell fate. Science *336*, 1440-1444.

321. Chipuk, J.E., Kuwana, T., Bouchier-Hayes, L., Droin, N.M., Newmeyer, D.D., Schuler, M., and Green, D.R. (2004). Direct activation of Bax by p53 mediates mitochondrial membrane permeabilization and apoptosis. Science *303*, 1010-1014.

322. Mihara, M., Erster, S., Zaika, A., Petrenko, O., Chittenden, T., Pancoska, P., and Moll, U.M. (2003). p53 has a direct apoptogenic role at the mitochondria. Mol Cell *11*, 577-590.

323. Leu, J.I., Dumont, P., Hafey, M., Murphy, M.E., and George, D.L. (2004). Mitochondrial p53 activates Bak and causes disruption of a Bak-Mcl1 complex. Nat Cell Biol *6*, 443-450.

324. Huang, T.T., Wuerzberger-Davis, S.M., Seufzer, B.J., Shumway, S.D., Kurama, T., Boothman, D.A., and Miyamoto, S. (2000). NF-kappaB activation by camptothecin. A linkage between nuclear DNA damage and cytoplasmic signaling events. J Biol Chem *275*, 9501-9509.

325. Baeuerle, P.A., and Baltimore, D. (1988). I kappa B: a specific inhibitor of the NF-kappa B transcription factor. Science *242*, 540-546.

326. Wu, Z.H., Shi, Y., Tibbetts, R.S., and Miyamoto, S. (2006). Molecular linkage between the kinase ATM and NF-kappaB signaling in response to genotoxic stimuli. Science *311*, 1141-1146.

327. Huang, T.T., Wuerzberger-Davis, S.M., Wu, Z.H., and Miyamoto, S. (2003). Sequential modification of NEMO/IKKgamma by SUMO-1 and ubiquitin mediates NF-kappaB activation by genotoxic stress. Cell *115*, 565-576.

328. McCool, K.W., and Miyamoto, S. (2012). DNA damage-dependent NF-kappaB activation: NEMO turns nuclear signaling inside out. Immunol Rev *246*, 311-326.

329. Reinhardt, H.C., Hasskamp, P., Schmedding, I., Morandell, S., van Vugt, M.A., Wang, X., Linding, R., Ong, S.E., Weaver, D., Carr, S.A., and Yaffe, M.B.

(2010). DNA damage activates a spatially distinct late cytoplasmic cell-cycle checkpoint network controlled by MK2-mediated RNA stabilization. Mol Cell *40*, 34-49.

330. Blasius, M., Forment, J.V., Thakkar, N., Wagner, S.A., Choudhary, C., and Jackson, S.P. (2011). A phospho-proteomic screen identifies substrates of the checkpoint kinase Chk1. Genome Biol *12*, R78.

331. Sellin, M.E., Holmfeldt, P., Stenmark, S., and Gullberg, M. (2011). Microtubules support a disk-like septin arrangement at the plasma membrane of mammalian cells. Mol Biol Cell *22*, 4588-4601.

332. Shen, B., Nolan, J.P., Sklar, L.A., and Park, M.S. (1997). Functional analysis of point mutations in human flap endonuclease-1 active site. Nucleic Acids Res *25*, 3332-3338.

333. Tsutakawa, S.E., Classen, S., Chapados, B.R., Arvai, A.S., Finger, L.D., Guenther, G., Tomlinson, C.G., Thompson, P., Sarker, A.H., Shen, B., Cooper, P.K., Grasby, J.A., and Tainer, J.A. (2011). Human flap endonuclease structures, DNA double-base flipping, and a unified understanding of the FEN1 superfamily. Cell *145*, 198-211.

334. Orans, J., McSweeney, E.A., Iyer, R.R., Hast, M.A., Hellinga, H.W., Modrich, P., and Beese, L.S. (2011). Structures of human exonuclease 1 DNA complexes suggest a unified mechanism for nuclease family. Cell *145*, 212-223.

335. Ip, S.C., Rass, U., Blanco, M.G., Flynn, H.R., Skehel, J.M., and West, S.C. (2008). Identification of Holliday junction resolvases from humans and yeast. Nature *456*, 357-361.

336. Constantinou, A., Gunz, D., Evans, E., Lalle, P., Bates, P.A., Wood, R.D., and Clarkson, S.G. (1999). Conserved residues of human XPG protein important for nuclease activity and function in nucleotide excision repair. J Biol Chem *274*, 5637-5648.

337. Shen, B., Singh, P., Liu, R., Qiu, J., Zheng, L., Finger, L.D., and Alas, S. (2005). Multiple but dissectible functions of FEN-1 nucleases in nucleic acid processing, genome stability and diseases. Bioessays *27*, 717-729.

338. Lee Bi, B.I., Nguyen, L.H., Barsky, D., Fernandes, M., and Wilson, D.M., 3rd (2002). Molecular interactions of human Exo1 with DNA. Nucleic Acids Res *30*, 942-949.

339. Otterlei, M., Bruheim, P., Ahn, B., Bussen, W., Karmakar, P., Baynton, K., and Bohr, V.A. (2006). Werner syndrome protein participates in a complex with RAD51, RAD54, RAD54B and ATR in response to ICL-induced replication arrest. J Cell Sci *119*, 5137-5146.

340. Cheng, W.H., Kusumoto, R., Opresko, P.L., Sui, X., Huang, S., Nicolette, M.L., Paull, T.T., Campisi, J., Seidman, M., and Bohr, V.A. (2006). Collaboration of Werner syndrome protein and BRCA1 in cellular responses to DNA interstrand cross-links. Nucleic Acids Res *34*, 2751-2760.

341. Tafel, A.A., Wu, L., and McHugh, P.J. (2011). Human HEL308 localizes to damaged replication forks and unwinds lagging strand structures. J Biol Chem *286*, 15832-15840.

342. Kee, Y., and D'Andrea, A.D. (2010). Expanded roles of the Fanconi anemia pathway in preserving genomic stability. Genes Dev *24*, 1680-1694.

343. Suhasini, A.N., Sommers, J.A., Muniandy, P.A., Coulombe, Y., Cantor, S.B., Masson, J.Y., Seidman, M.M., and Brosh, R.M., Jr. (2013). Fanconi Anemia Group J Helicase and MRE11 Nuclease Interact to Facilitate the DNA Damage Response. Mol Cell Biol.

344. Peng, M., Litman, R., Xie, J., Sharma, S., Brosh, R.M., Jr., and Cantor, S.B. (2007). The FANCJ/MutLalpha interaction is required for correction of the cross-link response in FA-J cells. Embo J *26*, 3238-3249.

345. Karanja, K.K., Cox, S.W., Duxin, J.P., Stewart, S.A., and Campbell, J.L. (2012). DNA2 and EXO1 in replication-coupled, homology-directed repair and in the interplay between HDR and the FA/BRCA network. Cell Cycle *11*, 3983-3996.

346. Cortazar, D., Kunz, C., Selfridge, J., Lettieri, T., Saito, Y., MacDougall, E., Wirz, A., Schuermann, D., Jacobs, A.L., Siegrist, F., Steinacher, R., Jiricny, J., Bird, A., and Schar, P. (2011). Embryonic lethal phenotype reveals a function of TDG in maintaining epigenetic stability. Nature *470*, 419-423.

347. Nakahira, M., Macedo, J.N., Seraphim, T.V., Cavalcante, N., Souza, T.A., Damalio, J.C., Reyes, L.F., Assmann, E.M., Alborghetti, M.R., Garratt, R.C.,

Araujo, A.P., Zanchin, N.I., Barbosa, J.A., and Kobarg, J. (2010). A draft of the human septin interactome. PLoS One *5*, e13799.

348. Morris, J.R., Boutell, C., Keppler, M., Densham, R., Weekes, D., Alamshah, A., Butler, L., Galanty, Y., Pangon, L., Kiuchi, T., Ng, T., and Solomon, E. (2009). The SUMO modification pathway is involved in the BRCA1 response to genotoxic stress. Nature *462*, 886-890.

349. Imai, Y., Kimura, T., Murakami, A., Yajima, N., Sakamaki, K., and Yonehara, S. (1999). The CED-4-homologous protein FLASH is involved in Fas-mediated activation of caspase-8 during apoptosis. Nature *398*, 777-785.

350. Povlsen, L.K., Beli, P., Wagner, S.A., Poulsen, S.L., Sylvestersen, K.B., Poulsen, J.W., Nielsen, M.L., Bekker-Jensen, S., Mailand, N., and Choudhary, C. (2012). Systems-wide analysis of ubiquitylation dynamics reveals a key role for PAF15 ubiquitylation in DNA-damage bypass. Nat Cell Biol *14*, 1089-1098.

351. Chahwan, R., Gravel, S., Matsusaka, T., and Jackson, S.P. (2013). Dma/RNF8 proteins are evolutionarily conserved E3 ubiquitin ligases that target septins. Cell Cycle *12*, 1000-1008.

352. Yan, J., and Jetten, A.M. (2008). RAP80 and RNF8, key players in the recruitment of repair proteins to DNA damage sites. Cancer Lett *271*, 179-190.

353. Crooks, G.E., Hon, G., Chandonia, J.M., and Brenner, S.E. (2004). WebLogo: a sequence logo generator. Genome Res *14*, 1188-1190.

354. Costantini, S., Colonna, G., and Facchiano, A.M. (2008). ESBRI: a web server for evaluating salt bridges in proteins. Bioinformation *3*, 137-138.

355. Maga, G., and Hubscher, U. (2003). Proliferating cell nuclear antigen (PCNA): a dancer with many partners. J Cell Sci *116*, 3051-3060.

356. Hutton, R.D., Roberts, J.A., Penedo, J.C., and White, M.F. (2008). PCNA stimulates catalysis by structure-specific nucleases using two distinct mechanisms: substrate targeting and catalytic step. Nucleic Acids Res *36*, 6720-6727.

357. Mesquita, R.D., Woods, N.T., Seabra-Junior, E.S., and Monteiro, A.N. (2010). Tandem BRCT Domains: DNA's Praetorian Guard. Genes Cancer *1*, 1140-1146.

358. Gilljam, K.M., Feyzi, E., Aas, P.A., Sousa, M.M., Muller, R., Vagbo, C.B., Catterall, T.C., Liabakk, N.B., Slupphaug, G., Drablos, F., Krokan, H.E., and Otterlei, M. (2009). Identification of a novel, widespread, and functionally important PCNA-binding motif. J Cell Biol *186*, 645-654.

359. Yu, X., Chini, C.C., He, M., Mer, G., and Chen, J. (2003). The BRCT domain is a phospho-protein binding domain. Science *302*, 639-642.

360. Gloeckner, C.J., Boldt, K., Schumacher, A., and Ueffing, M. (2009). Tandem affinity purification of protein complexes from mammalian cells by the Strep/FLAG (SF)-TAP tag. Methods Mol Biol *564*, 359-372.

361. Gloeckner, C.J., Boldt, K., and Ueffing, M. (2009). Strep/FLAG tandem affinity purification (SF-TAP) to study protein interactions. Curr Protoc Protein Sci *Chapter 19*, Unit19 20.

362. Wu, N., and Yu, H. (2012). The Smc complexes in DNA damage response. Cell Biosci *2*, 5.

363. Yazdi, P.T., Wang, Y., Zhao, S., Patel, N., Lee, E.Y., and Qin, J. (2002). SMC1 is a downstream effector in the ATM/NBS1 branch of the human S-phase checkpoint. Genes Dev *16*, 571-582.

364. Kim, S.T., Xu, B., and Kastan, M.B. (2002). Involvement of the cohesin protein, Smc1, in Atm-dependent and independent responses to DNA damage. Genes Dev *16*, 560-570.

365. Kitagawa, R., Bakkenist, C.J., McKinnon, P.J., and Kastan, M.B. (2004). Phosphorylation of SMC1 is a critical downstream event in the ATM-NBS1-BRCA1 pathway. Genes Dev *18*, 1423-1438.

366. Luo, H., Li, Y., Mu, J.J., Zhang, J., Tonaka, T., Hamamori, Y., Jung, S.Y., Wang, Y., and Qin, J. (2008). Regulation of intra-S phase checkpoint by ionizing radiation (IR)-dependent and IR-independent phosphorylation of SMC3. J Biol Chem *283*, 19176-19183.

367. Potts, P.R., Porteus, M.H., and Yu, H. (2006). Human SMC5/6 complex promotes sister chromatid homologous recombination by recruiting the SMC1/3 cohesin complex to double-strand breaks. Embo J *25*, 3377-3388.

368. Kim, J.S., Krasieva, T.B., LaMorte, V., Taylor, A.M., and Yokomori, K. (2002). Specific recruitment of human cohesin to laser-induced DNA damage. J Biol Chem *277*, 45149-45153.

369. Bauerschmidt, C., Arrichiello, C., Burdak-Rothkamm, S., Woodcock, M., Hill, M.A., Stevens, D.L., and Rothkamm, K. (2010). Cohesin promotes the repair of

ionizing radiation-induced DNA double-strand breaks in replicated chromatin. Nucleic Acids Res *38*, 477-487.

370. Nahas, S.A., Lai, C.H., and Gatti, R.A. (2005). Post-irradiation phosphorylation of structural maintenance chromosome 1 (SMC1) is independent of the Fanconi protein pathway. Int J Radiat Oncol Biol Phys *61*, 1167-1172.

371. Grompe, M., and D'Andrea, A. (2001). Fanconi anemia and DNA repair. Hum Mol Genet *10*, 2253-2259.